INFLUENCE OF INCREASING SURFACE HUMIDITY ON WINTER WARMING

AT HIGH ALTITUDES THROUGH THE 21ST CENTURY

by

IMTIAZ RANGWALA

A dissertation submitted to the Graduate School-New Brunswick

Rutgers, The State University of New Jersey

In partial fulfillment of the requirements

For the degree of

Doctor of Philosophy

Graduate Program in Environmental Sciences

Written under the direction of

Prof. James R. Miller

And approved by

New Brunswick, New Jersey

October, 2008

ABSTRACT OF THE DISSERTATION

Influence of Increasing Surface Humidity on Winter Warming at High Altitudes through the 21st Century

By IMTIAZ RANGWALA

Dissertation Director:

Prof. James R. Miller

This dissertation examines the influence of low-level atmospheric humidity in mediating the rate of surface warming, particularly at high altitude regions, during the late 20th century and the 21st century. The focus is on observations and global climate model projections (IPCC SRES A1B scenario) for China, the Tibetan Plateau (TP) and the San Juan Mountain (SJM) in southwest Colorado. For China, the analysis suggests large surface warming despite significant decreases in insolation until the middle of the 21st century. Both the past and future warming in China occurs primarily as a result of the lower and upper atmospheric water vapor feedbacks, triggered by the increase in anthropogenic greenhouse gases, which in turn causes an increase in downward longwave radiation (DLR). For the TP and the SJM region, I find that increases in surface specific humidity (q) leads to relatively large increases in DLR. This effect is enhanced in colder months and at higher altitudes, and the winter warming in the TP is about twice the warming during other seasons. For the TP, the model shows that for the highest elevations the largest warming between 1950-2100 occurs during winter and spring. The

increases in DLR influenced by increases in q during winter, and increases in absorbed solar radiation influenced by decreases in snow cover extent during spring are, in part, the reason for a large warming trend over the plateau. These two effects appear to produce the model's elevation dependent warming trend. For the SJM region, the observations show that q has been increasing at more than 10% per decade from October through January between 1990-2005, when the region experienced the largest increases in surface temperatures. Moreover, only during these months do diurnal changes in humidity explain the large variability in the corresponding changes in temperature. The largest changes in DLR also appear to occur during these months. Large increases in DLR during January and December coincide with large increases in temperatures and, in part, indicate the causes for a large warming trend during these months.

Acknowledgements

This dissertation would not be possible without the involvement and encouragements of several people both who were available in person and those whose work produced a deep impression on me to take a longer academic journey that I did.

The seed for venturing into a Ph.D. was unknowingly sown in the summer of 2000 when I first read about the Gaia Hypothesis in the very first book written on it by James Lovelock. It did have a deep impression on me to venture into the realm of Earth System Science which I attempted to facilitate in my remaining years at Rutgers as a graduate student.

The curriculum for Earth System Science is not formalized at Rutgers and it is true for most institutions. Nevertheless, there exists a potential to study it by integrating one's coursework and research from several disciplines – in my case from Environmental Sciences, Ecology, Oceanography, Geography, Geology and Human Ecology. Attending seminars and taking courses within these departments had been a very enriching experience. However, the major task of pinning down a research topic and an advisor remained formidable for me for a long time. Therefore, I was certainly glad to meet Dr. Paul Falkowski and take his most amazing course - "History of the Earth System".

When the stars were well placed, I met Dr. Jim Miller and put my case before him. The rest had been a fruitful collaboration and a concentrated research that also sustained the consciousness of the Earth System Science at all times. My deep gratitude goes to Dr. Miller for his trust in my candidacy, his open-minded outlook and for being such a kind and smiling human being. This Ph.D. would not have happened but for him and his counseling.

I am very thankful for a wonderful committee that presided my Ph.D. work. It, of course, felt like the company of friends who appreciated my efforts and helped me at all stages. Thanks to Dr. Dave Robinson for his ever-accessibility, advices and support with proof-reading and data. Thanks to Dr. Ming Xu for the data on China and his long discussions on the issues of environmental change in that region. Thanks to Dr. Tony Broccoli for his presence in the ENR building, teaching a brilliant course - "Mechanisms of Past Climate Change", and on steering and overseeing the progress of my research in whatever capacity he could.

I have been very fortunate to get an opportunity to work on the case of the San Juan Mountains in the summer of 2007 with a mini-grant from Mountain Studies Institute at Silverton, CO. Thanks to Dr. Koren Nydick for her trust in me to do something useful. This experience did not only epitomize my venture into climate change in the mountain regions but also took me into the mountains. My research on the San Juan Mountains, which has several components in climatology and hydrology, has provided numerous perspectives and opened doors on near future possibilities for work as a climate scientist.

My sincere appreciation to Dr. Gary Russell at NASA-GISS for his ever-prompt help with my queries related to the GISS-AOM model throughout this work. I would like to sincerely acknowledge several people and agencies for the climate and hydrology data for the San Juan Mountain region - High Plains Regional Climate Center (HPRCC), National Climatic and Data Center (NCDC) and National Resource and Conservation Services (NRCS) for climate and snow data; United States Geological Survey (USGS) and Colorado Department of Water Resources (CDSS) for streamflow data; Chris Landry and the Center for Snow and Avalanche Studies (CSAS) for climate and energy fluxes data at high elevation sites in San Juan Mountains; David Inouye and Dan Jones at Rocky Mountain Biological Lab for the long-term humidity data for Gothic, CO when no other humidity data was available. Many thanks to Neil Ramchandani for his very important help with compiling and analyzing the data on the San Juans in the last two months of this Ph.D. work.

No graduate work is possible without a proper and consistent form of financial support. I am deeply grateful to the Undergraduate Instructions in Life Sciences for providing me that support during my tenure as a Ph.D. student. Special thanks to Dr. Gregg Transue for allowing me to be a teaching assistant for his dynamic course- Biology 100, throughout that period.

I am deeply thankful for the involvement and interaction of the faculty in various disciplines at Rutgers, particularly Ecology, Environmental Sciences and Oceanography. I would specifically like to acknowledge the assistance of Dr. Peter Strom and Dr. John Reinfelder for their generous assistance and guidance in their capacity as a graduate director, and to Dr. Lily Young for greatly improving the graduate student life in her capacity as our department's chair.

To my colleagues, primarily in Environmental Sciences and Ecology, I would say that it was worth doing this Ph.D. just to meet them. Special thanks to Guanseelan Alagappan, Qiao Feng, Priya Narasingarao and Sarat Kannepalli for their involvement at different stages of this Ph.D. work. To Naseem, my sister, I am grateful for her charming presence at Rutgers. To Kritee, my wife, for her largest involvement both towards this work and outside it, I could only say that she was the wind beneath my wings. To my family in India and my zen family in New Jersey I am in debt of their profound love and support.

And, lastly, I would like to dedicate this Ph.D. to my mom and dad for their unconditional love, unwavering patience and everlasting support.

Table of contents

List of tables

List of illustrations and figures

Chapter 1: Introduction

The present earth is experiencing an energy imbalance of close to 1 W/m^2, which is probably unprecedented in its history [*Hansen et al.*, 2005]. This imbalance arises from a decrease in the outgoing longwave radiation (OLR) from the earth due to a rapid accumulation of greenhouse gases in its atmosphere and the thermal inertia of its ocean, while the incoming solar radiation (insolation) remains relatively unchanged. On a global average, this imbalance has caused the observed increases in the surface air temperature, on both land and ocean, by 0.74°C ± 0.18°C between 1906-2005, according to the fourth assessment report (AR4) of the Intergovernmental Panel on Climate Change (IPCC) [*Trenberth et al.*, 2007]. The report shows that, globally, the land temperatures (0.27 °C/decade) have increased twice as fast as the ocean temperatures (0.13 °C/decade) after 1979.

According to the IPCC-AR4 report, the two main periods in the 20th century which show a warming trend are 1910-1945 and 1976-2000. The warming trend in land-surface air temperature from 1976 to 2000 is about twice as fast, though with greater interannual variability, than the trend from 1910 to 1945. The period 1946-1975 does not show any significant increase in temperature, however it coincides with a non-significant, but regionally more marked, cooling over the Northern Hemisphere. Overall, warming in the Southern Hemisphere has been much more uniform than the Northern Hemisphere over the lifetime of the instrumental record. Moreover, observations show a steady increase in the heat content of the world ocean (~2 × 10^{23} joules), from surface to 3000 meter depth, during the latter half of the 20th century [*Levitus et al.*, 2000].

Global observations of surface insolation from 1960 to 1990 suggest a general decline of 4-6% in sunlight on the land surface [*Wild et al.*, 2005 and references therein]. However, since the late 1980s there appears to be an increasing trend in insolation at several locations where a good record exists [*Wild et al.*, 2005]. These trends in insolation could have possibly masked the greenhouse warming before the 1990s, which became more evident in the 1990s.

According to the IPCC- AR4 report [*Trenberth et al.*, 2007], the 20th century warming has been significant over most of the world's surface and, in the recent decades, some regions have warmed substantially while a few have shown a slight annual cooling. This warming shows significant spatial variability, particularly in the extra-tropics. Eleven of the 12 years, between 1995 and 2006, rank among the 12 warmest years on record since 1850. The report suggests that, between 1979 and 2005, warming is generally larger in the extra-tropics with strongest warming trends in northwest North America, Greenland, northwest Europe, and east and northeast Asia.

Observations in the high altitude regions of the planet during the latter half of the 20th century have suggested that these regions have been relatively more sensitive to climate change in the recent past [*Beniston*, 2003; *Diaz and Bradley*, 1997; *Giorgi et al.*, 1997; *Liu and Chen*, 2000]. These regions have warmed at a greater rate (1-2 ^{o}C in the last century) than the rest of the planet, with greater increases in daily minimum temperatures than the daily maximum temperatures [*Diaz and Bradley*, 1997]. Moreover, within these mountain regions, there is an elevation dependency in surface warming, i.e. greater warming rates at higher altitudes [*Diaz and Bradley,* 1997; *Liu and Chen,* 2000]. In contrast, there are also regions such as the Front Range of the Rocky Mountains in

Colorado, USA, which have experienced cooling at the highest elevation, possibly owing to increases in local precipitation regime and decreases in insolation [*Pepin and Losleben,* 2002]. Modeling studies have suggested snow-albedo feedback to be the most important factor in causing this elevation dependent surface warming over the different mountain regions [*Chen et al.*, 2003; *Giorgi et al.*, 1997].

A rapid and secular warming trend at high altitude regions would significantly and, possibly, irreversibly modify the hydrological cycles in these regions [*Nijssen et al.*, 2001]. An increase in warming tends to decrease winter and spring snowpack leading to a change in the pattern of seasonal streamflow – generally a reduction in summer flows [*Arnell*, 2003; *Dettinger and Cayan*, 1995; *Saunders et al.*, 2008]. These hydrological changes could imply a wide range of environmental impacts on humans and ecosystems of the mountain regions as well as the downstream regions. In addition to changes in seasonal river flow, a greater evaporation owing to a greater warming in the elevated regions may cause increased desiccation of vegetation during the summer months [*Beniston*, 2003].

In this dissertation, I focus on high altitude regions in the northern hemisphere mid-latitudes to understand the nature and causes of climate change observed in these regions in the latter half of the 20^{th} century. I examine feedbacks that might enhance warming rates in the mountainous regions, with an emphasis on the impact of changes in lower atmospheric water vapor in these regions during the late 20^{th} century and projected for the 21^{st} century. Increases in surface specific humidity have been suggested, in part, to be responsible for a rapid increase in surface warming across the central Europe in the late 20^{th} century by *Philipona et al.* [2005]. They suggest that these increases in specific humidity cause significant increases in the downward longwave radiation (DLR) onto the surface producing a rapid surface warming. Observations from the Swiss Alps have shown that the increases in DLR owing to specific humidity changes are particularly large at very low specific humidity levels [*Rucksthul et al.*, 2007], which are likely to occur at high elevations and during the cold season. The mid-latitude boundary layer, particularly at high altitudes, is expected to be under-saturated in longwave absorption in the water vapor absorption lines. Therefore, an increase in surface water vapor content during winter when the specific humidity is lowest will cause a large increase in the DLR at the surface

Other factors also evaluated include changes in snow cover trends and atmospheric aerosol burden. The study regions include (i) China and its major mountain region, the Tibetan Plateau, and (ii) the San Juan Mountain (SJM) region in southwest Colorado. Our current understanding of the 20th century climatic trends in each of these regions is further discussed in the subsequent sections.

1.1 China

There have been several recent papers reporting significant changes in climate variables over China during the latter half of the 20th century [*Kaiser*, 2000; *Kaiser and Qian*, 2002; *Liu et al.*, 2004a; *Liu et al.*, 2005; *Liu et al.*, 2004b; *Qian et al.*, 2006; *Thomas*, 2000]. These variables include surface insolation, surface air temperature, cloud cover, surface vapor and air pressure, precipitation and evaporation. The changes have both spatial and temporal variability. The observations suggest (a) an increase in surface air temperature [*Liu et al.*, 2004b] (b) reductions in daily temperature range [*Liu et al.*, 2004b], insolation [*Che et al.*, 2005; *Kaiser and Qian*, 2002; *Liu et al.*, 2004a; *Qian et al.*, 2006] and estimated potential evapotranspiration [*Thomas*, 2000] for most geographical regions, (c) a decrease in cloud amount [*Kaiser*, 2000; *Qian et al.*, 2006], (d) an increase in surface air pressure [*Kaiser*, 2000], and (e) an increase in the intensity and reduction in the frequency of precipitation, except in northwest China [*Liu et al.*, 2005].

The causes for these changes are not yet clearly understood. It is possible that some combination of both global- and regional-scale forcings has led to the observed behavior of the climate variables. On the global scale, the increase in radiative forcing due to increasing greenhouse gases and the associated changes in atmospheric circulation are likely to have caused a portion of the observed changes. At the regional scale, the climate variables could be influenced by the increase in atmospheric aerosols caused by the rapid rate of development in China over the last 5 decades of the 20th century (e.g. [*Giorgi et al.*, 2003; *Qian et al.*, 2003]. Large-scale land-use changes may also be a factor [*Fu*, 2003]. An equilibrium modeling study by *Menon et al.* [2002], using the GISS SI2000 12-layer model, reported that the alteration in the regional atmospheric circulation caused by the direct radiative effects of black carbon aerosols over China, produced the observed temperature and precipitation trends over China. These regional trends primarily include increases in summer floods in south China and drought in north China, and moderate cooling in southeast China.

This study analyzes simulations from the global coupled atmosphere-ocean model based on *Russell et al.* [1995] to elucidate the underlying mechanisms that are likely to have caused the observed warming over China from 1950-2000 despite significant decreases in surface insolation over most of the region. Both the global- and regional-scale forcings are likely to persist, even intensify, in the first half of the 21st century. It is, therefore, crucial to understand the trends in climate variables that might emerge as a result of expected changes in the global and regional forcings during the 21st century. This study, therefore, also examines potential changes in the climate variables for the 21st century over China.

1.2 Tibetan Plateau

In recent years, there has been much interest in the nature of climate change in the Tibetan Plateau during the late 20th century. It is understood that this region may be one of the most sensitive to global climate change [*Du et al.*, 2004; *Liu and Chen*, 2000]. However, climate observations are not comprehensive in space over the plateau. Most of the climate data are available from weather stations that are located in the eastern half of the plateau which is more inhabited and where the average altitude is relatively lower.

Previous studies on the Tibetan Plateau suggest that the warming there during the latter half of the 20th century started earlier (early 1950s) than the northern hemisphere trend (mid-1970s) [*Liu and Chen*, 2000; *Niu et al.*, 2004], though it experienced a sudden jump in the mid-1980s [*Niu et al.*, 2004]. Moreover, the plateau had one of the highest rates of warming between 1955 and 1996 in the northern hemisphere [*Liu and Chen*, 2000]. This warming has been largest during the winter months [*Du et al.*, 2004; *Liu and Chen*, 2000; *Shenbin et al.*, 2006; *You et al.*, 2007] and is estimated to be twice as large as the mean annual trend [*Liu and Chen*, 2000]. However, the comparison between winter and annual warming rates varies greatly among other studies [*Du et al.*, 2004; *Shenbin et al.*, 2006; *You et al.*, 2007]. Fall has the next highest warming rate; while summer and spring show relatively less warming [*Du et al.*, 2004; *Liu and Chen*, 2000; *Shenbin et al.*, 2006; *You et al.*, 2007].

Using an extensive selection of weather stations (178) within the Tibetan Plateau, *Liu and Chen* [2000] found a differential increase in the rate of surface warming dependent primarily on the elevation of the observing station for the 1960-1990 period. *Duan and Wu* [2006] reported increases in low level nocturnal cloud cover over central and eastern parts of the plateau between 1961-2003, despite decreases in total cloud cover during the same time period. They suggest that these increases in the low-level cloud cover explain, in part, the increases in minimum temperatures over the plateau in the latter half of the 20th century.

In this dissertation, I examine the potential effects of seasonal changes in surface water vapor on downward longwave radiation (DLR) and on the surface warming observed in the plateau between 1961-2000 at different elevations. Measurements of surface specific humidity (q) and DLR at different elevations in the Swiss Alps by *Rucksthul, et al.* [2007] suggest large increases in DLR to changes in q during the cold seasons, when the absolute water vapor in the surface boundary layer is relatively low. I use their observed relationship between q and DLR to examine whether increases in surface water vapor over the Tibetan Plateau are, in part, responsible for the large warming during the winter months over the plateau between 1961 and 2000, particularly at higher altitudes.

I also examine the output from a transient experiment of a global climate model to (a) investigate presence of the observed pattern of climate changes over the plateau in the latter half of the 20th century, (b) examine potential changes through the 21st century and (c) elucidate the mechanisms for these climate changes.

1.3 San Juan Mountains

The San Juan Mountain (SJM) region, located between 37-38.5 ^{o}N, 105.5-109 ^{o}W, forms an east-west oriented belt of the Rocky Mountain range in the southwest Colorado (Figure 1.1). Hydrologically, this region contributes significantly to the annual flow in major streams and rivers in the southwest US, such as the Colorado and the Rio Grande. Climate change in this region in the form of increased warming and changes in precipitation will have important consequences on the pattern of streamflow and hence its effect on humans and ecosystems [*Arnell*, 2003; *Beniston*, 2003; *Dettinger and Cayan*, 1995; *Nijssen et al.*, 2001] .

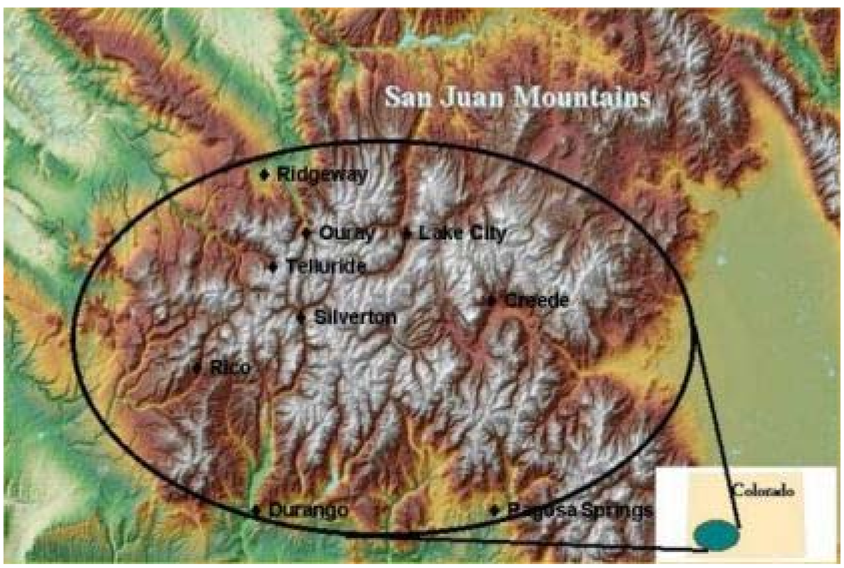

Figure 1.1 San Juan Mountain region located in the southwest of Colorado

Long-term trends in the climate and hydrological variables in the region have not been systematically analyzed previously. However, recent studies have suggested that the interior southwest US, which includes the SJM region, has experienced one of the largest increases in surface warming between 2001-2007 [*Redmond*, 2007; *Saunders et al.*, 2008], which has been linked, in part, to significant changes in the hydrological variables such as precipitation, snowpack and streamflow [*Saunders et al.,* 2008]. Therefore, the intention of this study is, in part, to investigate trends in climate (temperature, precipitation) and hydrological (snow water equivalent, snow-depth, humidity and stream-flow) variables for the 20th century and to assess interrelationships among these trends. In similarity to the analysis for the Tibetan Plateau, the effects of changes in specific humidity on the warming trend in the SJM region are evaluated.

Methodology and the information on observations and the model are described in chapter 2. Chapters 3, 4 and 5 discuss the findings from the analysis on China, the Tibetan Plateau and the San Juan Mountain region, respectively. Chapter 6 provides conclusions and future directions.

Chapter 2: Methodology

The basic approach to understanding the climate trends and evaluating the mechanism of climate change in the study regions includes (a) compilation of the observed and modeled data, (b) trend analysis and graphing of these datasets, and (c) assessment of correlations among various climate and hydrological variables. Sections 2.1 and 2.2 discuss specific approaches used in investigating the climatic trends and mechanisms for China and the Tibetan Plateau, and section 2.2 for the San Juan Mountain region.

2.1 China and Tibetan Plateau

For China, the observed variables analyzed include annual mean measurements of surface air temperature, surface insolation, cloud cover, and surface vapor pressure. The observations for surface insolation (85 stations) and vapor pressure (305 stations) from 1954 to 2000 are obtained from *Liu et al.* [2004], and their trends are consistent with sunshine duration and vapor pressure trends reported in *Kaiser and Qian* [2002] and *Kaiser* [2000], respectively. Figure 2.1 shows the location and elevation of these stations. The annual mean surface temperature observations from 305 stations between 1955-2000 are obtained from *Liu et al.* [2004a]. The observations for cloud cover from 537 stations between 1954-2000 are obtained from *Qian et al.* [2006] which closely correlate with the cloud cover data from 1954-1996 in *Kaiser* [2000] from 196 stations.

All observation stations are first-order observation stations (also referred to as “basic and reference stations” operated by the China Meteorological Administration) across China which provide a daily database meeting the World Meteorological Organization’s standards. To estimate the mean over the whole country, each climate variable, except insolation, is spatially averaged according to an area-based weighting factor in which each station controls an area determined by a Thiessen polygon [*Liu et al.*, 2004a]. The model averages are also effectively area weighted. Insolation observations are available at 85 out of the 305 stations for which the observations for temperature and vapor pressure are also available. The 85 stations are well distributed across China and have correlation coefficients greater than 0.98 with the 305 stations [*Liu et al.*, 2004a]. This indicates that they are representative of the whole country. Additionally, the trends in climate variables from these two groups of stations are very similar.

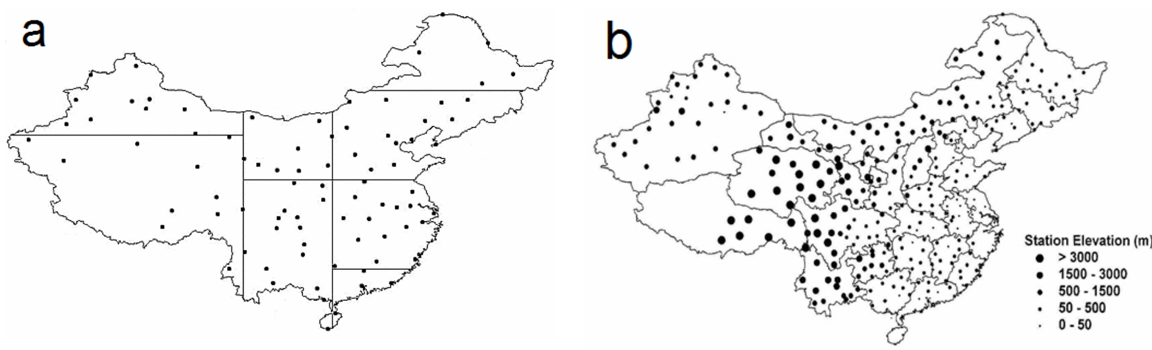

Figure 2.1 Spatial locations of the **(a)** 85 [reproduced from *Liu et al.*, 2004] and **(b)** 305 stations [reproduced from *Liu et al.*, 2004a]

For the Tibetan Plateau, the observations include surface air temperature, surface specific humidity (q), cloud cover and precipitation from 1961 to 2000 which are obtained from the dataset described in *Xu et al.* [2006]. The data quality is same as that discussed for China. For this study, the Tibetan Plateau region lies between 80 - 105 ^{o}E and 27 - 39 ^{o}N. There were 43 observation stations identified over the plateau, and most of them are located on the eastern side of the plateau where the average elevation is relatively lower (Figure 2.2a).

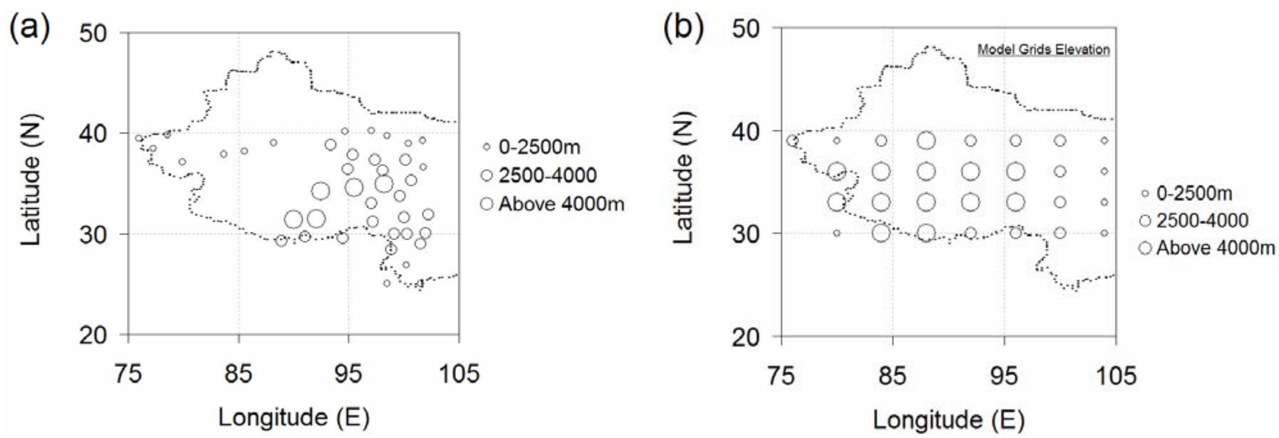

Figure 2.2 Location and elevation range of **(a)** 43 observation stations and **(b)** 29 model grids used in the Tibetan Plateau study. Size of circles indicates elevation.

The 4×3 degree grid global coupled atmosphere-ocean model, GISS-AOM (Goddard Institute of Space Studies – Atmosphere Ocean Model, NASA), based on *Russell et al.* [1995; http://aom.giss.nasa.gov] is used to simulate trends in the selected climate variables over China. Most of the model results presented here are based on output from a single model experiment (GHG + Sulfate). The initial state of this simulation was based on a 200 year spin-up run of initial ocean conditions [*Levitus et al.*, 2000]. From 1850 to 2000, this simulation uses observed greenhouse gases and estimated spatial distributions of atmospheric sulfate burden from *Boucher and Pham* [2002] (Figure 1a). For the 21st century, greenhouse gases are observed up to year 2003 followed by SRES A1B [*Houghton et al.*, 2001]; the sulfate burden is from SRES A1B [*Pham et al.*, 2005]. Two additional model experiments whose results are presented here are (a) the control experiment, which keeps the atmospheric composition fixed at 1850 values, and (b) the GHG experiment, which keeps sulfate aerosols fixed at 1850 values.

Output from two model experiments, GHG + Sulfate and control, identical to those analyzed for the China study, are analyzed to assess the nature of climate change in the

Tibetan Plateau. The plateau region considered in the model simulations has 29 grid cells, which are situated between 80^{o}E - 110^{o}E and 27^{o}N - 39^{o}N (Figure 2.2b). To extract the elevation dependent climate trends in the plateau, we organized the model outputs into 3 different elevation regions: 0-2500m, 2500-4000m, and 4000-5300m. There are respectively 6, 10 and 13 grid cells associated with these regions. The modeled trends in climate variables are shown as anomalies, which are calculated based on the difference between the GHG + Sulfate and control simulations. The output from the model experiment is analyzed for the surface energy balance over the plateau between 1950 and 2100.

2.3 San Juan Mountains, Colorado

The study area primarily includes the 12 counties described in Table 2.1 (see Figure 2.3 for the county map). However, a few observation stations on the southern fringes of Montrose and Gunnison counties are also included. A comprehensive digitized record (number of stations, n ~ 25) of climate observations such as temperature and precipitation for the selected study region is only available after 1948. There are many fewer stations (n ~ 5) that inform us about the climatic trend in early half of the 20th century. For temperature and precipitation, the long-term observations are only available from the National Weather Service (NWS) stations. More recently, since the mid 1980s, weather observations are also available from the SNOTEL sites, managed by the National Resources Conservation Service (NRCS), which has been primarily interested in the measurement of snow water equivalent (SWE). There are long-term observations of the SWE at the SNOTEL sites. Moreover, information on SWE and snow-depth is also available from the Snow Course sites, some of which go as far back as the mid-1930s.

Table 2.1 The SJM study region primarily comprises these 12 counties

1	Archuleta
2	Conejos
3	Dolores
4	Hinsdale
5	La Plata
6	Mineral
7	Montezuma
8	Ouray
9	Rio Grande
10	Saguache
11	San Miguel
12	San Juan

The streamflow observations are obtained from the gages maintained by the United States Geological Survey (USGS; n = 34) and Colorado's Decision Support Systems (CDSS; n = 22) maintained by the Colorado Division of Water Resources. A station was selected for analysis only if it included observations for the 1985-2005 period because we are particularly interested in investigating changes in streamflow in recent decades. To compile the data from all stations, the data are normalized by 1990-2005 mean because the data for this period are available for each of the selected stations.

Information on all the climate and hydrological observation stations used in the analysis is provided in Appendix A (Tables A1-A5). All data collected are compiled as monthly averages before analysis. For temperature, missing data in the middle of the record are estimated based on the observations available from adjacent months because absence of data affected a realistic estimation of annual and seasonal means and trends. Moreover through this process, the use of available data included in the analysis is maximized. The criteria adopted for filling in the missing data include the following: (i) missing monthly averaged data are calculated as the mean of available observations from the nearest five years in both the past and future for the same month, (ii) if the total observations adjacent to a missing monthly value do not total five, past or future, then the estimation for the missing data is calculated based on the mean of nearest four, three, two or one year/s, past and future; based on maximum availability of observations, and (iii) in absence of observation for even one year, past or future, the missing data is made equivalent to the nearest past or future value for the same month, whichever is available. Overall, less than 5% of the temperature data was filled in.

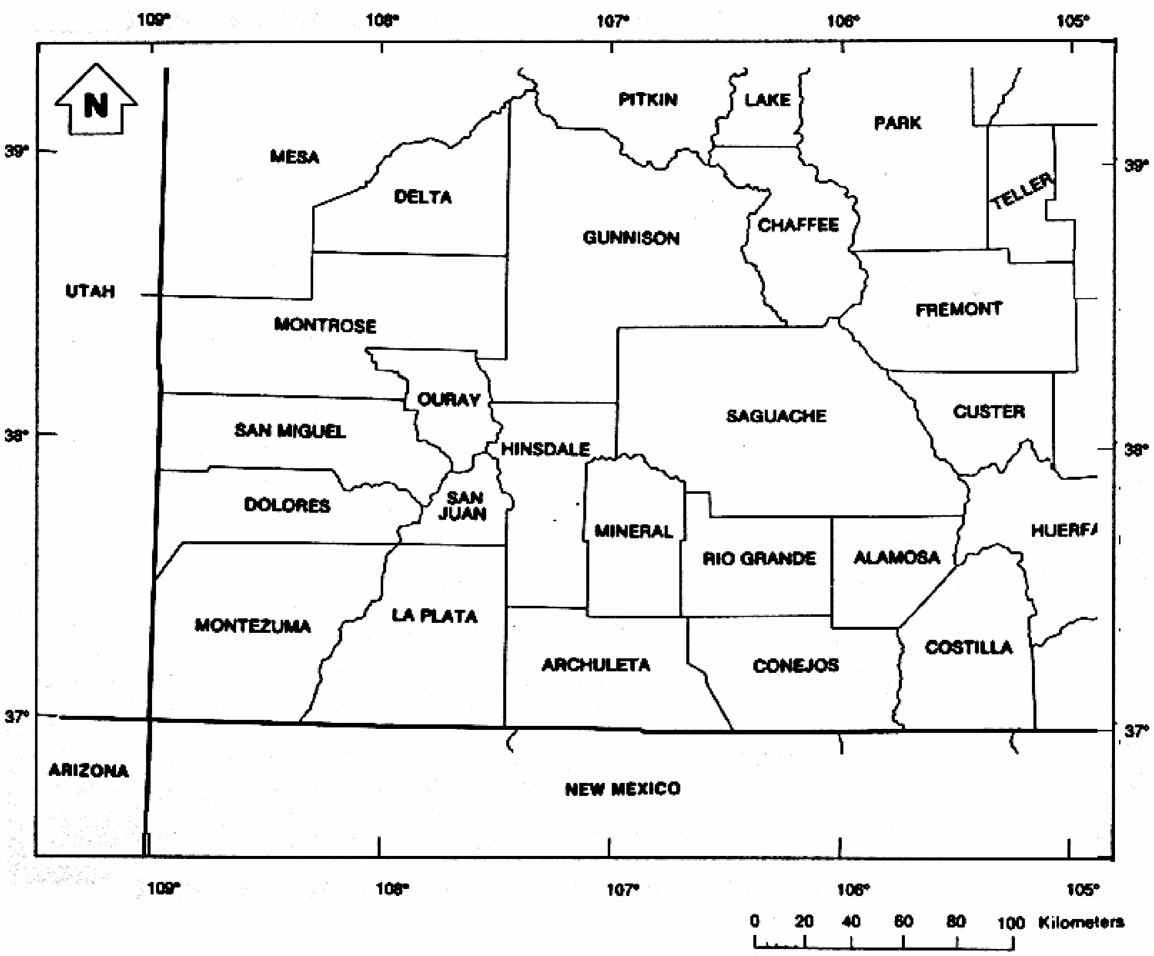

Figure 2.3 Southwest Colorado county map. (Source: US Dept. of Commerce)

The precipitation analysis is divided into snowfall (Nov-May) and monsoon precipitation (Jul-Aug). The snowfall and monsoon precipitation data from the NWS sites, and the SWE and snow-depth data from the SNOTEL and Snow Course sites are normalized by the mean of the data for the 1960-1990 period. The snowfall and monsoon precipitation data from the SNOTEL sites are normalized by the mean of the data for the 1990-2005 period due a shorter observation period available for these sites. This difference in the base value of time period used for normalization creates an offset between the absolute anomalies of NWS and SNOTEL sites. This offset is countered, without affecting the trends of the absolute anomalies, by subtracting the absolute anomalies obtained for SNOTEL sites from the difference in the means of NWS and SNOTEL data over the period for which the SNOTEL data are available. Missing values in precipitation from NWS sites are filled in similarly to temperature.

Caution is recommended in the interpretation of SNOTEL and Snow Course data. *Julander* [2008] suggests that (a) changes in the physical surrounding (e.g. vegetation) and distribution of snowpack, and (b) changes in instrumentation could create an artificial trend in the data. Moreover, use of thermistors and timing of daily data reporting can affect the accuracy of temperature measurements at the SNOTEL sites.

Effects of changes in specific humidity (q) on winter warming in the recent decades are evaluated in section 5.2. I could not find long-term humidity trends for any site within the study region, therefore I used relative humidity observations available for the 1990-2007 period from Gothic, CO (38°57'N & 106°59'W; elev. 9474 ft), which is slightly north of the study region. The EPA weather station at the Rocky Mountain Biological Laboratory (RMBL; rmbl.org) in Gothic, CO has hourly relative humidity and temperature measurements, which are used to calculate specific humidity trends between 1990-2005. Moreover, temperature trends at Gothic between 1990-2005 are similar to trends observed for the SJM region, therefore I expect the humidity trends from Gothic might also be representative of the humidity changes in SJM for this time period.

The relationship between q and downward longwave radiation (DLR) for the SJM region is obtained from their hourly measurements at two high elevation sites from 2005-2007 in the SJM region near Silverton, CO, maintained by the Center for Snow and Avalanche Studies (CSAS; www.snowstudies.org) in Silverton. These sites are Swamp Angel Study Plot (SASP; 37° 54' 25" N, 107° 42' 41" W; elev. 11,050 ft) and Senator Beck Study Plot (SBSP; 37° 54' 25" N, 107° 43' 30"; elev. 12,200 ft). The q-DLR relationship obtained from these sites is used to estimate seasonal changes in DLR based on changes in q at Gothic between 1990-2007.

Chapter 3: Late 20th and 21st Century Climate Change In China

Analysis of observations and global climate model experiments to elucidate past and future changes in surface insolation and warming in China

In this section, I analyze observations and simulations from the global coupled atmosphere-ocean model based on *Russell et al.* [1995], discussed in section 2.1, to elucidate the underlying mechanisms that are likely to have caused the observed warming over China from 1950-2000 despite significant decreases in surface insolation over most of the region. Both the global- and regional-scale forcings are likely to persist, even intensify, in the first half of the 21st century. It is, therefore, crucial to understand the trends in climate variables that might emerge as a result of expected changes in the global and regional forcings during the 21st century. This chapter will examine potential changes in the climate variables for the 21st century over China. Section 3.1 describes and compares the observed and modeled changes in climate variables, such as temperature, insolation, cloud cover and vapor pressure, during the last half of the 20th century. Section 3.2 describes the projected changes in the 21st century. A discussion of the findings is provided in section 3.3.

3.1 Climate change between 1950 – 2000

Figure 3.1 shows that there is a decreasing trend in surface insolation and cloud cover and an increasing trend in surface temperature and water vapor pressure in both model and observations (see also Table 3.1). Between 1950 and 1975, there is no appreciable trend in cloud cover, temperature and surface vapor pressure in the observations or model simulation. For the same period, both model and observations show a decrease in insolation. Modeled and observed trends presented hereafter are from 1950-2000. The observed reduction in insolation is 3.27 W/m^2 per decade which is significantly greater than the model reduction of 0.68 W/m^2 per decade (Figure 3.1a). The observed increase in surface temperature in China is 0.19°C per decade [*Liu et al.*, 2004a], compared to 0.12°C per decade for the model (Figure 3.1b).

Table 3.1 Observed and modeled trends (per decade) in climate variables over China for three time periods: 1950-2000, 1950-1975 and 1975-2000. For each climate variable, 51 annual values were least square fitted to a parabola. The trends are equal to ten times the slope of the parabola over the various time periods.

Climate Variables	1950-2000		1950-1975		1975-2000	
	Observed	Model	Observed	Model	Observed	Model
Sulfate Burden (mg/m^2)	+0.57	-	+0.59	-	+0.55	-
Insolation (W/m^2)	-3.27	-0.68	-3.85	-0.70	-2.69	-0.68
Temperature (°C)	+0.19	+0.12	+0.01	-0.07	+0.38	+0.31
Cloud Cover (%)	-0.73	-0.08	-0.30	+0.08	-1.22	-0.24
Vapor pressure (mb)	+0.08	+0.03	-0.01	-0.02	+0.17	+0.07

Most of the simulated increase in surface vapor pressure occurs after 1975, which is similar to the modeled trends in temperature (Figure 3.1d). The simulated increase in vapor pressure in the upper (200mb) and middle troposphere (500mb) is 9% and 4%, respectively; it is 2% at the surface. The sudden decrease in observed cloud cover, -0.73 % per decade, starting around 1975 (Figure 3.1c) is correlated with the rise in temperature (r = -0.52). The model, however, shows a much smaller decrease in cloud cover although the correlation of the latter with temperature (r = -0.47) is similar.

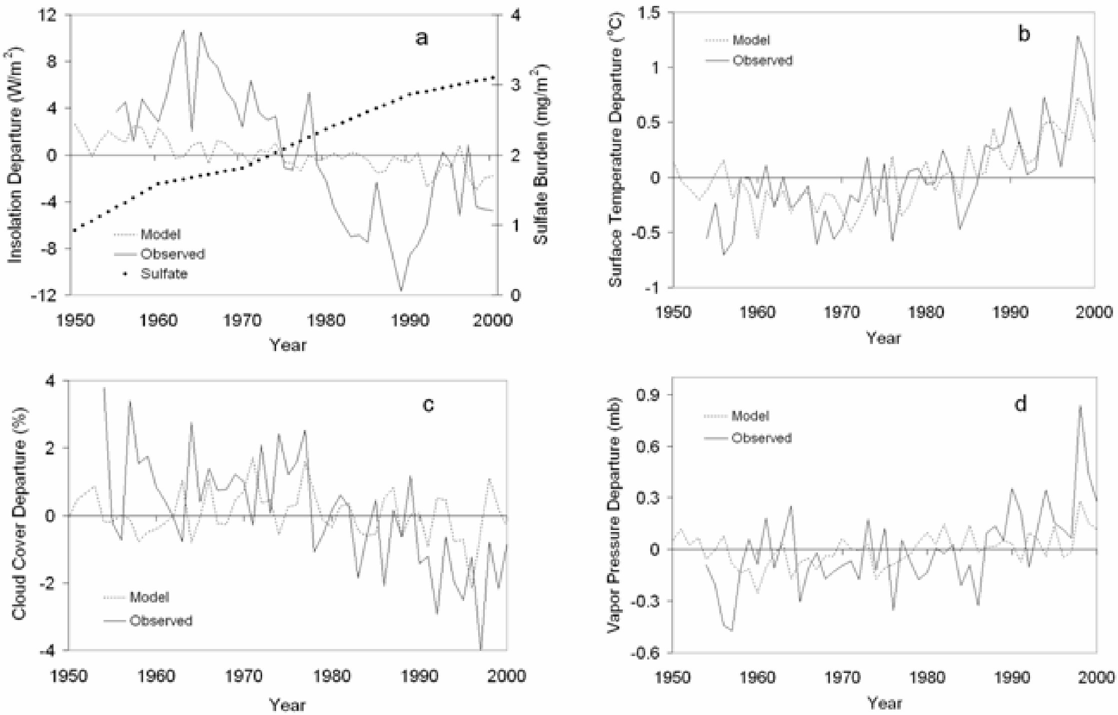

Figure 3.1 Departures from the 1950 to 2000 mean for observations and model for (a) insolation, W/m^2 [*Liu et al.*, 2004] and atmospheric sulfate burden, mg/m^2 [*Boucher and Pham*, 2002] (b) surface temperature, ^{o}C [*Liu et al.*, 2004a], (c) cloud cover, % [*Qian et al.*, 2006], and (d) surface vapor pressure, mb [*Liu et al.*, 2004].

The reduction in surface insolation over China appears to be primarily forced by the atmospheric aerosol loading (Figure 3.1a). This is further supported by noting that there is a decreasing trend (modeled and observed) in cloud cover (Figure 3.1c). The partial correlation between the observed insolation and sulfate aerosol trends from 1955 to 2000 is -0.81, and between the observed insolation and cloud cover is -0.45. The spatial distribution of sulfate aerosols in the model is similar to the observed mean aerosol extinction coefficient (AEC) across China from 1984-1998 estimated by *Kaiser and Qian* [2002]. Sulfate aerosols in the model affect the radiation directly, but their indirect effects on clouds are not included in the model. Furthermore, the model captures only 21% of the observed reduction in surface insolation, which suggests, among other possibilities that either black and organic carbon aerosols and dust have a greater role to play in the observed solar dimming over China than sulfate aerosols alone [*Chameides et al.*, 1999; *Qian et al.*, 2003], or the model insolation has lower sensitivity to changes in sulfate aerosols.

It is interesting to note that, in both model and observations, the surface temperature over China increases during the same period when surface insolation decreases with the contrast being much greater in the observations. The increase in surface temperature could be caused by an increase in downward longwave radiation (DLR) due to the increase in greenhouse gas forcing and the associated water vapor feedbacks, which overcompensates for the reduction in insolation. The partial correlation between the observed CO_2 and temperature trends from 1959-2000 is 0.70, and between the observed surface vapor pressure and temperature is 0.75. However, there is a weak correlation ($r = 0.34$) between the observed CO_2 and surface vapor pressure. Moreover, the partial correlation between the modeled DLR and CO_2 from 1950-2000 is 0.77, and between the modeled DLR and surface vapor pressure is 0.83.

The model's DLR, which is affected by greenhouse gases and clouds, increases by 4.3 W/m^2 while the insolation decreases by 3.4 W/m^2 from 1950-2000. Assuming other variables are constant, the change in surface temperature associated with a change in DLR can be estimated using the relationship, $\Delta B/B = 4*\Delta T/T$, derived from the Stefan-Boltzmann law for black body radiation, where ΔB and ΔT are changes in DLR and temperature, respectively. This calculation yields $\Delta T = 1.03^{o}C$ when $\Delta B = 4.3$ W/m^2. However, the model simulates a surface temperature increase of $0.61^{o}C$ from 1950-2000. The discrepancy between the calculated and the modeled surface temperature increase is caused, in part, by a 0.6 W/m^2 decrease in insolation absorbed by the surface between

1950 and 2000 (Figure 3.2c). Furthermore, the discrepancy between the observed and modeled rate of surface warming by a factor of 1.5, from 1950-2000, is likely caused by a 2.5 times higher rate of increase in the observed surface vapor pressure (Figure 3.1d; see also Table 3.1), which could amplify the DLR from the near surface atmosphere.

Philipona et al. [2005] present a similar scenario for warming in Central Europe from 1995-2002. Their ground based radiation measurements show a decrease in annual average insolation of 1.1 W/m^2 and an increase in annual average DLR of 5.3 W/m^2. This leads to an increase of 0.8^oC in annual average temperature. They separate different forcings contributing to the increase in DLR from increases in (a) clouds (1.4 W/m^2), (b) greenhouse gases except water vapor (0.35 W/m^2), (c) water vapor (0.79 W/m^2) and (d) temperature (2.72 W/m^2) to suggest that the water vapor forcing in the lower atmosphere is about 2.3 times the anthropogenic greenhouse gas forcing in the regions where sufficient water is available for evapotranspiration.

An additional mechanism that could produce surface warming in spite of a significant decrease in surface insolation over China during the latter half of the 20st century, particularly from 1970 to 1995, is a relatively greater reduction in latent heat fluxes to compensate for the decrease in surface insolation. *Liepert et al.* [2004] performed equilibrium climate simulations to elucidate the changes in the global terrestrial surface energy budgets between the pre-industrial (1880s) and the present day (1980s) situations produced by the difference in the atmospheric loading of greenhouse gases and aerosols. Their model, which included parameterizations for both direct and indirect aerosol effects, showed a relatively greater reduction in the strength of latent heat fluxes in the present day scenario, to compensate for the reduction in surface insolation. Their model also produced a 0.6°C warming in the present day condition despite a 0.52 W/m^2 decrease in the net surface insolation.

The direct observation of evaporation across China is unavailable. However, measurements of potential evapotranspiration from observed meteorological data over China from 1951-1993 show a significant decreasing trend [*Thomas*, 2000]. Decreases in potential evapotranspiration south of 35°N are most strongly associated with sunshine duration. Our model suggests a small decrease in evaporation (-1.3 mm/decade) from 1950 to 2000. The simulated decrease in evaporation would be greater if black and organic carbon aerosols and aerosol indirect effects are included in the model [*Ramanathan et al.*, 2001; *Roderick and Farquhar*, 2002].

Overall, the modeled trends in the climate variables discussed above have the same sign as the observed, although the modeled changes in surface insolation, temperature and vapor pressure are smaller than the observed changes. The sharp increase in temperature during the latter half of the 20th century despite "solar dimming" appears to occur, in part, because of the simultaneously increasing greenhouse gas forcing and associated water vapor feedbacks. Overall, the model appears to offer a conservative estimate of the change in the climate variables discussed here. In the next section, we examine the trends and interrelationships among these variables for China during the 21st century under the prescribed forcings of greenhouse gases and atmospheric sulfate burden.

3.2 Climate change in the 21st century

The modeled surface insolation shows a small declining trend between 1850 and 1950, following which there is a sharp and continuous decline in insolation by 6 W/m^2 by the year 2020 (Figure 3.2a). This appears to be caused by the increase in atmospheric sulfate burden. In fact, the model predicts a gradual reduction in annual cloud cover for the 21st century (Figure 3.2a), which will enhance the insolation during that period. Insolation increases in the latter half of the 21st century; however, it does not reach the pre-1950 values even under the decreasing cloud cover trend during the 21st century. This is because the atmospheric sulfate burden is still above pre-1950 values.

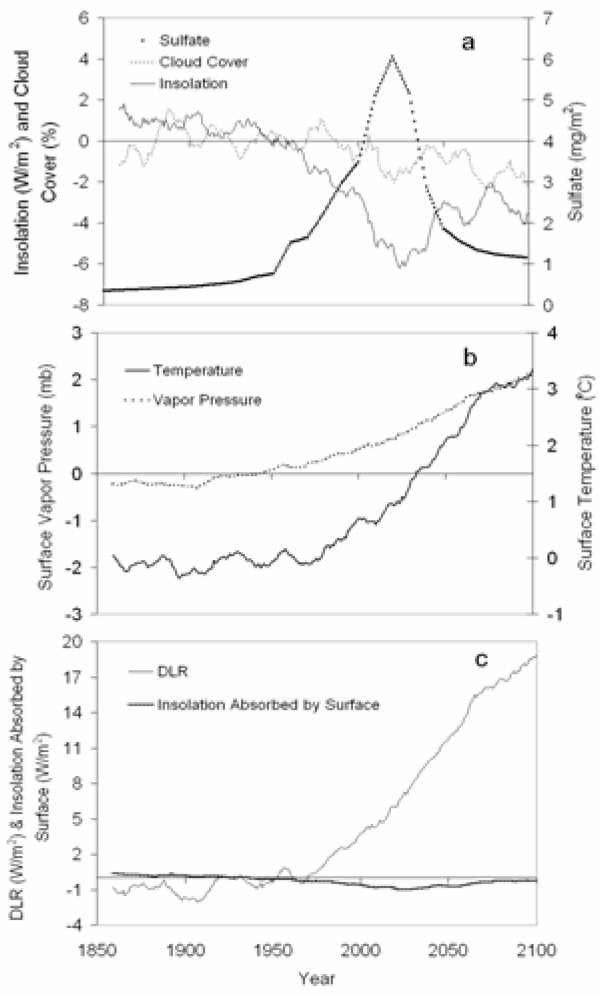

Figure 3.2 Departures in (a) insolation (W/m^2) and cloud cover (%), (b) surface temperature (^{o}C) and vapor pressure (mb), and (c) DLR (W/m^2) and insolation absorbed by the surface (W/m^2) simulated over China from 1850 to 2100. Simulations are 10 year running mean of annual departures from the 1850-1999 mean. Annual mean values of the atmospheric sulfate burden (mg/m^2) shown are based on *Pham et al.* [2005].

In spite of a decrease in surface insolation of 6 W/m^2 (from the 1850-1999 mean) in the first half of the 21st century, followed by a recovery of 2 W/m^2 in the latter half, a continuous increase in surface temperature is simulated for the entire 21st century over China. The 3 ^{o}C temperature increase from 1975-2100 (Figure 3.2b) appears to be related to an increase in DLR of 19 W/m^2 over China for the same time period (r = 0.98; Figure 3.2c), which is significantly greater than the increases in sensible heat (0.6 W/m^2) and latent heat (3.5 W/m^2) fluxes. Our calculation suggests that for a DLR increase of 19 W/m^2 the temperature increases by about 3.8^{o}C, which is slightly higher than the simulated increase in surface temperature (3^{o}C). This difference could be partly due to a concomitant decrease in insolation absorbed by the surface during the 21st century (Figure 3.2c). The partial correlation of the modeled DLR during the 21st century, with atmospheric CO_2 concentration and surface vapor pressure is 0.79 and 0.80.

Modeling experiments [*Hall and Manabe*, 1999] as well as the analysis of observed climate variables [*Rákóczi and Iványi*, 1999-2000] have shown that the water vapor feedback induced by atmospheric warming, which is triggered by an increase in anthropogenic greenhouse gases, is a much more important mechanism in amplifying DLR than the anthropogenic greenhouse gases alone. Moreover, the water vapor feedback is a combination of both the lower and the upper tropospheric water vapor feedback. The midlatitude atmospheric boundary layer over China may not be optically saturated to the longwave radiation from the surface. Therefore, an increase in the lower atmospheric water vapor content can directly increase the infrared heating of the surface. The modeled increase in surface vapor pressure at the end of the 21st century is 15%

higher than the 1850-1950 mean, a period during which there is little change in surface vapor pressure (Figure 3.2b).

Moreover, the modeled increase in vapor pressure during the 21st century is 25% at 500 mb and 80% at 200 mb, which is similar to the results from another GCM simulation performed by *Soden et al.* [2005]. They analyzed satellite measurements of clear-sky radiances, which are sensitive to water vapor concentration in the upper troposphere, to demonstrate moistening of the upper troposphere from 1982-2000. This observed moistening is also in accord with the increase in moistening of the upper troposphere simulated with satellite-observed sea surface temperatures. The outgoing longwave radiation is suggested to be very sensitive to the changes in the upper tropospheric humidity [*Held and Soden*, 2000]. Therefore, the moistening of the mid and upper troposphere can make the troposphere substantially more opaque to outgoing longwave radiation, thereby warming the troposphere as a whole and contributing to warming the surface and the lower troposphere in the 21st century. However, the relative importance of the lower and upper level water vapor feedbacks in increasing the DLR over China could not be quantified from our modeling experiments.

Cloud cover, which can also significantly affect DLR, is decreasing during the 21st century (Figure 3.2a), and is, therefore, not expected to cause the simulated increase in DLR (Figure 3.2c). Comparison of trends in climate variables between the GHG + Sulfate and GHG experiments shows that atmospheric sulfate will tend to suppress the warming until the middle of the 21st century (Figure 3.3a). A smaller increase in surface temperature between 1960 and 2060 in the GHG + Sulfate experiment is accompanied by a smaller increase in surface vapor pressure (Figure 3.3c), and consequently a smaller increase in DLR (Figure 3.3b), in comparison to the GHG experiment. As the difference in surface insolation between the two experiments becomes smaller after 2060, there are smaller differences between the two experiments for temperature, vapor pressure and DLR.

3.3 Discussion

The simulation of climate variables for China from 1950 to 2000 by the GISS-AOM model produces similar trends as observed although the magnitude of the modeled changes is smaller. The observed warming of 1^{o}C from 1950 to 2000 despite a 3.27 W/m^2 per decade decrease in surface insolation appears to be in large part the result of an increase in DLR, which is a consequence of an increase in anthropogenic greenhouse gases and the associated atmospheric water vapor feedbacks. The surface vapor pressure over China increases by 0.40 mb during that period. *Philipona et al.* [2005] suggest that an increase in DLR resulting from an increase in surface vapor pressure, triggered by an increase in anthropogenic greenhouse warming, caused the bulk of surface warming observed in Central Europe from 1995-2002 in spite of a decreasing trend in surface insolation.

For the 21st century, the model predicts a downward trend in surface insolation until the middle of the 21st century forced by the atmospheric sulfate burden, after which it has an upward trend as the atmospheric sulfate burden decreases. The model also predicts a continuous rise in surface temperature and surface vapor pressure during the 21st century. These changes are much greater than for the period from 1850-2000.

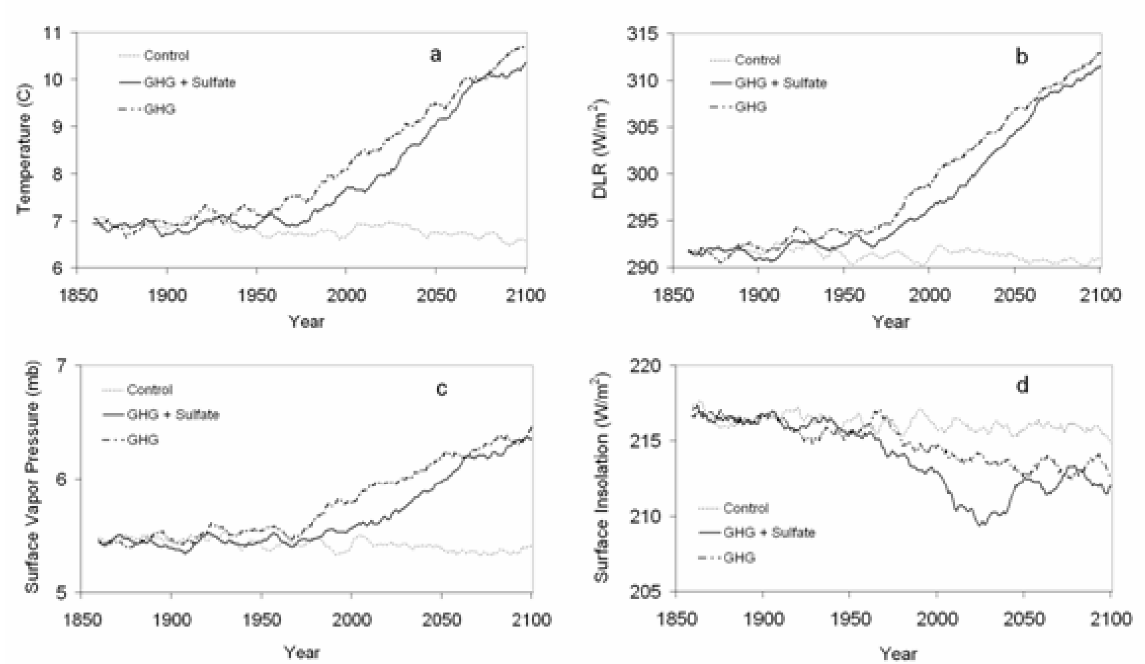

Figure 3.3 Trends in (a) temperature (^{o}C), (b) DLR (W/m^2), (c) surface vapor pressure (mb) and (d) surface insolation (W/m^2) over China from three different model experiments having (1) no greenhouse and sulfate aerosol forcings (Control), (2) greenhouse forcing only (GHG) and (3) both greenhouse and sulfate aerosol forcings (GHG + Sulfate). Line plots are 10 year running mean. Outputs from the GHG experiment were corrected for the offset over the whole period.

Surface warming in China during the 21st century despite the decreasing trend in surface insolation, is caused by a combination of changes in energy budgets near the surface and in the upper atmosphere. Near the surface, an increase in surface vapor pressure, triggered by an increase in anthropogenic greenhouse gases, leads to increased infrared heating of the surface. In the upper troposphere, a decrease in the outgoing longwave radiation, due to an increase in greenhouse gases and the associated upper-troposphere water vapor feedback, would produce a general warming of the troposphere which will be transmitted to the surface. The outgoing longwave radiation at the top of the atmosphere is highly sensitive to changes in upper tropospheric humidity and the observations suggest that the latter has increased in the past two decades in accord with the predictions made by most GCMs [*Soden et al.*, 2005].

The model insolation decreases between 1950-2000 are 4-5 times less than the observed decreases in insolation. Among other possibilities, the smaller decreases in model insolation suggest that either black and organic carbon aerosols and dust have a greater role to play in the observed solar dimming over China than sulfate aerosols alone [Chameides *et al*., 1999; Qian *et al*., 2003], or the model insolation has lower sensitivity to changes in sulfate aerosols. Menon *et al.* [2002] were able to simulate the observed summer cooling trend in southeast China only through the inclusion of black carbon aerosols in their model in addition to the non-absorbing aerosols. Exclusion of the indirect aerosol effects as well as the direct radiative effects of black and organic carbon aerosols, and mineral dust in the model are likely to have caused the conservative prediction of the changes in climate variables from 1950-2000. Therefore, the large changes in annual mean insolation, temperature and vapor pressure at the surface predicted by the model for China in the 21st century, may also be conservative estimates.

Chapter 4: Late 20th and 21st Century Climate Change In The Tibetan Plateau

Evaluating the influences of water vapor, snow cover and atmospheric aerosol in a global climate model

In this chapter, I examine output from the transient experiments of the model used in chapter 3, to (a) compare the modeled and observed patterns of climate change over the Tibetan Plateau in the latter half of the 20th century, (b) examine potential changes through the 21st century and (c) elucidate the mechanisms for these climatic changes. Section 4.1 describes the observed climate change over the plateau between 1950-2000. Section 4.2 describes the results of modeled changes in climate variables between 1950-2100. Influences of changes in humidity and snow cover extent on the pattern of warming, both observed and simulated, are described in sections 4.3 and 4.4, respectively. Section 4.5 examines the mechanisms for an elevation dependent warming (EDW) over the plateau and section 4.6 provides a brief discussion.

4.1 Observed climate change between 1950-2000

Observations from the 43 stations within the plateau region describe a warming trend of 0.24°C/decade for the 1961-2000 period. Since we have specific humidity observations at only these 43 stations, we first compare the annual temperature trends based on these stations with those of the larger dataset of *Liu and Chen* [2000] to verify if these 43 stations are representative of the larger dataset. Figure 4.1a shows that elevation based annual warming trends between 1961-1990 based on the 43 stations are similar to the trends reported by *Liu and Chen* [2000] for the same time period, however the rates of warming calculated in their study are slightly lower. Their lower warming rates may be partly due to their inclusion of more lower elevation stations to the east of our study area where the warming rates are lower.

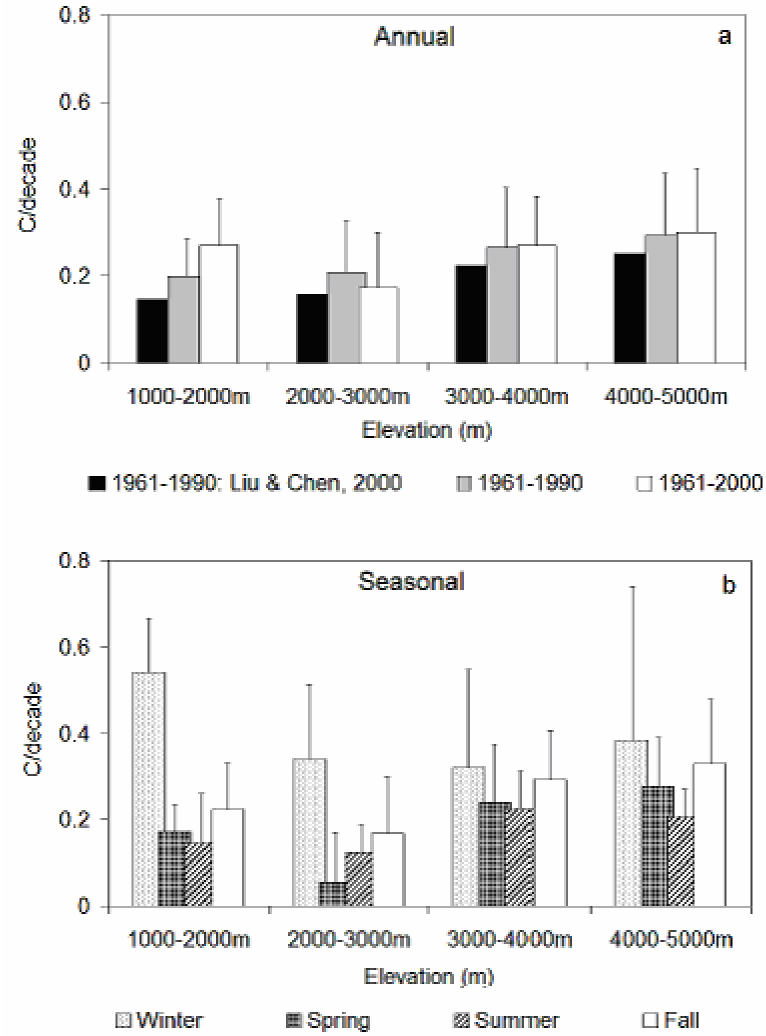

Figure 4.1 (a) Elevation based trends in the annual temperatures (C/decade) over the Tibetan Plateau. Annual trends are plotted for two different time periods – 1961-1990 and 1961-2000. Annual trends for the 1961-1990 period from *Liu and Chen* [2000] are shown for comparison. The corresponding number of stations at different elevation ranges between our study and *Liu and Chen* [2000] are 13-42 (1000-2000m), 9-22 (2000-3000m), 13-32 (3000-4000m) and 7-5 (4000-5000m), respectively. **(b)** Seasonal temperature trends based on the observations in this study for the 1961-2000 period. The error bars represent standard deviations.

Figure 4.1b shows that for the 1961-2000 period, winter, followed by fall, has warmed most rapidly at all elevations. Spring and summer months, which show significantly lower warming rates in the region during the 1961-1990 period, demonstrate greater increases in temperatures when the 1961-2000 period is considered. A rapid increase in spring warming and a slackening in the rate of winter warming appear to have occurred during the last decade of the 20^{th} century. Figure 4.1a also shows an elevation dependent warming (EDW) in the region based on the 43 stations as suggested by *Liu and Chen* [2000] for the 1961-1990 period. However, when we include the last decade (1991-2000), the EDW trends become weaker.

For the 1961-2000 period, Figure 4.2a shows the largest temperature increases during winter. Figures 4.2b-c indicate that daily minimum temperatures over the plateau have increased much more rapidly than the daily maximum temperatures in all seasons and at all elevations except at the lowest elevation during fall. There are also similar increases in maximum temperatures during winter, summer and fall, whereas winter has the largest increases in minimum temperatures. At the highest elevations, maximum temperatures increase most in summer. At lower elevations, the largest increases occur in winter and fall. There are statistically insignificant decreasing trend (about –0.1% sky cover per decade) in cloud cover during all seasons and these decreases are largest at 4000-5300m during winter, spring and summer (Figure 4.2d). Figures 4.2e-f show that increases in q are larger at higher elevations during winter and spring, whereas for summer, they are largest at 0-2500m. Similarly, Figures 4.2g-h indicate large increases in precipitation over the plateau at higher elevation during winter and spring; however increases in summer precipitation is largest at 0-2500m.

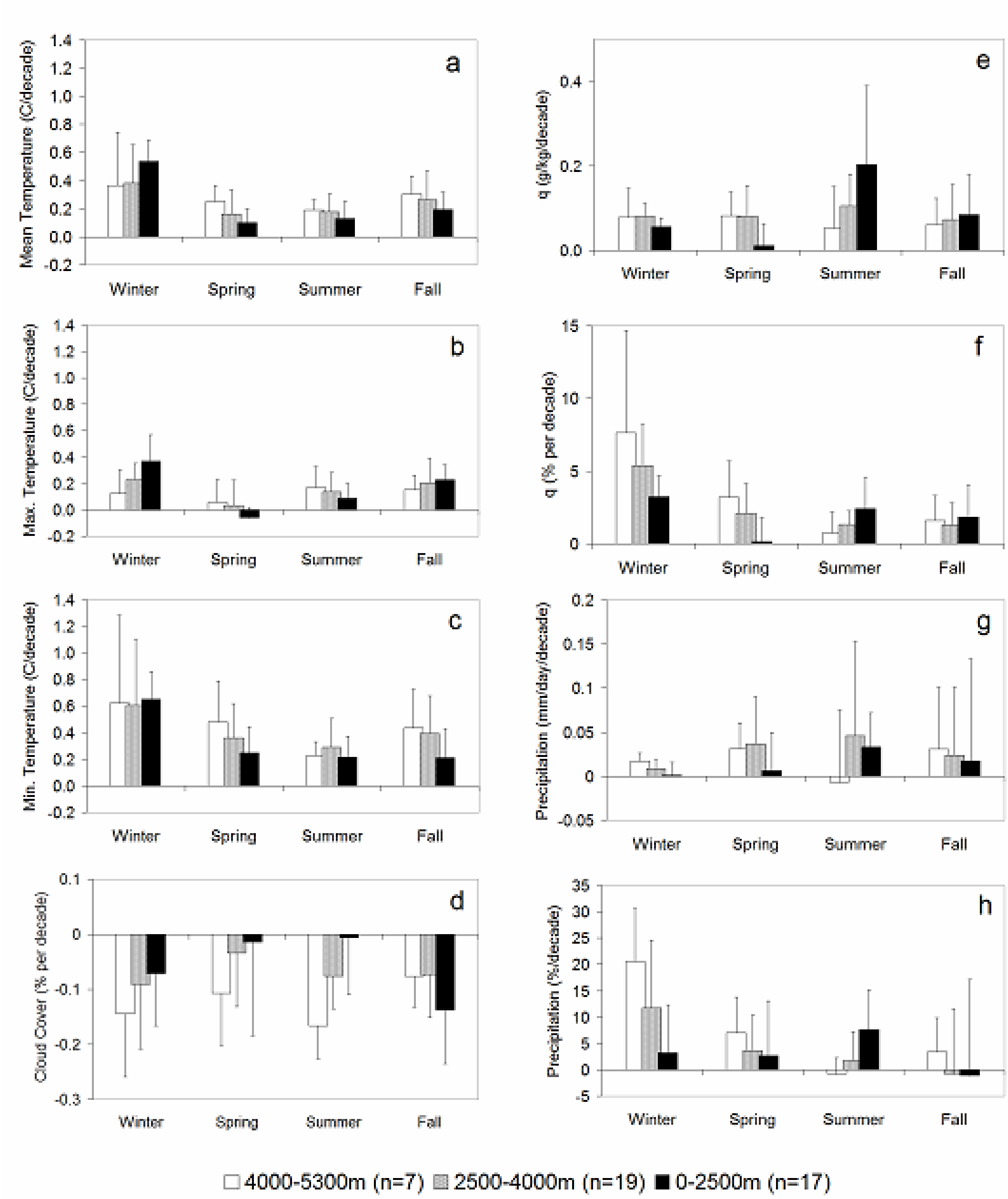

Figure 4.2 Seasonal changes per decade in the observed (a) mean, (b) maximum, and (c) minimum temperature (^oC), (d) cloud cover (%), (e) specific humidity (g/kg), (f) specific humidity (normalized), (g) precipitation (mm/day) and (h) precipitation (normalized) from 1961 to 2000 at three different elevation regions in the Tibetan Plateau. "n" is the number of observation stations associated with each elevation region. Error bars represent standard deviations.

4.2 Simulated climatic changes over the Plateau between 1950-2100

Figure 4.3a shows that the plateau region warmed by 4°C over the entire period of the simulation. Most of this warming occurred after 1950, and the largest rate of warming

(0.52°C/decade) occurred between 2020 and 2060 at all elevations. For the 1961-2000 period, the simulated surface-warming rate is 0.25°C/decade, which is similar to the observed trend (0.24°C/decade) as described in section 4.1. The observed warming trend for the plateau is greater than the late 20th century warming trend of 0.19°C/decade reported for all of China by *Liu et al.* [2004] and 0.12°C/decade in the model simulation (see section 3).

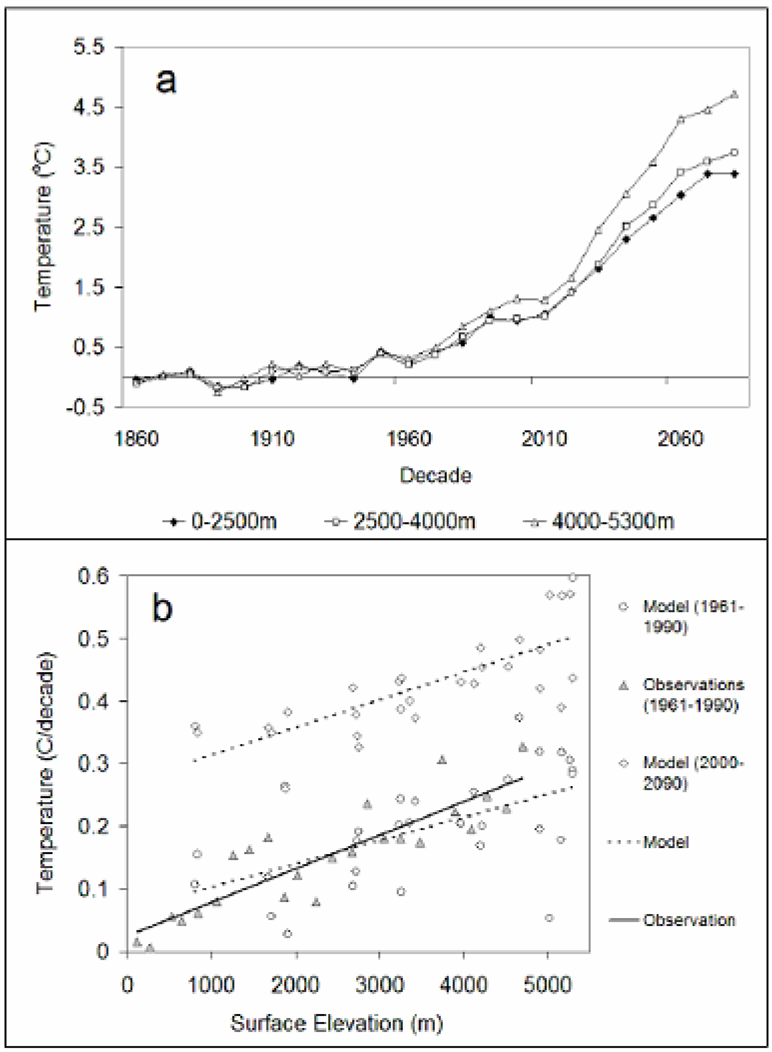

Figure 4.3 (a) Decadally averaged anomalies in surface temperature simulated over the Tibetan Plateau from 1851 to 2100 at three different elevation ranges **(b)** Observed [1961-1990; from *Liu and Chen,* 2000] and modeled (1961-1990 and 2000-2090) trends in surface temperature (C/decade) in the Tibetan Plateau as related to the elevation of the observing station and the model grid, respectively.

Figures 4.4a-b shows spatial pattern of linear trends in observed and modeled temperature over the plateau in the latter half of the 20th century and the 21st century. Figure 4.4a exposes the scarcity of observations on the western side of the plateau, where the mean elevation is higher and the model simulates higher rate of warming during, both, the late 20th and the 21st century. Therefore, the mean observed warming rate of 0.24°C/decade for the 1961-2000 period might be a conservative estimate.

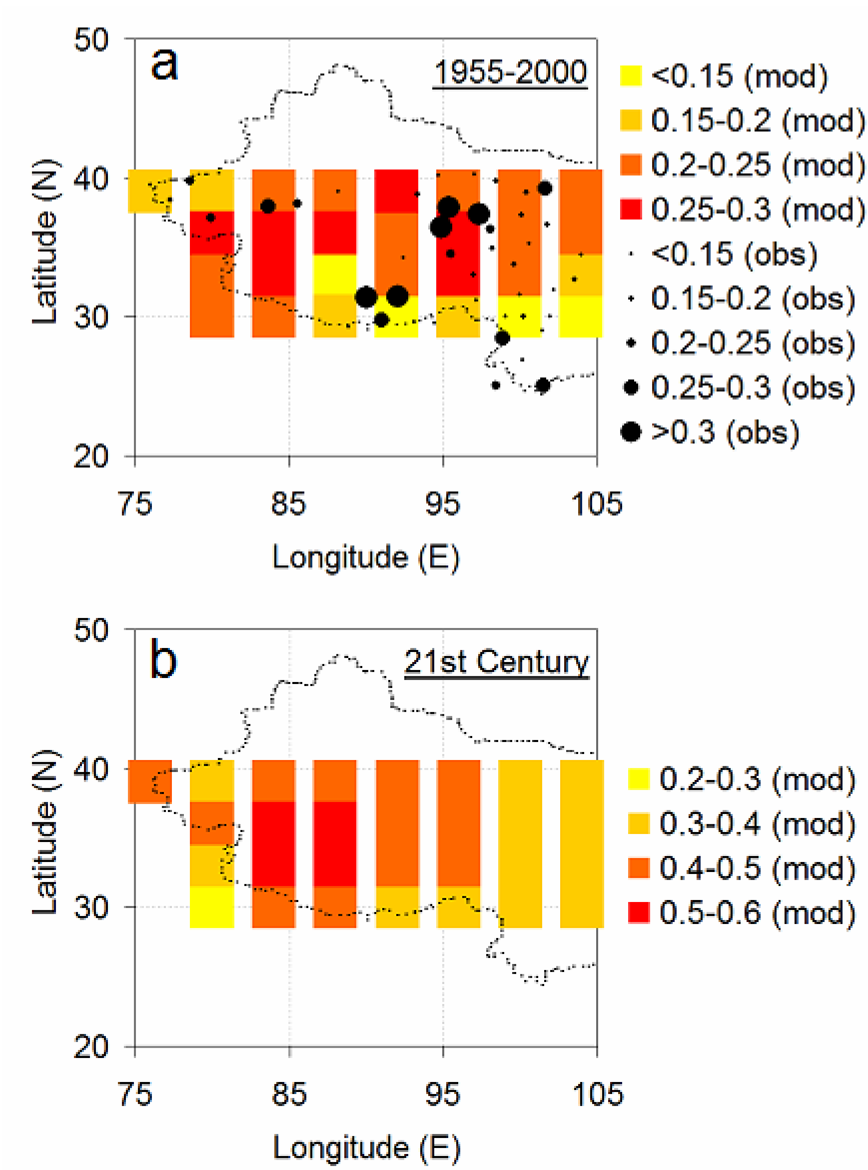

Figure 4.4 (a) Observed and modeled temperature trends (C/decade) over the Tibetan Plateau between 1955-2000. **(b)** Modeled temperature trends during the 21st century. Dark circles describe observed trends and colored squares describe modeled trends.

Moreover, the model experiment demonstrates an EDW trend over the Tibetan Plateau between 1951 and 2100. Figure 4.3a shows increases in surface temperatures by 5, 4 and 3.5°C between 1950 and 2100 from the highest to the lowest elevation ranges, respectively. The EDW trend becomes larger in the latter half of the 21st century. For the 1961-1990 period, the model demonstrates an EDW of 0.037°C/decade/1000m over the plateau which is smaller than the observed trend of 0.054°C/decade/1000m obtained by *Liu and Chen* [2000] as shown in Figure 4.3b. During the 21st century, the model's EDW trend is similar to that observed in the late 20th century. However, there is almost a doubling of the actual warming rate at all elevations during the 21st century (Figure 4.3b).

For the 21st century, the model projects the largest warming during winter and spring months at higher elevations (Figure 4.5a). Moreover, warming during these months started earlier than in summer and fall. Even the lower elevation regions (< 2500m) show a similar seasonal contribution to the warming trend in the model, however the differences amongst the seasonal contributions to the total warming are smaller. Moreover, Figure 4.5a shows that the EDW for the 21st century is significantly greater during winter and spring than it is in summer and fall.

Figure 4.5b shows the modeled change in surface energy budgets during the 21st century. There are large increases in DLR (downward longwave radiation) and ULR (upward longwave radiation) at all elevations and all seasons. However during winter, the increases in DLR are larger than ULR particularly at 4000-5300m. During spring and summer, there are large increases in absorbed solar radiation (ASR) at 4000-5300m and 2500-4000m. At 0-2500m, there are large increases in latent heat fluxes and decreases in sensible heat fluxes during all seasons except spring. There is negligible change in sensible heat fluxes at higher elevations; however latent heat fluxes show large increases during winter and spring at 2500-4000m and during summer at 4000-5300m.

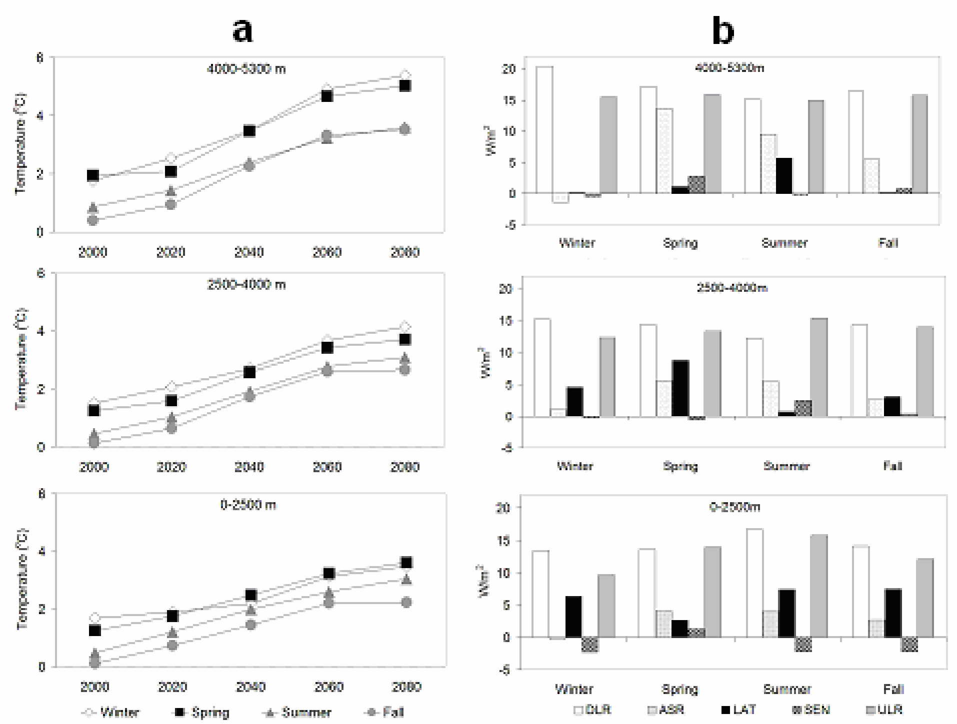

Figure 4.5 (a) Modeled anomalies in the seasonal surface temperature for the 2000-2090 period relative to the pre-industrial conditions, and **(b)** changes in surface energy fluxes between two decades – "2081-2090" minus "2001-2010" – over the Tibetan Plateau at three different elevation ranges. Surface energy fluxes plotted, in order, are DLR (downward longwave radiation), ASR (absorbed solar radiation), LAT (latent heat fluxes), SEN (sensible heat fluxes), and ULR (upward longwave radiation).

In concurrence with elevation dependent increases in temperature (Figure 4.6a) between 1950 and 2100 over the plateau, Figures 4.6 d-g show that there are elevation-based increases in surface vapor pressure, ASR, DLR and latent heat fluxes. Figure 4.6b shows that there is a significant elevation-based decrease in snow cover and that there is a small decreasing trend in cloud cover except at 4000-5300m (Figure 4.6c). The atmospheric sulfate burden increases between 1950-2030 and is followed by a decreasing trend for the rest of the 21st century (Figure 4.6h). The largest increases in sulfate burden occur at the lowest elevations, where the sulfate concentrations are more than three times higher compared to the highest elevations between 1980-2040.

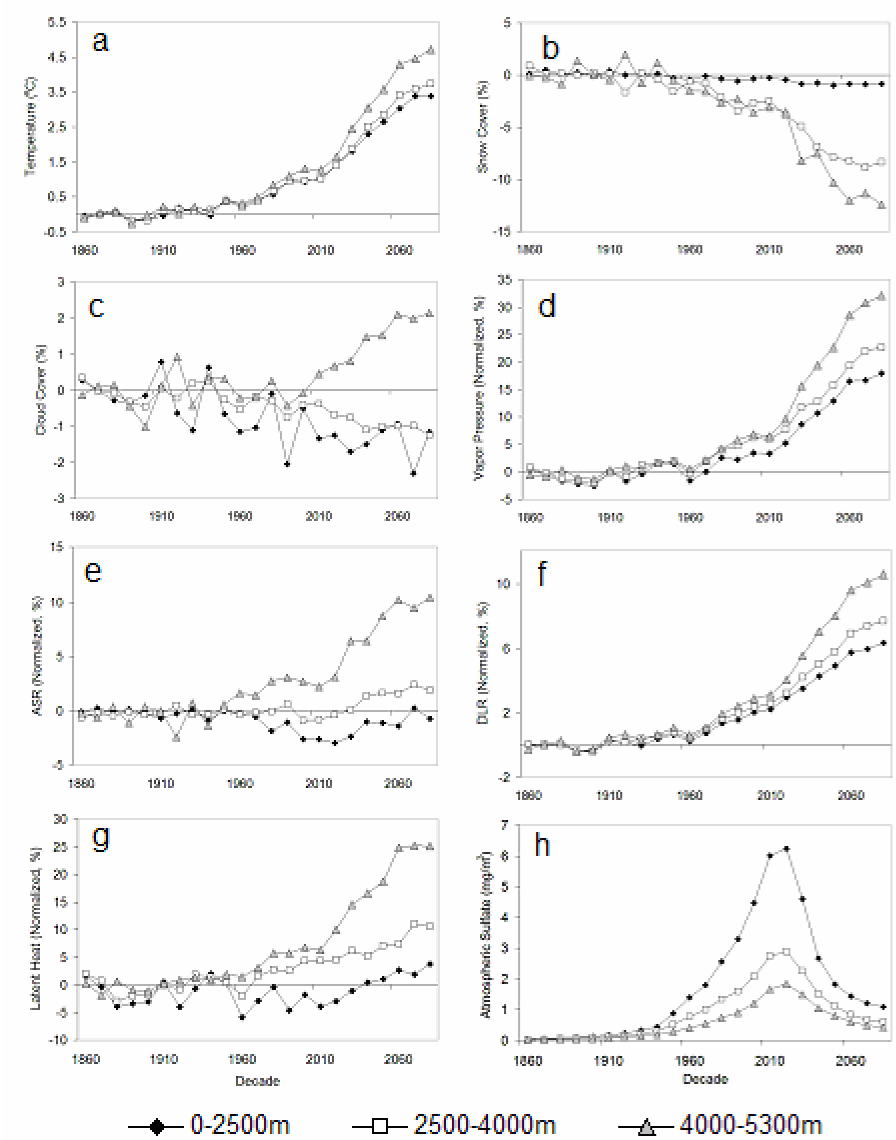

Figure 4.6 Decadally averaged anomalies in the modeled climate variables – (a) temperature (°C), same as Figure 4.3a, (b) snow cover (%), (c) cloud cover (% sky cover), (d) vapor pressure (normalized, %), (e) ASR (normalized, %), (f) DLR (normalized, %), (g) surface latent heat fluxes (normalized, %) and (h) atmospheric sulfate burden (mg/m^2) based on *Boucher and Pham* [2002] *and Pham et al.* [2005] – over the Tibetan Plateau between 1851 to 2100 at three different elevations.

4.3 Effect of surface water vapor on winter warming

Both the observations and model demonstrate a prominent winter warming over the plateau for the 1961-2000 period. The model simulation projects this pattern to continue during the 21st century (Figure 4.5a). Evaluation of surface energy fluxes suggests that greater increases in DLR, relative to ULR, during the winter months at all elevations are associated with a greater warming of the plateau during winter (Figure 4.5b).

Figures 4.6d and f show that the modeled changes in DLR correspond to the changes in surface vapor pressure. Partial correlations indicate that vapor pressure is positively correlated ($r = 0.5 - 0.7$) to DLR at all elevations, though not as strongly as to surface temperature ($r > 0.85$). The large increases in modeled DLR during winter appear to be associated with a greater sensitivity for the atmospheric absorption of longwave radiation at low atmospheric water vapor content which occurs during the cold season. This effect, therefore, also becomes larger at higher elevations. *Ruckstuhl et al.* [2007] present observational evidence from the Alps to support this conclusion. They suggest an enhancement in the absorption of outgoing longwave radiation in the atmospheric window (8-13 μm) at higher elevations where the average atmospheric vapor concentrations are lower. This absorption gain should be greatest during the winter months when the atmospheric water vapor content is lowest over the plateau.

Figure 4.7 shows the modeled relationship between DLR and surface specific humidity (q) for each season and elevation range. The model's power law relationship ($DLR=156.6*q^{0.34}$), obtained using all the data points shown in Figure 4.7, is comparable to the power law relationship of *Ruckstuhl et al.* [2007] for all sky conditions in the Swiss Alps. The model's power law does better in capturing the relationship between DLR and q at higher elevations (2500-5300m), whereas the power law from *Ruckstuhl et al.* [2007] does better at 0-2500m. The model shows a slightly higher sensitivity of DLR to q as compared to the sensitivity from the power law relationship of *Ruckstuhl et al.* [2007]

when q is higher than 0.7 g/kg, e.g., the model sensitivity is 1.6 % higher during winter at 4000-5300m where the average observed q is 1.1 g/kg between 1961-2000.

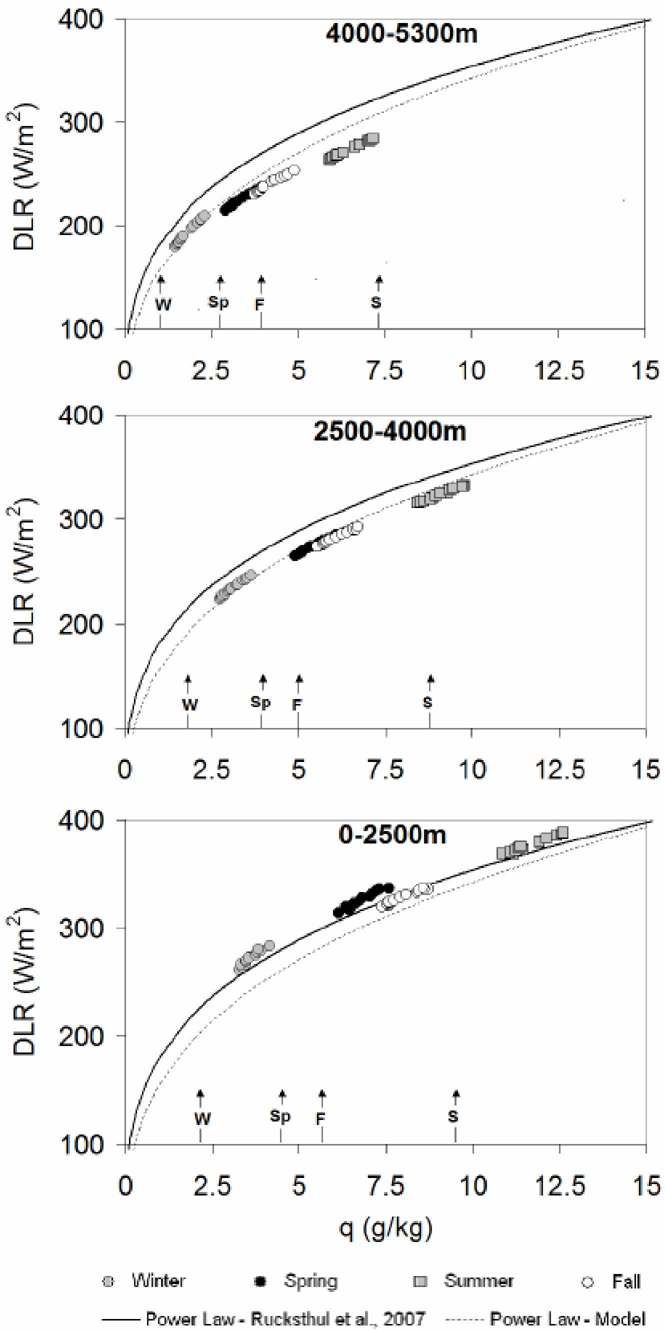

Figure 4.7 Seasonally resolved modeled relationship between DLR and q for three different elevation regions in the Tibetan Plateau. Each point is a decadally averaged value for the period between 1950 and 2100. For each season the points move upward and to the right with time. The power law curves are DLR=181.4*$q^{0.29}$ [*Ruckshtul et al.*, 2007] and DLR=156.6*$q^{0.34}$ (model). The arrows indicate the location of mean values of observed q over the plateau for the 1961-2000 period during winter (W), spring (Sp), summer (S) and fall (F).

Table 4.1 Comparison of sensitivities (λ) of DLR to q between relationships obtained from the model and *Rucksthul et al.* [2007] at different elevations in the Tibetan Plateau. λ ($W.m^{-2}.kg.g^{-1}$) measurements are based on the average values of q ($g.kg^{-1}$) between 1961-2000

Elevation	4000-5300m		2500-4000m		0-2500m	
	λ (model)	λ (Rucksthul et al.)	λ (model)	λ (Rucksthul et al.)	λ (model)	λ (Rucksthul et al.)
Winter	50.5	49.7	38.1	36.7	32.3	30.7
Spring	27.2	25.5	21.8	20.2	19.9	18.3
Summer	14.4	12.9	12.8	11.3	12.0	10.6
Fall	22.2	20.5	18.8	17.1	17.5	15.9

I calculated seasonal increases in DLR over the Tibetan Plateau resulting from the observed increases in q for the 1961-2000 period based on the sensitivity obtained from the power law relationships of *Rucksthul et al*. [2007] and the model as described in Table 4.1. The change in DLR for each season can be calculated as $\Delta DLR = \lambda * \Delta q$, where Δq is the observed change in q from 1961-2000. Figure 4.8 shows similar increases in DLR estimated using both power law relationships. Calculations of ΔDLR based on the estimated λ suggest large increases in DLR during cold seasons at 4000-5300m (15 and 11 W/m^2 for winter and spring, respectively) and 2500-4000m (10 and 7 W/m^2 for winter and spring, respectively) (Figure 4.8). These large increases in DLR during winter and spring months at high altitudes can, in part, facilitate a more prominent warming of the surface during these months, particularly increases in the minimum temperature (Figure 4.2c). For the 21st century, further warming of the atmosphere under the continuing greenhouse gas forcing will increase the atmospheric water vapor content. As the q values during cold seasons are expected to stay in the range that has large sensitivities to DLR during the 21st century, we expect large increments in the absorption and re-emission of longwave radiation in the surface boundary layer. Therefore, for most of the

21st century, we expect a large warming trend in winter at high elevation due to increases in the surface water vapor over the plateau.

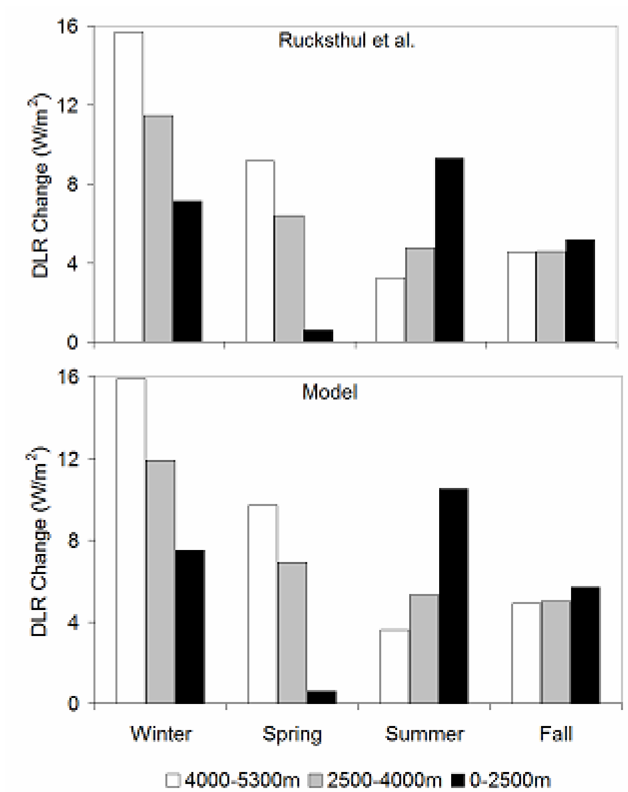

Figure 4.8 Seasonally estimated DLR changes from the observed q changes over the three elevation regions of the Tibetan Plateau for the 1961-2000 period. Estimations of changes in DLR are compared between sensitivities of DLR to q obtained from the power law relationship of *Rucksthul et al.* [2007] (above) and the model (below).

Modeled increases in DLR over the plateau appear to be primarily associated with increases in q between 1950-2100 (Figure 4.9). The changes in DLR and q are strongly correlated, particularly, at the highest elevation ($r > 0.99$). Furthermore, Figure 4.9 shows that smaller increases in q at 4000-5300m are associated with large increases in DLR during the cold season (winter, early spring and late fall). The sensitivity of DLR to q becomes increasingly greater when q is less than 2.5 g/kg. Changes in the modeled cloud cover are small and not correlated with changes in DLR over the plateau, except during winter at 4000-5300m (Figure 4.10). However, even for the latter case, only the partial correlation of DLR to q is significant. Moreover, the observed cloud cover is decreasing between 1961-2000 except at the lowest elevations (Figure 4.5c); the largest decreases are at 4000-5300 during winter and summer months. *Duan and Wu* [2006] suggest increases in the observed low level nocturnal cloud cover over the plateau between 1961-2003, even though the total cloud cover is decreasing during this period. However, there does not appear to be any apparent elevation dependence to this phenomenon in their analysis.

For the 21st century, the largest increase in modeled DLR at higher elevations occurs in winter (Figures 4.5b, 4.8). Wintertime increases in DLR at 4000-5300m are 40% higher than the increases at 0-2500m. These increases will tend to warm the higher elevations more than the lower elevations during winter.

4.4. Effect of snow cover extent on warming in spring and fall

The model, unlike the observations, does not show as large a warming during fall in the plateau (Figure 4.5a). For both the model and observations, fall has a slightly higher water vapor content than spring. Observations show similar increases in q for spring and fall between 1961-2000. Considering similar sensitivities of DLR to q during both spring and fall, the water vapor influences on DLR during fall are not significant enough to cause the larger observed warming of the surface as compared to spring.

Observed increases in the maximum temperature at all elevations during fall are much larger than during spring between 1961 and 2000; the minimum temperature increases are similar for both seasons. We propose that this phenomenon is, in part, associated with changes in snow cover in the region. *Xu et al.* [2007] report a widespread decrease in precipitation over the plateau during the summer months between 1960 and 2000, and significant increases during spring. The latter is consistent with the increases in spring snow depth [*Zhang et al.*, 2004] and cloud cover [*Li et al.*, 2005] over the plateau since the mid-1970s. The observations used in our study suggest that precipitation increases during winter and spring with smaller decreases during fall (low elevation) and summer (high elevation) (Figure 4.2g-h). Therefore, the large increases in the maximum temperature during fall relative to spring in the plateau from 1960-2000 could be, in part, a result of a possible increase in snow cover extent during spring and a reduction during fall. Snow on the ground greatly reduces the absorption of solar radiation at the surface hence suppressing the maximum temperature more than the minimum temperature [e.g. *Leathers et al.*, 1995]. Moreover, comparable increases in the minimum temperatures during these two seasons can be partly explained by similar increases in DLR.

The model simulation shows that the largest increase in maximum and minimum temperatures occurs in spring followed by winter in the latter half of the 20th century. Fall has the smallest increases in both. This pattern is mostly explained by a large decrease in snow cover during spring (2500 – 5300m), summer (> 4000m) and winter (2500-4000m), while fall had the smallest change in snow cover. For the 21st century, Figure 4.11 shows that there are large decreases in snow cover (>10%) at 4000-5300m during spring, fall and summer, and at 2500-4000m during winter and spring. This corresponds with increases in the surface absorption of incoming solar radiation. There is little change in the snow cover at 0-2500m because there is very little annual snowfall associated with these regions in the model.

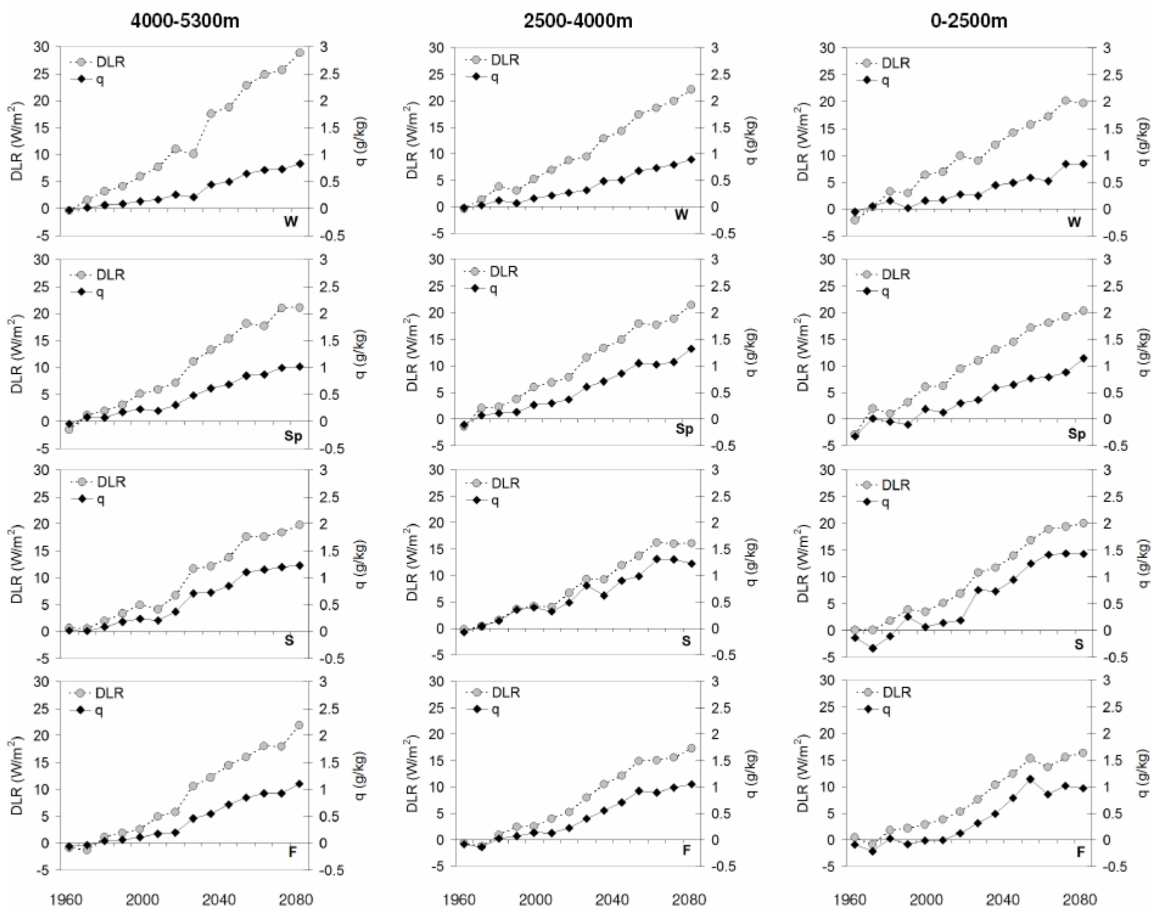

Figure 4.9 Seasonal changes in decadal means with respect to 1950s in DLR (W/m^2; left axis) and q (g/kg; right axis) for each decade between 1960s and 2090s at the three elevation regions in the Tibetan Plateau.

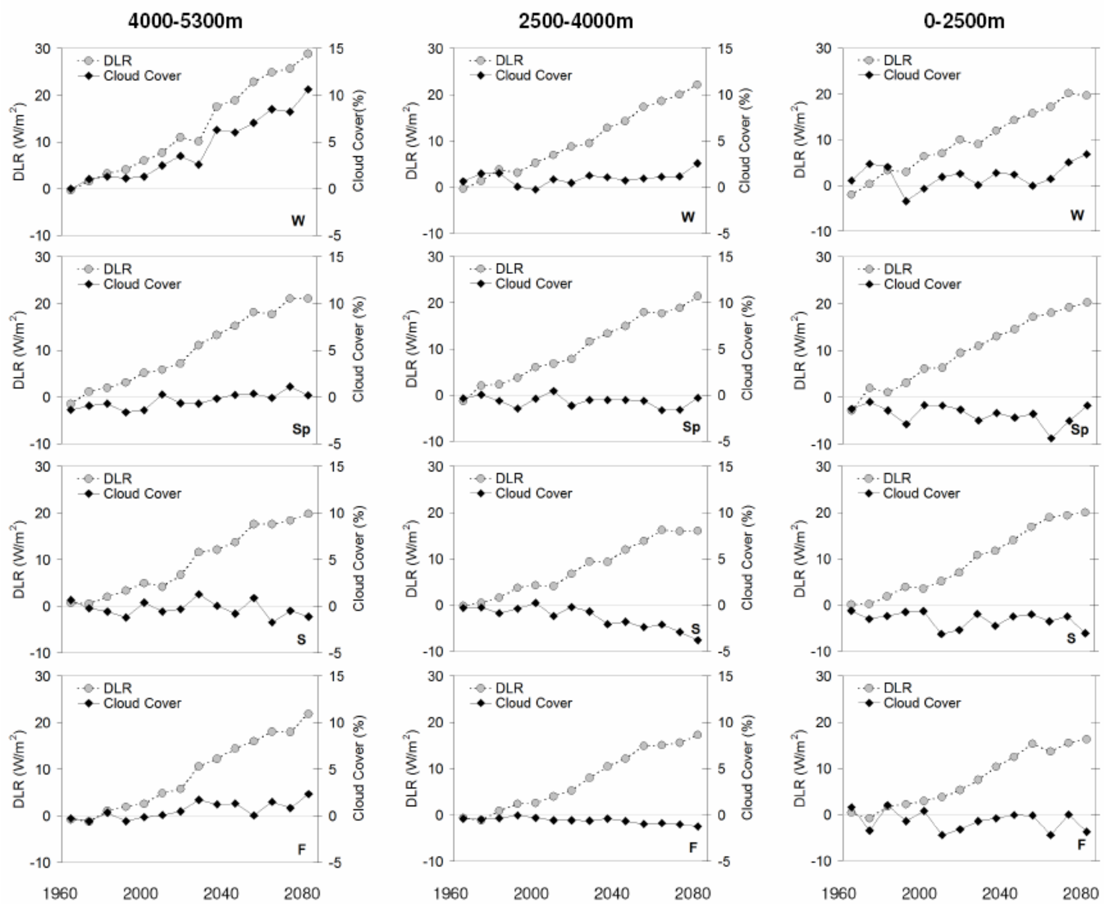

Figure 4.10 Same as Figure 4.9 but for DLR (W/m^2) and cloud cover (%)

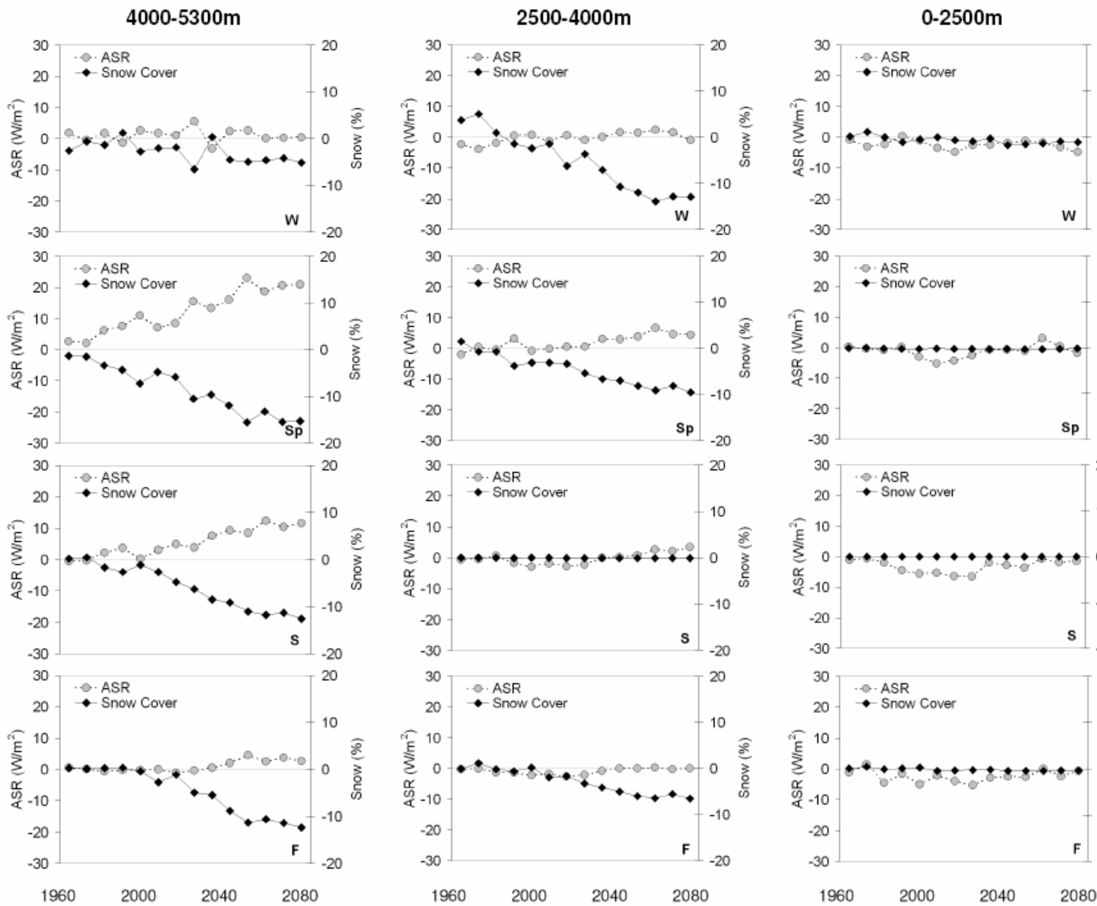

Figure 4.11 Same as Figure 4.9 but for ASR (W/m^2) and snow cover (%)

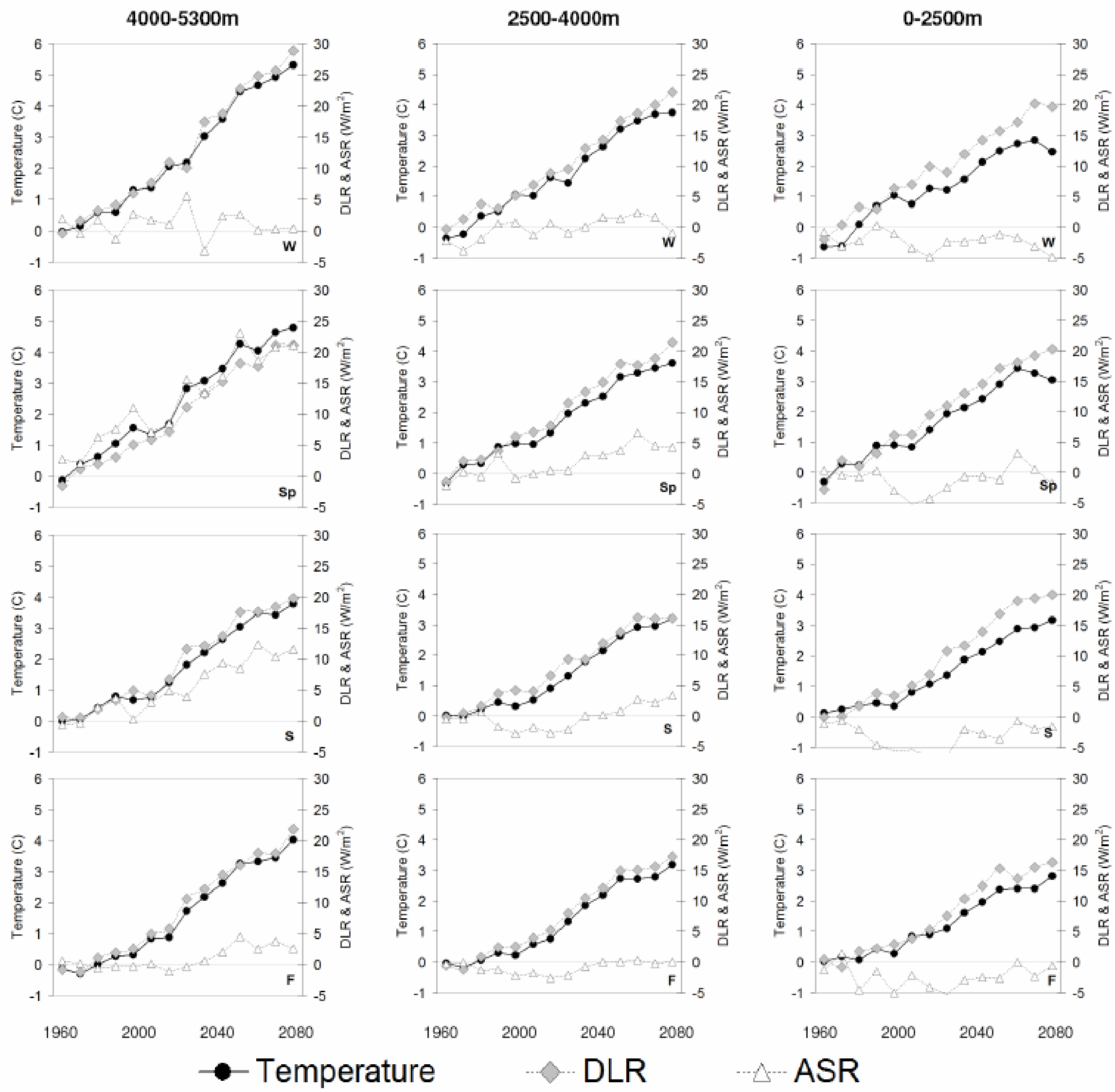

Figure 4.12 Same as Figure 4.9 but for temperature (C), DLR (W/m^2) and ASR (W/m^2)

As the region warms during the 21st century, we expect continuous reduction in snow cover during spring and summer at higher elevation as suggested by the model. This effect would accelerate the surface warming during spring and summer through the mechanism of snow-albedo feedback. It is possible that the last decade of the 20th century is already exhibiting this process when one accounts for a sudden increase in spring and summer temperatures at high elevations as described in section 4.1.

During the 21st century, Figure 4.11 shows that ASR increases significantly more at the highest elevation than at the lower elevations during spring and summer despite a small increasing trend in cloud cover at higher elevations (Figure 4.10). The cloud cover generally decreases at the lower elevations. Therefore, the greater increases in the simulated ASR trends at higher elevations appears to be primarily associated with greater decreases in snow cover at higher elevations (> 2500m) during the 1961-2100 period, whereas the lower elevation regions have little snow cover extent in the model. The elevation-based decreases in snow cover during spring and summer will, therefore, cause larger warming at higher elevations through the snow-albedo feedback mechanism.

4.5 Effect of aerosols on surface warming

Figure 4.11 shows decreases in ASR between 1970 and 2040 in the lower elevations. These decreases are particularly large during summer. Annually, these decreases appear to be associated with increases in the atmospheric aerosol burden between 1970 and 2040 (Figure 4.6h). The trends in the atmospheric sulfate burden over low-elevation regions are at least two times higher than at high-elevation sites, both in past estimates and the projected scenario. Seasonally, the largest aerosol burden occurs during summer.

Moreover, the model projects large increases in the atmospheric sulfate burden until the middle of the 21st century over the low elevation regions in the plateau, particularly during the warm season (May – September), which reduce the net solar radiation at the surface and, hence, the ASR. This factor further intensifies the EDW in the plateau by differentially decreasing the ASR in the lower elevation regions.

The spring and summer temperatures have risen sharply over the plateau in the last decade of the 20th century, and this trend is likely to continue and accelerate during the

21st century under the influence of the global greenhouse warming. A continuous increase in warming during spring and summer in the 21st century will increasingly influence the extent of snow cover in the high elevation regions. Therefore, the EDW phenomenon may intensify, particularly during the early half of the 21st century, due to elevation dependent increases in DLR and ASR as predicted by the model.

4.6 Conclusions

In this chapter, we have used a global climate model to understand the mechanisms for the observed climate change reported over the Tibetan Plateau in the latter half of the 20th century [*Du et al.*, 2004; *Liu and Chen*, 2000; *Niu et al.*, 2004; *Xu et al.*, 2007] and to examine potential climatic changes through the 21st century.

The model simulation generates a 4°C warming between 1951-2100 over the Tibetan Plateau relative to the pre-industrial climate under the SRES A1B scenario. The largest warming rates in the model occur during winter and spring. For the 1961-2000 period, the simulated warming is similar to the observed trend. The model experiment also generates an EDW trend over the plateau between 1951-2100. This trend becomes larger in the latter half of the 21st century. An EDW over the plateau is simulated for all seasons in the model between 1950-2100, however the effect is more significant during winter and spring (Figure 4.12). For the 1961-2000 period, the model's EDW trend is comparable to the observed trend reported by *Liu and Chen* [2000]. Similar to the temperature trend, there are elevation based increases in surface vapor pressure, absorbed solar radiation (ASR), downward longwave radiation (DLR) and latent heat fluxes, and decreases in the snow cover between 1951-2100. The increases in atmospheric sulfate burden, which peak around 2030 and decrease in the latter half of the 21st century, are much larger at lower elevations than at the higher elevations.

The analysis of the model simulation suggests that an accelerated wintertime warming results from large increases in DLR during the winter months. These increases in DLR are sensitive to changes in specific humidity, particularly when the specific humidity is low [*Ruckstuhl et al.*, 2007], which occurs most prominently during the winter months and at high elevations. This mechanism, therefore, tends to cause the largest net increases in DLR at higher elevations during the winter months in the model and consequently appears to cause an EDW in the plateau during winter. This mechanism is also important during spring and fall, although it is not as strong.

Another factor in the warming is the snow albedo effect. There are large increases in ASR at higher elevation, particularly during spring and summer, which can increase the surface temperature. These increases in ASR are largely associated with decreases in snow cover. Previous modeling studies have also suggested that snow-albedo feedback is one of the primary factors in causing an EDW in the high mountain regions [*Chen et al.*, 2003; *Giorgi et al.*, 1997].

Moreover, there is a decreasing trend in ASR in the low elevation region in the early half of the 21st century due to large increases in the atmospheric sulfate burden relative to the high elevation sites. The net effect of changes in snow cover and atmospheric sulfate burden is to produce an elevation dependent increase in ASR during the 21st century. Observations suggest that snow cover over the plateau has not been significantly affected during spring in the latter half of the 20th century. However, as the greenhouse warming continues into the 21st century, the surface warming during spring and summer is likely to accelerate, particularly at higher elevations, due to a continuous reduction in the snow cover.

The analysis suggests that the Tibetan Plateau would experience a large warming ($4^{o}C$) during the 21^{st} century under the SRES A1B scenario. This warming is likely to be more pronounced at the higher elevations in the plateau due to (a) increases in DLR caused by surface humidity increases during cold seasons and (b) increases in ASR caused by decreases in the snow cover extent during spring and summer, and (c) larger aerosol concentrations at lower elevations. The elevation-based changes in surface energy balance affected by changes in surface humidity, snow cover and atmospheric aerosol will also tend to produce an EDW trend over the plateau during the 21^{st} century.

Chapter 5: 20th Century Climate Change In The San Juan Mountains In Southwest Colorado

Investigating long term trends in climate and hydrological variables and explaining the causes for a rapid climate change in the region between 1985-2005

Results from chapter 4 demonstrated the importance of increases in specific humidity in accelerating warming during the cold season in the high altitude region of the Tibetan Plateau during the late 20th century and the 21st century. In this chapter I examine another high altitude region – the San Juan Mountains in southwest Colorado – to determine whether the effects of changes in specific humidity on winter warming are similar. Description of the region is provided in section 2.3 (see also Figure 2.3 for the region's map). Trends in temperature and hydrological variables (precipitation, snow water equivalent, snowdepth and streamflow) in the San Juan Mountain (SJM) region during the 20th century are examined. The available digitized instrumental record is used to investigate interrelationships among these variables in order to understand the mechanisms involved in triggering long- and short-term climate and hydrological changes. Since this region is much smaller than the Tibetan Plateau, the resolution of the global climate model is too coarse to allow a similar analysis of potential climate change through the 21st century.

Section 5.1 describes the temperature trends in the SJM region during the 20th century. Section 5.2 analyzes the effect of changes in surface specific humidity on a winter warming trend during recent decades. Section 5.3 describes the 20th century trends in precipitation, snowdepth and snow water equivalent (SWE) and their relationship with the warming in recent decades. Section 5.4 discusses a long-term streamflow trend and a relationship among precipitation, snowdepth and streamflow in recent decades. Section 5.5 provides a brief discussion.

5.1 Temperature trends in the 20th century

The analysis of surface air temperature in the San Juan Mountain (SJM) region from 1906-2005 suggests an increase in the mean annual temperature by 1^{o}C in the region during the first half of the 20th century (Figure 5.1). There is a gradual cooling of about 0.5^{o}C between 1960 and 1980 which is followed by a recovery to the 1960 level. A period of relatively little trend occurs between 1985 to 1995, which is then followed by a rapid and secular increase in surface temperature by about 1^{o}C between 1996-2005. Overall, it appears that the mean annual surface air temperature in the region has increased by about 2^{o}C over the 100-year period, considered in this study. Moreover temperature trends from the SNOTEL sites in the region also suggest a 1 ^{o}C increase in surface air temperature from 1985-2005; most of this increase happens during the 1996-2005 period which is correlated (r = 0.68) with the NWS temperature trends.

There is less confidence in the temperature trend between 1906-1948 owing to a much smaller number of stations for which the record is digitized during that period. Nonetheless for the 1906-2005 period, when temperature trends are compared between observations collected from all available data and observations from only three stations for which data are available between 1906-1910, there is a strong correlation (r = 0.95) between the two trends (Figure 5.2).

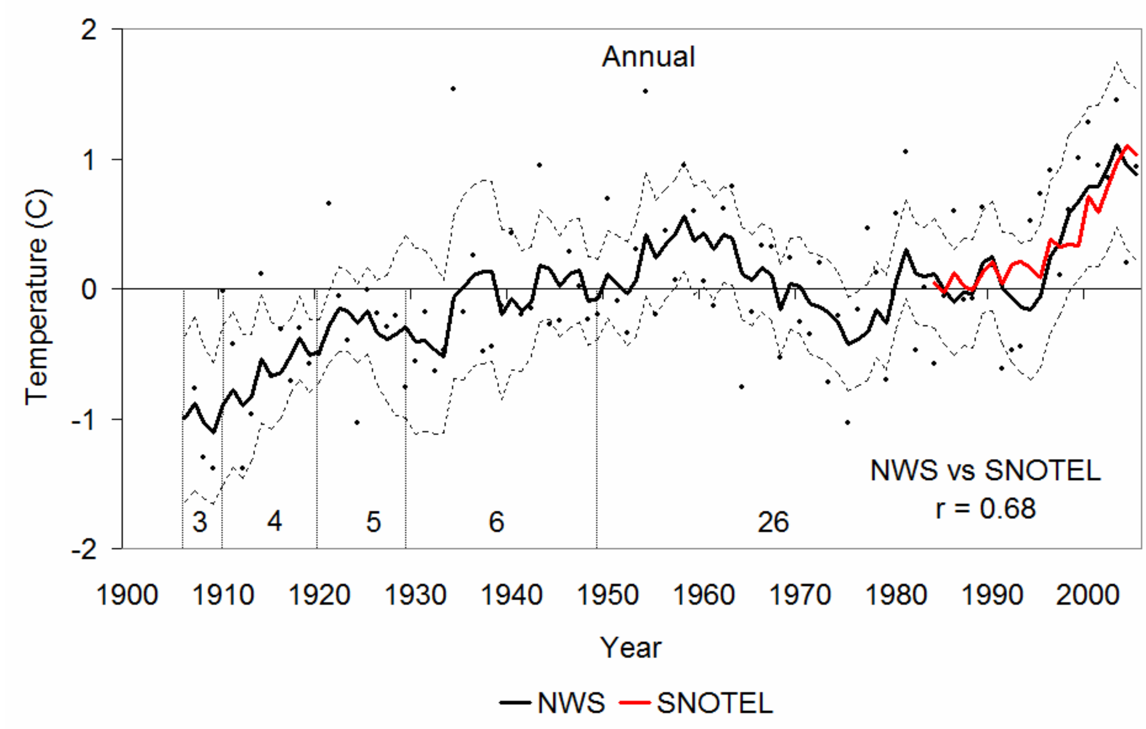

Figure 5.1 Anomalies in the mean annual surface air temperature from 1906-2005 in the San Juan Mountain region. Dark circles describe the absolute value of the anomalies in the surface temperature obtained from the NWS 1st and 2nd order stations. The trend described by the thick dark line is a 5-year running mean of the data. The dashed lines demonstrate the average deviation of data about the mean. The anomalies are calculated against the mean for the 1960-1990 period. The red line shows the trend (5-year running mean) in the surface temperature anomalies from the SNOTEL sites. The numerical values describe the number of weather stations from which the average anomalies were extracted between the time periods marked by the vertical dashed lines.

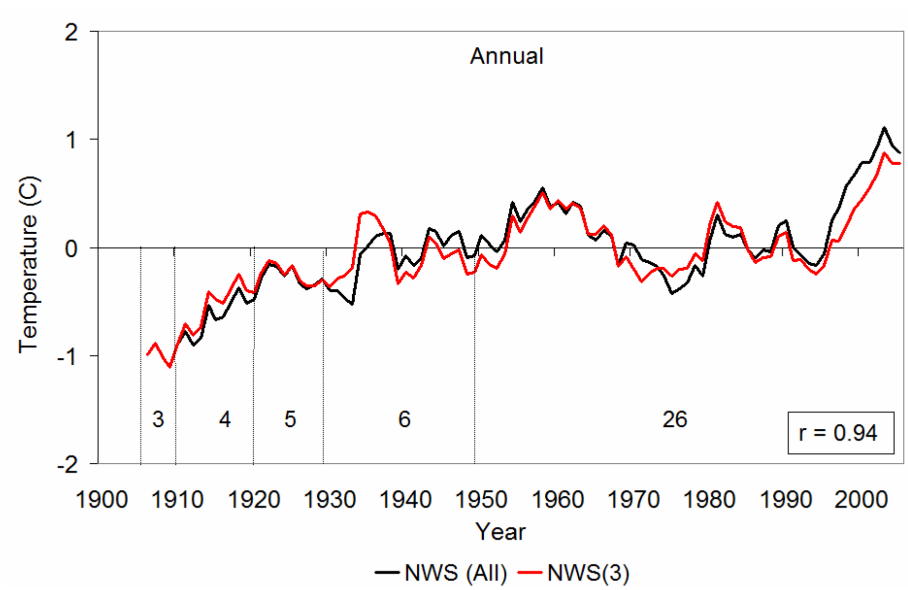

Figure 5.2 Same as Figure 5.1 except that the red curve shows a temperature trend from only the three NWS stations for which there exist a digitized record between 1906-1910.

The trends in annual maximum temperatures are similar to the annual mean temperatures (r = 0.90). These include a gradual warming of 1.5°C between 1906-1940, a weak warming trend between 1940-1960, a cooling of 1°C between 1960-1985, and an abrupt warming of about 1.5°C between 1985-2005 (Figure 5.3). The latter is also observed at the SNOTEL sites (r = 0.71).

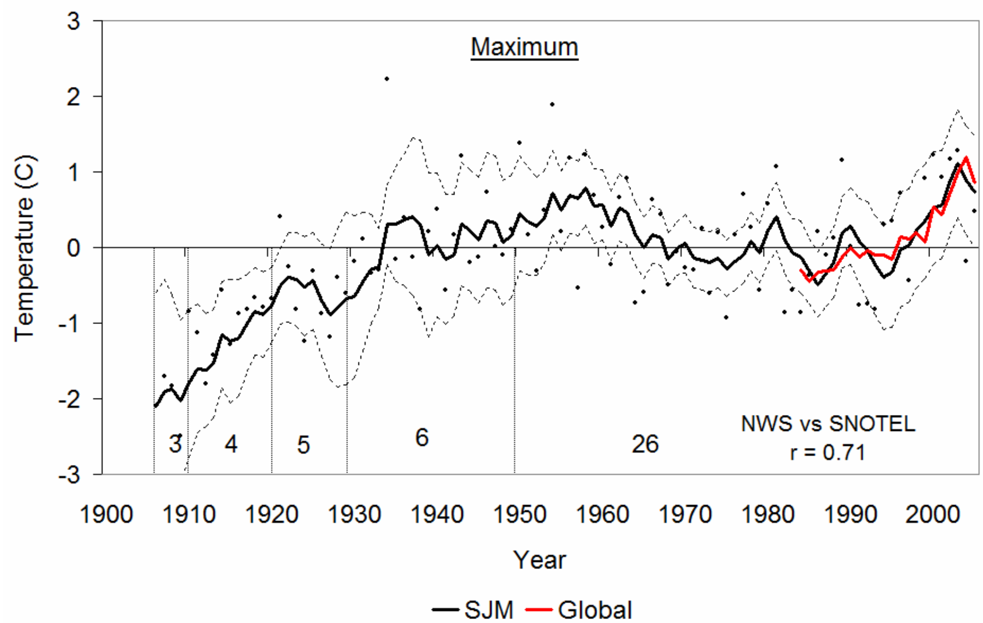

Figure 5.3 Same as Figure 5.1 but for the mean annual maximum temperature.

The annual minimum temperatures in the SJM region show little trend for most of the observational record prior to 1995, except a 0.5°C cooling between 1970 and 1980 (Figure 5.4). A secular warming of 1°C has occurred between 1995-2005, which is similar to the increase observed at the SNOTEL sites (r = 0.73). Unlike SNOTEL trends, the NWS trends show a very high increase in minimum temperature (1°C) within a period of less than 5 years, starting in 1995, followed by near constant temperatures until 2005.

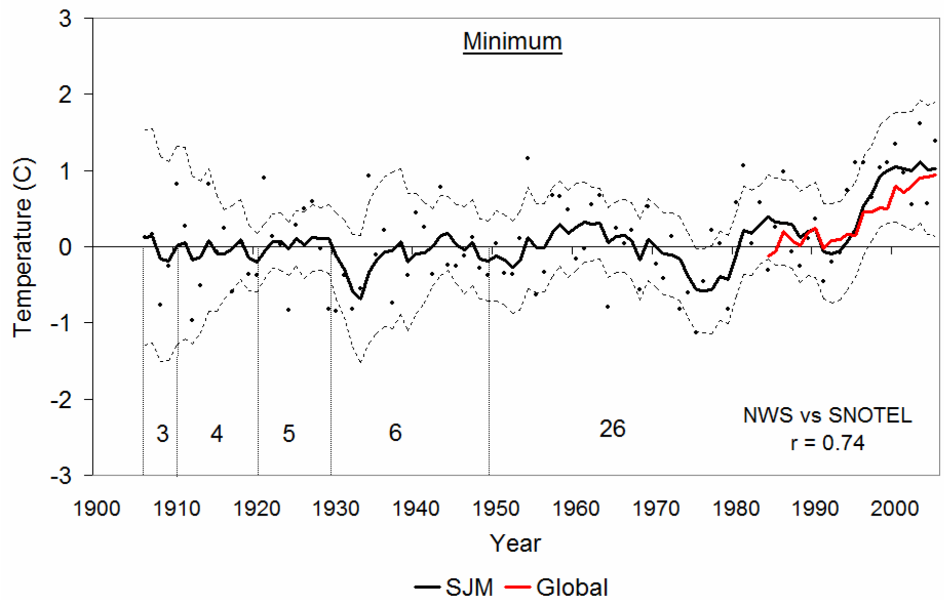

Figure 5.4 Same as Figure 5.1 but for the mean annual minimum temperature.

The trend in annual diurnal temperature range (DTR; maximum - minimum temperature) shows an increase of 2.5°C between 1906 and 1935, no apparent trend between 1935 and 1980, and decrease by at least 0.5°C between 1980 and 2005 (Figure 5.5). The increase in DTR from 1906 to 1935 appears to be due to an increase in maximum temperature. However, the decreases in DTR between 1980 and 2005 appear to be, in part, associated with the increase in the minimum temperature.

Overall, it appears that the climate of the SJM region has warmed by 2°C during the 1906-2005 period. The warming has occurred primarily during the 1906-1940 and 1995-2005 periods. It appears that most of the warming between 1906-1940 is related to increases in the maximum temperature. However, there is less confidence in making this inference owing to a much smaller number of station records for that period and a large variability in data, particularly in the minimum temperature. On the other hand, there is much higher confidence in trends from the most recent decades (1985-2005) owing to a larger number of NWS station records as well as the additional records from the SNOTEL sites in the region.

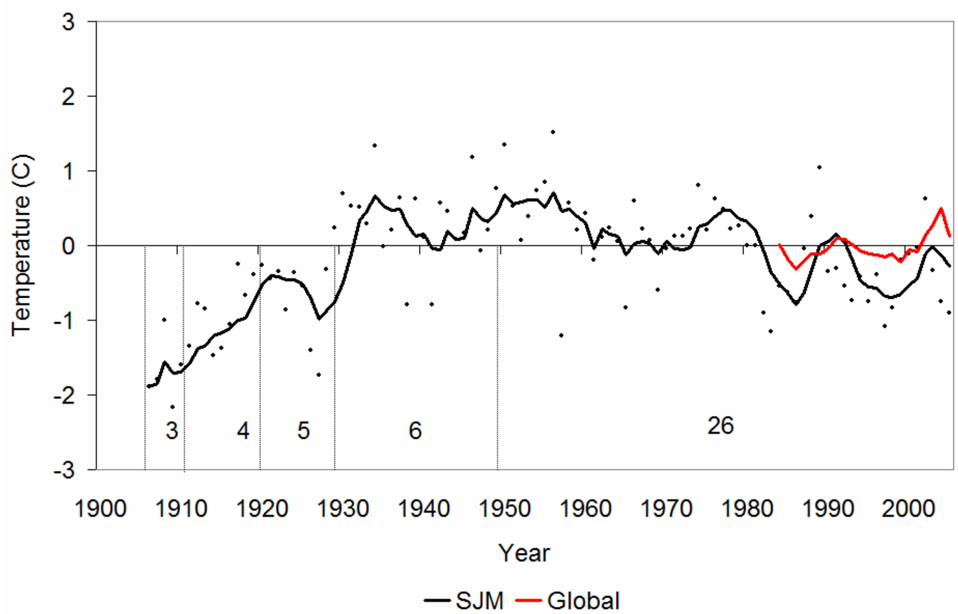

Figure 5.5 Same as Figure 5.1 but for the diurnal temperature range (DTR).

During the 1995-2005 period, increases in the minimum temperature occur earlier, and are slightly greater than the increases in maximum temperature. Table 5.1 shows that temperatures are correlated between the NWS and SNOTEL sites on an annual basis. However, this correlation tends to vary seasonally. For instance, the correlation is much greater between the two sites during spring.

Table 5.1 Correlations (r) of annual and spring temperatures between the NWS (26) and SNOTEL (23) sites.

Temperature	Correlation (r)
Annual (Daily Average)	0.68
Annual (Daily Maximum)	0.71
Annual (Daily Minimum)	0.73
Spring (Daily Average)	0.93
Spring (Daily Maximum)	0.85
Spring (Daily Minimum)	0.93

Figure 5.6 shows trends in daily average, maximum, minimum and seasonal temperatures at both the NWS and SNOTEL sites during the three decades: 1975-1985, 1985-95 and 1995-2005. Comparing warming trends during these three periods, it is apparent that the largest warming occurs during the 1995-2005 period in all the panels in the figure; the exceptions being (a) greater increases in the minimum temperature between 1975-1985 at the NWS sites, (b) similar increases in the summer and spring temperatures during the 1975-1985 and 1995-2005 periods at NWS sites and (c) greater winter warming during the 1985-1995 period at the SNOTEL sites.

Figure 5.7 shows a comparison of annual and seasonal temperature trends between the NWS and SNOTEL sites between 1985-2005, a period for which the SNOTEL data are available. At the NWS sites, mean annual temperature increases by 0.55^{o}C/decade. The increase in the minimum temperature (0.7^{o}C/decade) is greater than the increase in the maximum temperature (0.5^{o}C/decade). On a seasonal basis, winter months experience the largest warming (1.0^{o}C/decade), which is more than two times the warming during spring (0.3^{o}C/decade), summer (0.4^{o}C/decade) and fall (0.55^{o}C/decade). At the SNOTEL sites, where the increases in surface temperatures are overall higher than the NWS sites, there is a similar increase in the average, maximum, minimum, winter and spring temperatures (~0.8^{o}C/decade); the summer increase is higher at 1.0^{o}C/decade and the fall is lower at 0.55^{o}C/decade. Prominent temperature increases at NWS sites occur during winter, and at SNOTEL sites during spring and summer.

Overall, there is a larger warming at the SNOTEL sites as compared to the NWS sites, except during winter. On an annual basis, the SNOTEL sites record about 20% higher warming rates than the NWS sites. During spring and summer, the warming at SNOTEL sites is two times higher than at NWS sites; the warming is similar at both sites during fall. Moreover, the variability in the warming is similar at both sites except during summer and fall when it is slightly lower at NWS sites.

The SNOTEL sites (average elevation = 10,500 ft) are about 2500 ft higher than the NWS sites (average elevation = 7,000 ft) and the former experiences the bulk of snowmelt later in the year than the NWS sites. It is further interesting to note that for the period of 1985-2005, there is higher correlation between the winter and annual trends in temperature for the NWS sites (r = 0.79), and between the spring and annual trends for the SNOTEL sites (r = 0.78). A weak correlation (r = 0.40) exists between the spring and annual trends for the NWS sites for the same time period. Therefore, depending on the elevation of a site, a specific season could be more important in influencing the trend in warming on an annual basis. Moreover during the last few decades, there appears to be a shift in the seasons for which the warming rate was the highest. For example, at the NWS sites, the spring months had significantly higher warming rates for 1975-1985 than winter, however, for 1985-1995 and 1995-2005, the winter months show higher warming rates than spring (Figure 5.6).

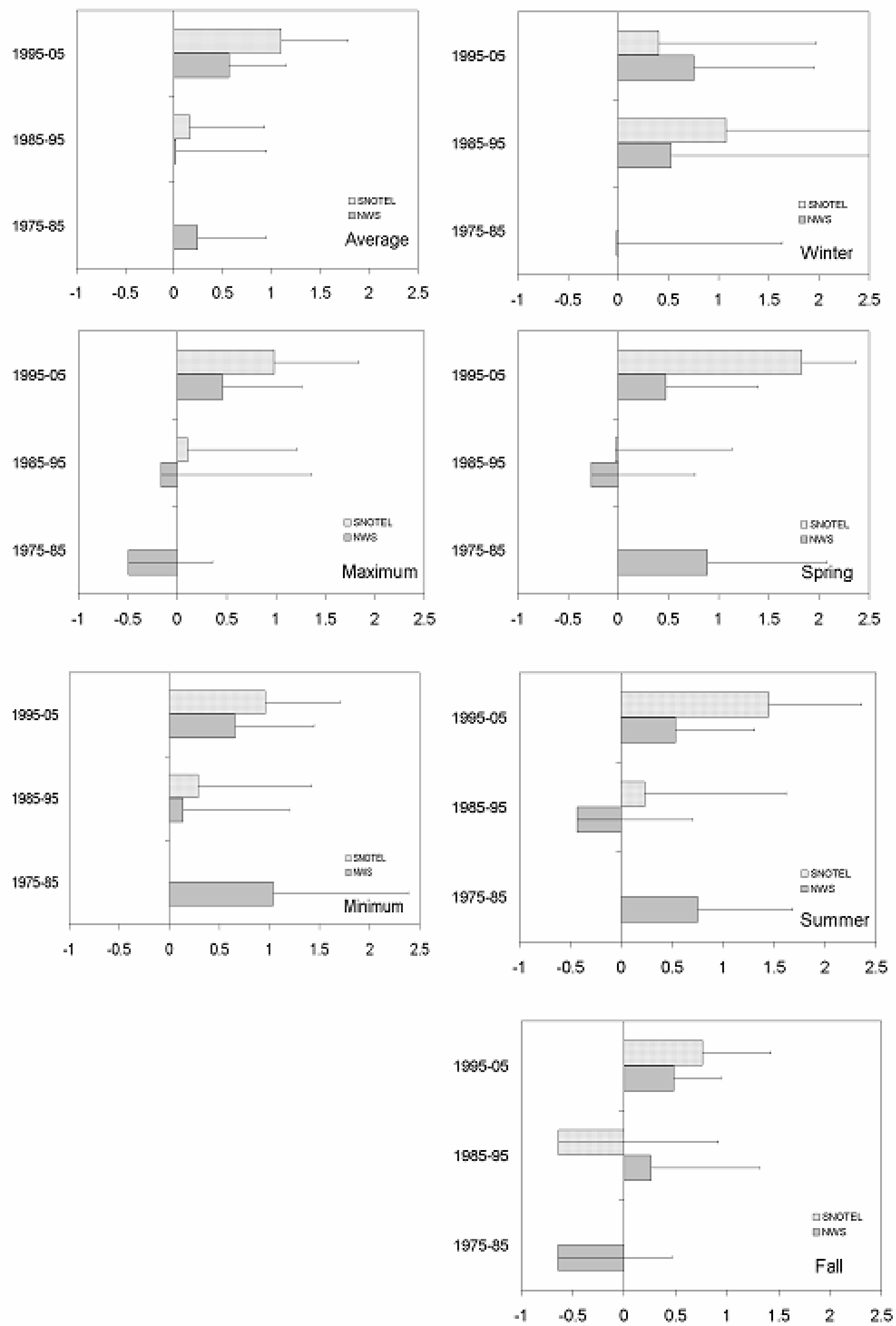

Figure 5.6 Mean trends in daily average, maximum, minimum, winter, spring, summer and fall surface air temperature (C/decade) from three recent decades 1975-85, 1985-95 and 1995-05 in the San Juan Mountain region from both the NWS and SNOTEL observation. Error bars show the standard deviation in the data from the mean.

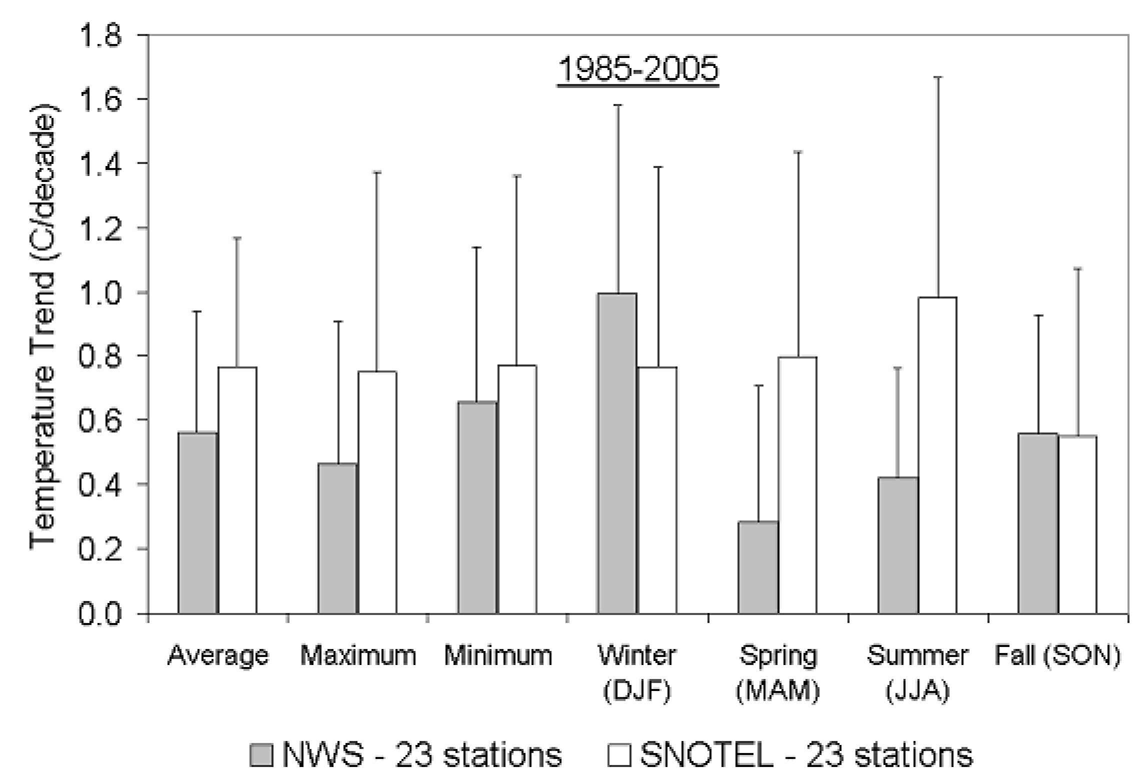

Figure 5.7 Mean trends in daily average, maximum, minimum, winter, spring, summer and fall surface air temperature (C/decade) during the 1985 - 2005 period in the San Juan Mountain region from both the NWS and SNOTEL observations. Error bars show the standard deviation in the data from the mean.

Unlike the maximum temperatures, the minimum temperatures in the region have increased more recently, since 1975. Moreover, it is interesting to find similar increases in the minimum and maximum temperatures at the SNOTEL sites. Review studies of late 20th century climate change at different mountain regions around the world by [*Beniston et al.*, 1997] and [*Diaz and Bradley*, 1997] find that minimum temperatures have increased two times more than maximum temperatures. Therefore, it is possible that at elevations corresponding to the SNOTEL sites in the SJM region there is a greater influence of certain climatic feedbacks, such as the snow-albedo feedback, which tend to increase the maximum temperature more than the minimum temperatures.

Figure 5.8 shows that the general pattern of warming in the SJM region during the 20th century is similar to the pattern observed at the global scale – (i) a gradual warming during the early half of the century, (ii) a mid-century cooling and (iii) a relatively rapid warming in the latter part of the century. In the SJM region, the surface warming is twice that of the global average during the 20^{th} century. The mid century cooling and the late century warming occurred later in the SJM region as compared to the global trend, however the latter occurred much more rapidly.

The SJM region experienced a cooling of about $1^{o}C$ between 1960-1980. A similar change was observed for the maximum temperatures. However, the minimum temperature increased by a few tenths of a degree (~$0.4^{o}C$) from 1955 to 1970, and decreased by more than $0.5^{o}C$ from 1970 to 1980. It is interesting to note that the period from 1950-1980 was predominantly La Niña as well as the cool phase (positive) of PDO (Pacific Decadal Oscillation), both of which are associated with warm and dry winters over the southwestern Colorado [*Edwards and Redmond*, 2005]. However, between 1960 and 1980, the winter temperatures are much lower than the mean for the 1960-1990 period. Overall, the relationship of winter temperatures to ENSO and PDO is unclear for the SJM region from 1950 to 1990, in fact the relationship appears to be just the opposite to the one proposed in *Edwards and Redmond* [2005]. One possible explanation for an increase in the minimum temperature and a decrease in the maximum temperature during the 1960s and 1970s could be related to the "solar dimming" phenomenon during this period, which is thought to be, in part, responsible for a global scale cooling (see Figure 5.8), though mostly restricted to the northern hemisphere, from 1940 to 1980 [*Stanhill and Cohen*, 2001; *Wild et al.*, 2005]. One of the direct effects of particulate pollution in the atmosphere is to reduce incoming solar radiation at the surface, thereby, causing a decrease in daytime heating of the surface and hence affecting the maximum temperature.

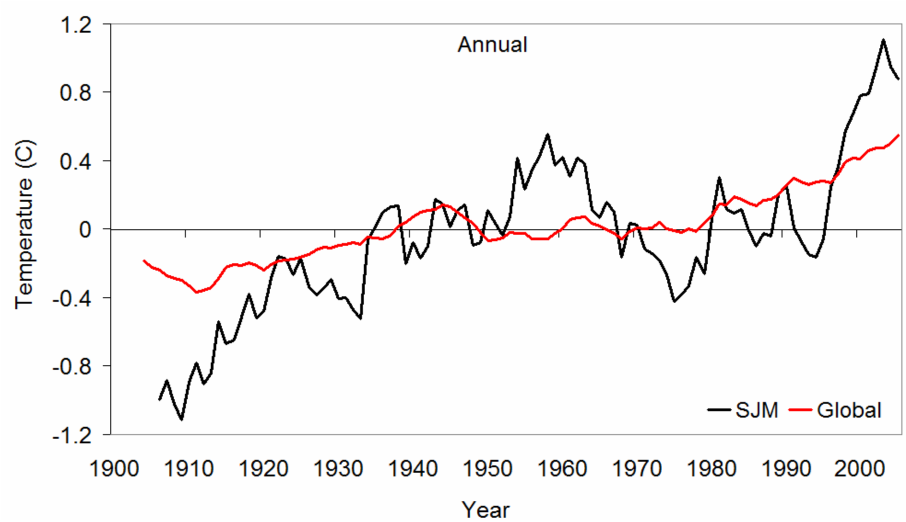

Figure 5.8 Comparison of SJM (all NWS stations) and global (land + ocean) surface air temperature anomalies. Curves are five year running mean. Global temperature anomalies are obtained from the National Climatic Data Center (**http://www.ncdc.noaa.gov/oa/climate/research/anomalies/anomalies.html#anomalies**)

Figure 5.9a provides a comparison of the warming trend in Western Colorado, which includes the study region, to other regions in the US during the recent decades (1985-2005). It appears that the warming in Western Colorado has been one of the highest in the contiguous US during the recent decades, particularly between 2000-2007 as shown by *Redmond* [2007] and *Saunders et al.* [2008] (see also Figure 5.9b) The 1985-2005 warming in the SJM is greater than the trend for Western Colorado. In subsequent sections I examine the causes for this rapid warming in the SJM region, particularly the role of specific humidity on winter warming. Subsequent sections will also examine the trends in snowfall, precipitation, and streamflow in the region and their interrelationships to this rapid warming trend in recent decades.

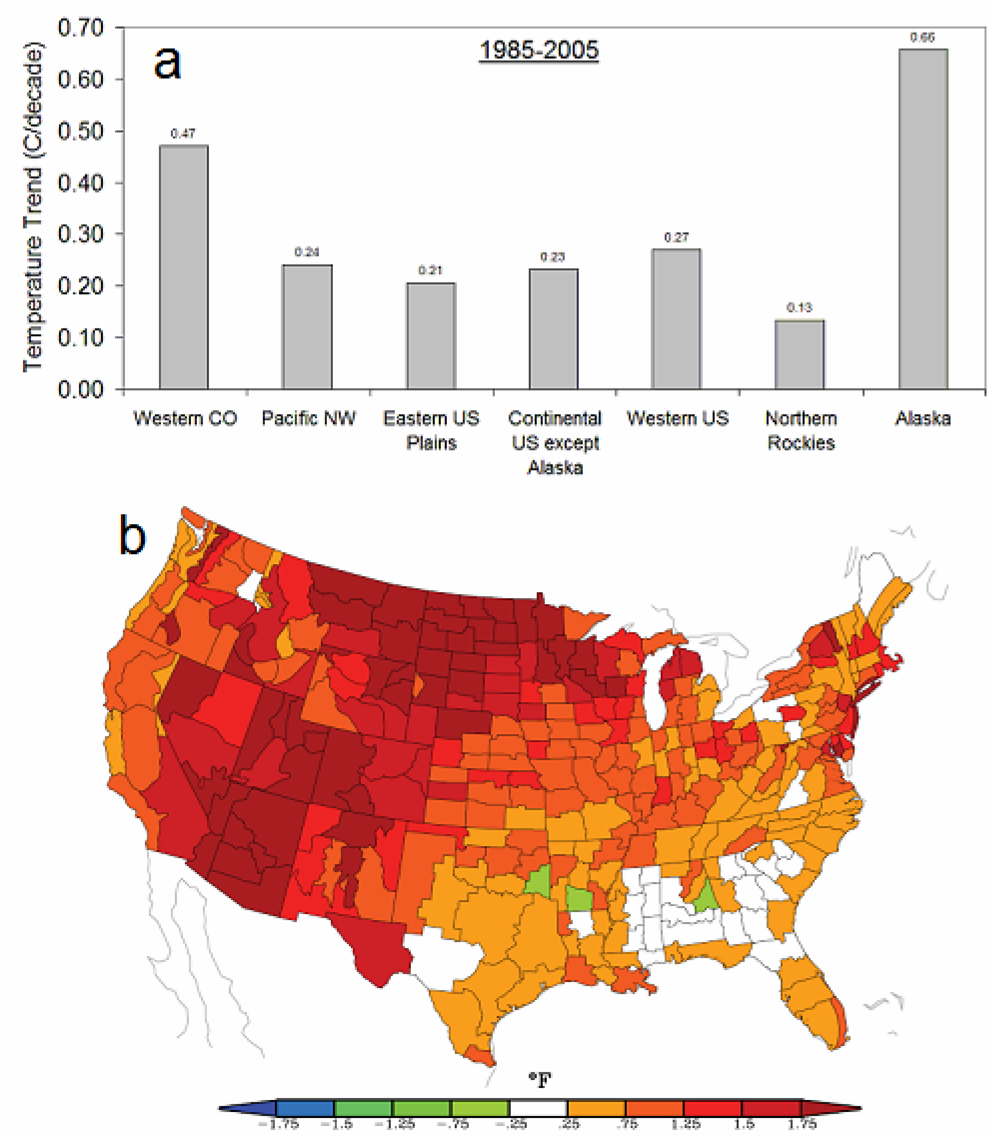

Figure 5.9 (a) Temperature trends (C/decade) across different geographic regions of the US compared to Western Colorado for the 1985-2005 period. Trends are estimated using the 5^{o} x 5^{o} gridded GHCN (Global Historical Climatology Network) land surface dataset provided by NCDC, NOAA. **(b)** Average temperatures in 2000 - 2007 compared to averages for 1901 - 2000. Source: Dr. Martin Hoerling, National Oceanic and Atmospheric Administration (reproduced from *Saunders et al.* [2008])

5.2 Effect of water vapor on the late 20th century warming

In this section I evaluate the effects of changes in specific humidity on the winter warming observed over the SJM region. This analysis is similar to the one done for the Tibetan Plateau in section 4.3. An investigation for any long-term humidity data in the

SJM region did not yield any successful result, not even for any observations during the last 15 years. The only comprehensive network of observations for humidity is available through the Real-time Observation Monitor and Analysis Network (ROMAN; http://raws.wrh.noaa.gov/roman), however it goes back only as far as 1997 and for fewer stations in the region. Moreover, the data are digitized on an hourly basis. Therefore, in absence of finding any long term humidity data from the SJM region I based my analysis on humidity data available from a single station at Gothic, CO, which is situated slightly north of the study region. Comprehensive hourly data from this station are available from 1990 to 2007. Details of the station are provided in section 2.3.

In Figures 5.10-5.12, I have compared monthly trends in the mean, maximum and minimum temperature between the SJM region (both NWS and SNOTEL sites) and the Gothic station between 1990 and 2005. The monthly temperature trends between the SJM region and Gothic are, for the most part, similar in sign and relative proportion of the magnitude on a monthly basis. An obvious cooling during February and significantly large warming during January, May and July are observed at both the SJM region and the Gothic station. Overall, the temperature changes at the Gothic station are similar to those in the SJM region.

The trends at the Gothic station appear to be more similar to the average trends from the SNOTEL sites. This might be partly due to a higher elevation of the Gothic (9,474 ft) station compared to the average elevation of the NWS stations (7,500 ft) in the SJM region. On a monthly basis, there are large differences in the magnitude of warming between NWS and SNOTEL sites (Figure 5.10). SNOTEL sites show higher warming trends during spring (April and May) and summer (June and July) months, whereas NWS stations show a higher warming trend during winter months (November through January). Moreover, at the Gothic station, the minimum temperature (Tmin) increases more than the maximum temperature (Tmax) during winter and the converse is true during spring and summer. A greater increase in Tmax during April and May could be suggestive of significant decreases in snow cover in the region as supported by monthly trends in the snowdepth shown in Figure 5.22. Larger Tmax increases during June and, particularly, July could be a result of decreases in cloud cover, which is supported, in part, by an indirect evidence that the monsoon (July-August) precipitation has been declining since the mid-1980s (Figure 5.25).

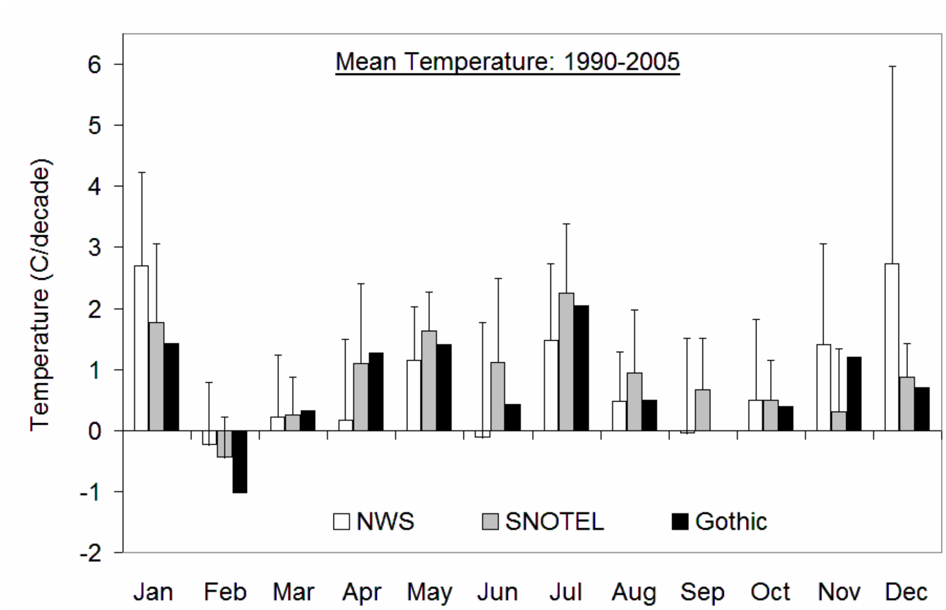

Figure 5.10 Linear trends in the mean temperature (C/decade) at the NWS and SNOTEL sites in the SJM region compared to Gothic, CO from 1990-2005.

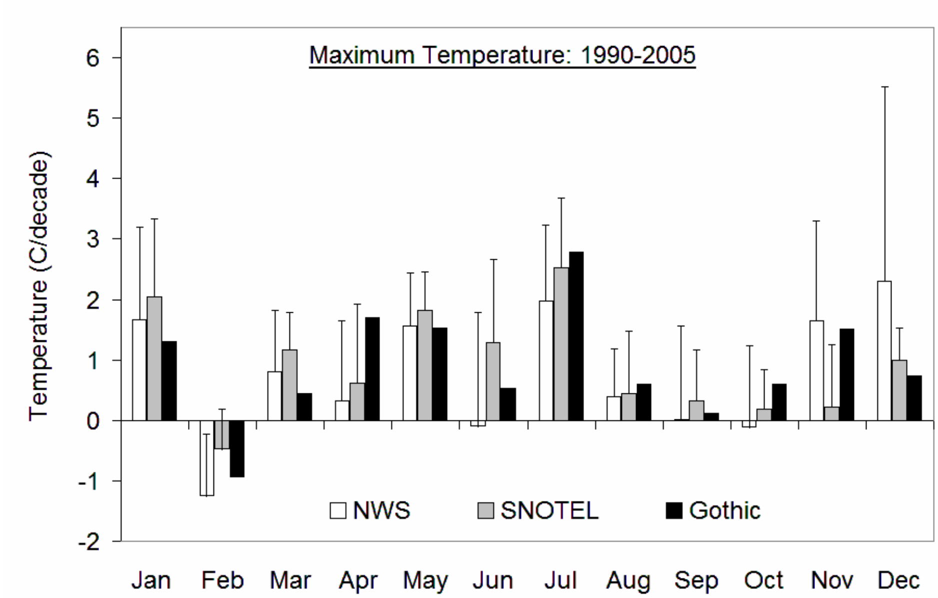

Figure 5.11 Same as Figure 5.10 but for the maximum temperature

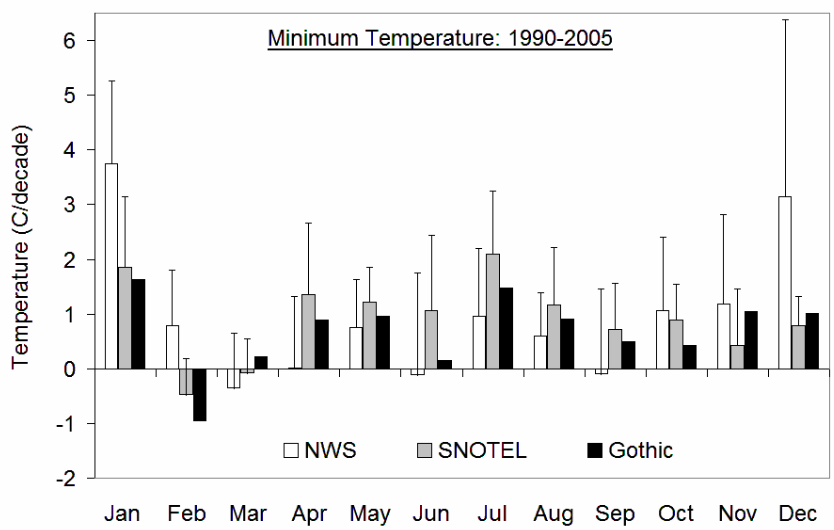

Figure 5.12 Same as Figure 5.10 but for the minimum temperature

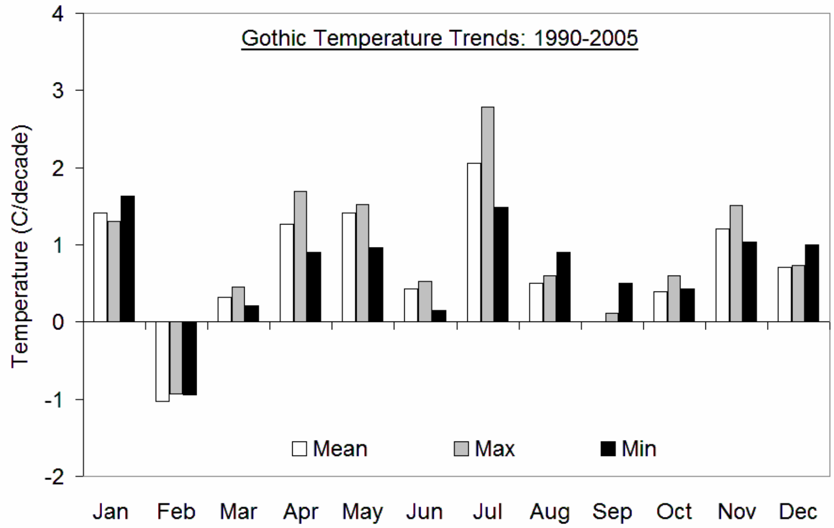

Figure 5.13 Linear trends in the mean, maximum and minimum temperature at Gothic, CO from 1990-2005.

On the other hand, the higher increases in Tmin during winter at Gothic could, in part, be caused by the humidity-downward longwave feedback mechanism discussed in section 4.3 for the Tibetan Plateau. Therefore in this section, I intend to examine the potential effects of increases in humidity on a warming trend during the winter months at Gothic as done for the Tibetan Plateau in section 4.3. Figure 5.14 shows the trends in the mean temperature and specific humidity (q) at Gothic from 1990-2005. Large increases in temperature occur in January, April, May, July and November. On an absolute basis, q increases in all months except September; the largest increases occur in January, June, July and October. However, the normalized increases in q are only obvious during the cold season particularly in January, October, November and December.

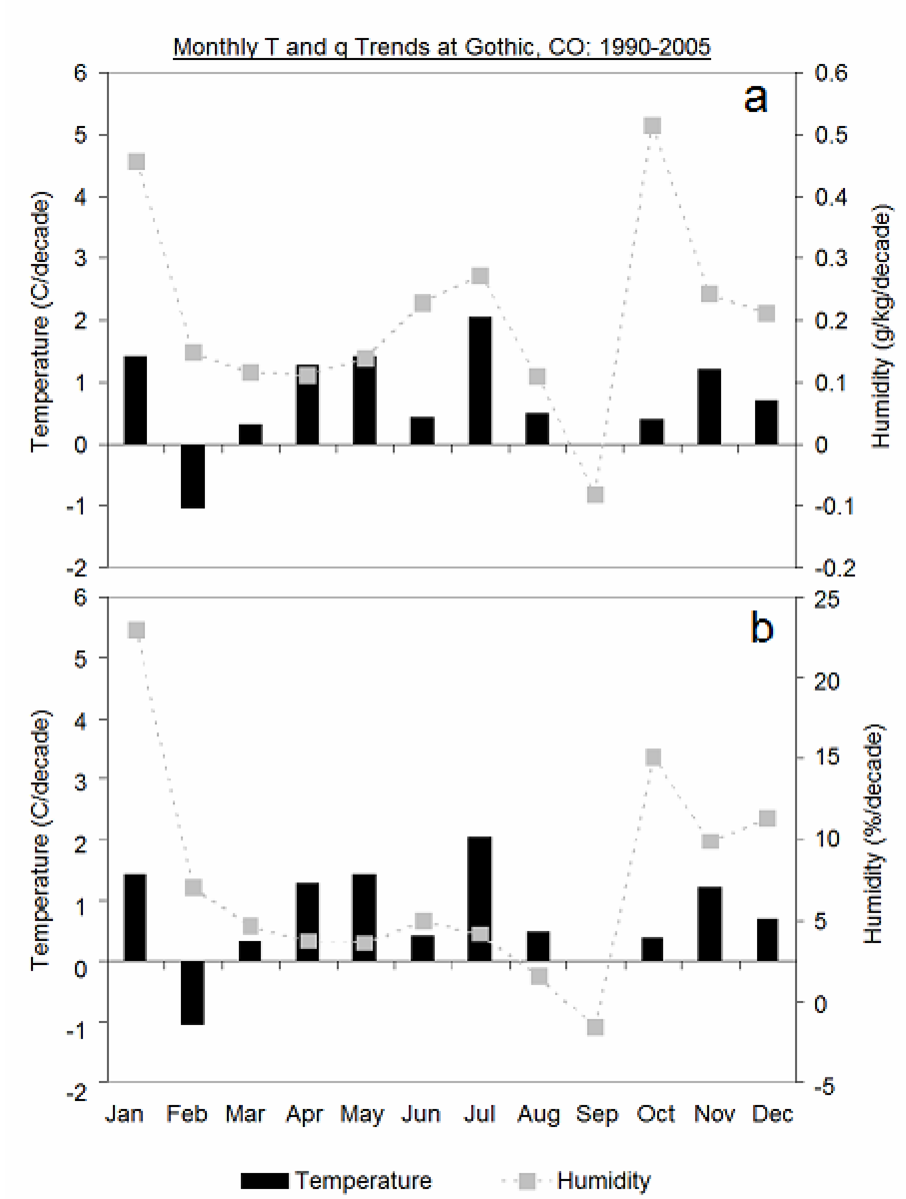

Figure 5.14 Monthly trends in the mean temperature (left axis) and humidity (right axis) at Gothic from 1990 to 2005. Humidity trends are plotted as **(a)** absolute values and **(b)** normalized by mean by respective monthly means for the 1990-2005 period.

Figure 5.15 shows a linear relationship in temperature changes (ΔT) to the changes in q (Δq) between consecutive days at the Gothic station for January, May, July and November using the whole record. The choice of these four months is based on the fact that these months experience the highest warming rate for the season they represent. The figure shows that, during January and November, there is a positive relationship between

ΔT and Δq; Δq tends to explain more than 50% of variability in ΔT. For May and July, there does not appear to be any relationship between ΔT and Δq.

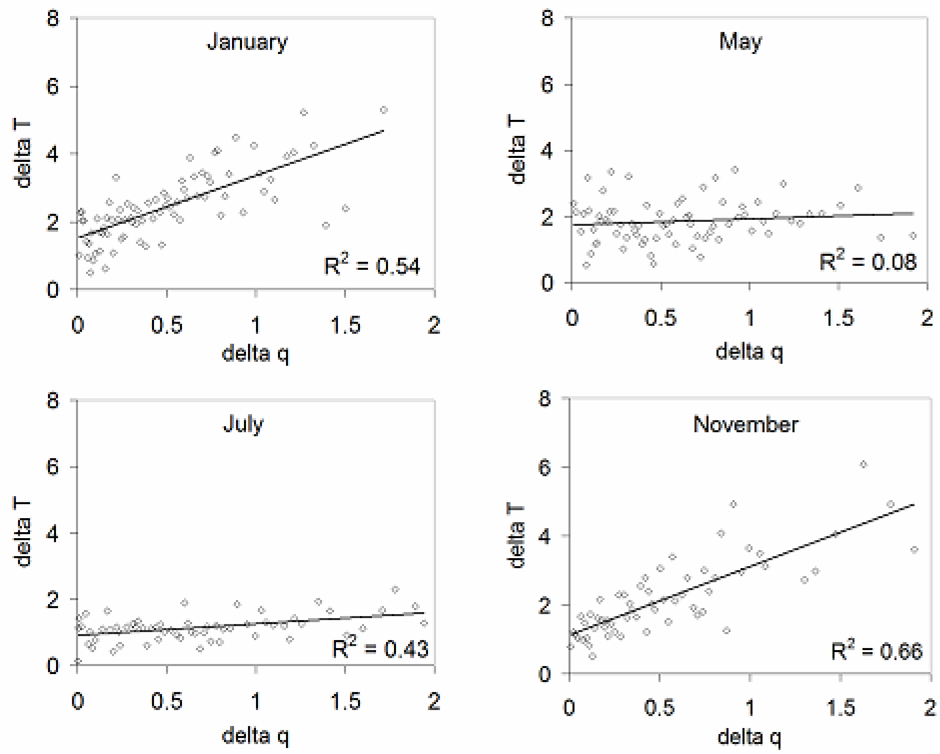

Figure 5.15 Relationship between changes in temperature (delta T) and humidity (delta q) during January, May, July and November at Gothic, CO obtained for the 1990-2007 period. Changes in T and q represent difference between the daily averages of two consecutive days. Each point in figure represents a weekly average of delta T and delta q values.

Moreover, the relationship between ΔT and Δq for February, as shown in Figure 5.16, is similar to January even though February is the only month that has experienced a cooling trend between 1990-2005. Therefore, both Figures 5.15 and 5.16 suggest that increases in temperature at Gothic are sensitive to increases in q during the cold seasons. As discussed in section 4.3, an increase in downward longwave radiation (DLR) is approximately proportional to the logarithm of low-level humidity owing to the distribution of lines of absorption and emission of thermal radiation by water vapor [*Ruckstuhl et al.,* 2007]. Therefore, changes in specific humidity (q) have a greater effect on DLR in cold seasons and higher elevations where the initial q is smaller. Figure 5.17 shows an estimation of the power law relationship between DLR and q for the SJM region based on the observations from two high elevation sites near Silverton, CO – SASP and SBSP (details provided in section 2.3). A slope at any location on the curve describes sensitivity (λ) of DLR to q. As q becomes smaller, the slope, and hence the sensitivity of DLR to changes in q becomes larger. Table 5.3 provides an estimation of monthly values of λ for Gothic. Monthly changes in DLR at the Gothic station based on changes in q between 1990 and 2005 are estimated by using the relationship between DLR and q in Figure 5.17.

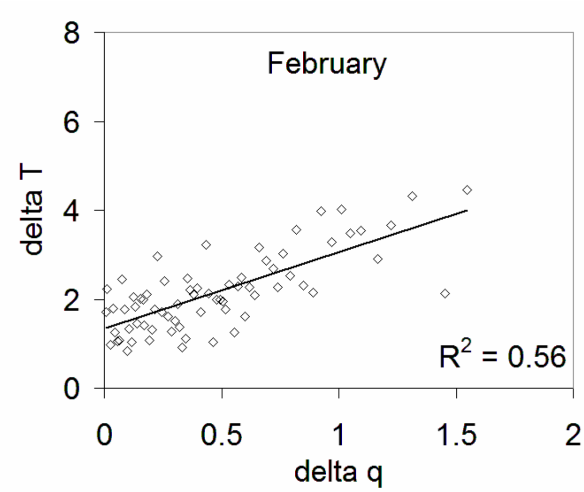

Figure 5.16 Same as Figure 5.15 but for February.

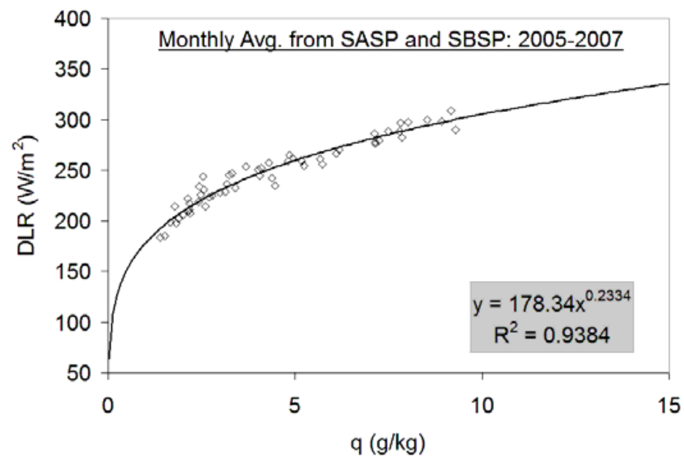

Figure 5.17 Relationship between monthly averaged DLR and q from two high elevation sites in the SJM region from daily observations made between 2005 and 2007.

As discussed in section 4.3, significantly large changes can be expected to occur in DLR over the SJM region owing to changes in q when the latter is less than 2.5 g/kg. Table 5.2 suggests that the period of November through February have large sensitivities of DLR to q. Figure 5.18 shows estimated changes in monthly DLR for Gothic between 1990 and 2005 based on observed changes in q and estimated λ values in Table 5.2. Largest DLR changes tend to occur in January, October, December and November. Large increases in DLR during January and December coincides with large increases in temperatures. Moreover during these months, the minimum temperature (Tmin) increases are greater than the maximum temperature (Tmax) unlike May and July, which also experience large warming trends, when the opposite is true (Tmax > Tmin). The large increases in Tmin during January and December suggest, in part, a greater influence of DLR on the warming trends in the SJM region during the winter months.

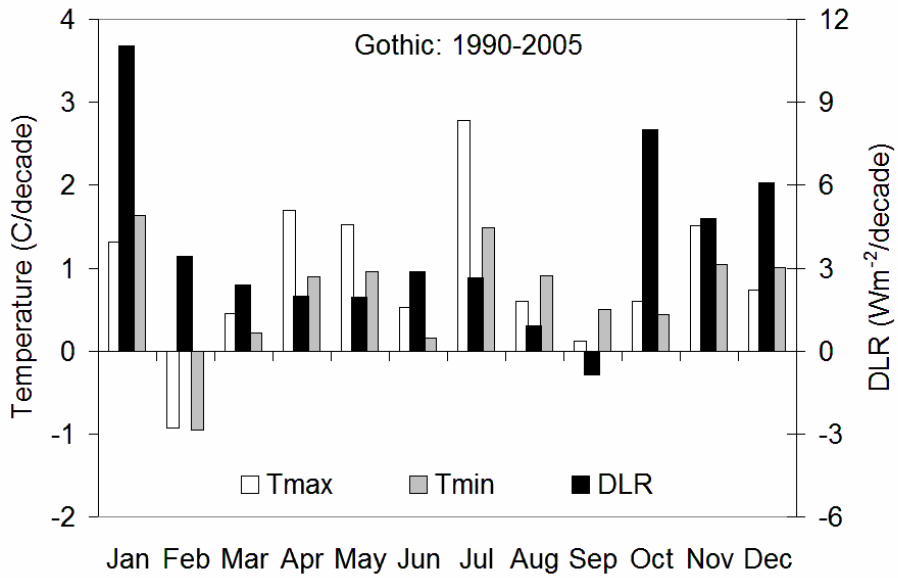

Figure 5.18 Linear trends in maximum and minimum temperature (left axis) and estimated DLR (right axis) for Gothic, CO from 1990 to 2005.

Table 5.2 Monthly estimates of λ (Wm^{-2}/gkg^{-1}) based on the slope of the power law curve described in Figure 5.19 at the monthly means of q (g/kg), also shown here, at Gothic between 1990-2005.

Month	q	λ
Jan	2.0	24.2
Feb	2.1	23.1
Mar	2.5	20.5
Apr	3.0	17.8
May	3.8	14.5
Jun	4.5	12.8
Jul	6.6	9.6
Aug	7.1	9.1
Sep	5.3	11.4
Oct	3.4	15.9
Nov	2.4	20.6
Dec	1.9	25.4

5.3 Effect of precipitation and snow amount on the late 20th century warming

The annual snowfall (Nov-May) in the SJM region between 1906-1990 does not have any long-term trend and varies between ± 20% of the mean for the 1960-1990 period (Figure 5.19). Generally, there is higher precipitation in the early half of the century (1906-1945) and lower in the middle of the century (1945-1970). However, there appears to be a decreasing trend since 1990. There is a 25% decrease in snowfall between 1995 and 2005, which is strongly correlated with the trends at the SNOTEL sites (r = 0.80). Moreover to validate the long-term trend, a comparison of trends between 4 long-term stations for which data are available before 1949 and all 22 stations shows a strong correlation (r = 0.87) for the 1949-2005 period.

Furthermore between 1936 and 2005, the trends in snowfall appear to be strongly correlated to the trends in SWE at both the SNOTEL and Snow Course sites (r ~ 0.83 for both sites, see Figure 5.20). SWE trends from both sites, which are very strongly correlated (r = 0.96), decrease by about 40% between 1995 and 2005. Furthermore, the snowdepth, which is very strongly correlated to the SWE (r = 0.99) at the Snow Course sites, decreases by about 25% between 1995 and 2005 (Figure 5.21).

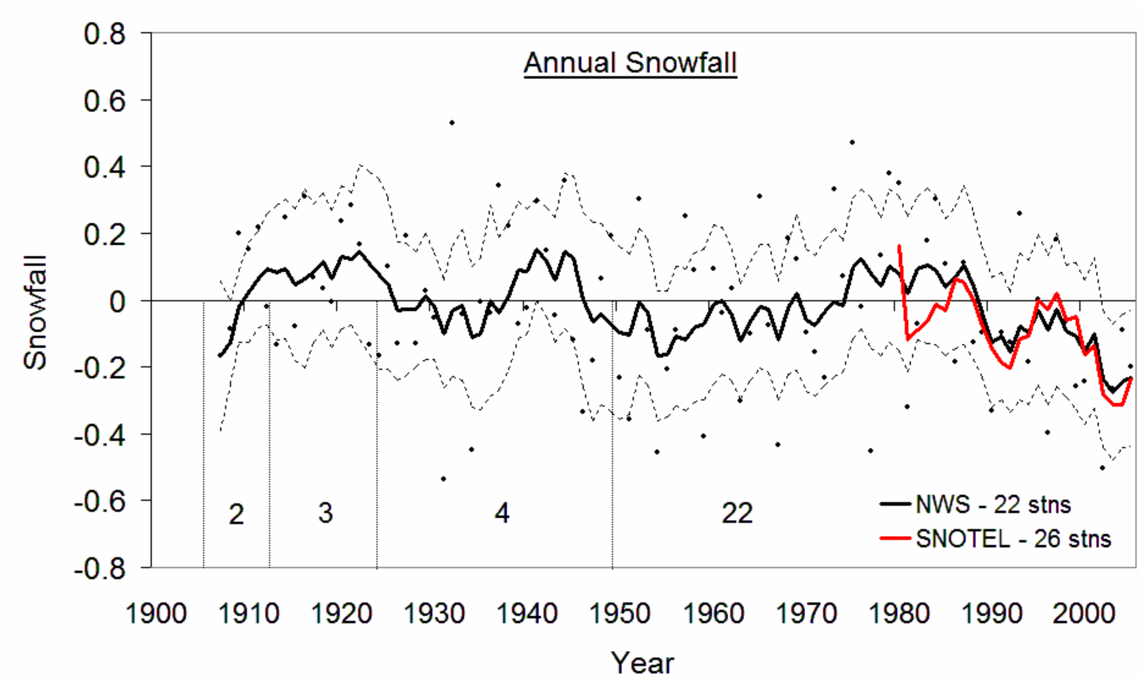

Figure 5.19 Same as 5.1 but for normalized snowfall trends. The anomalies are normalized by the mean of the 1960-1990 period.

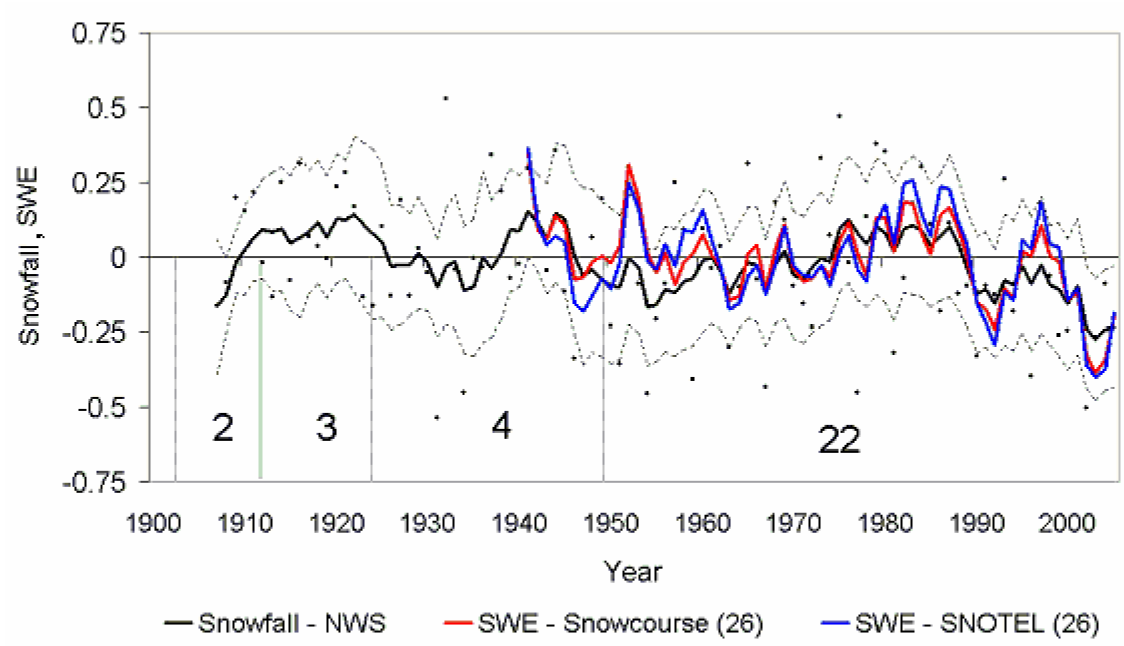

Figure 5.20 Same as 5.19 but the red and blue curves describe normalized SWE trends for Snow Course and SNOTEL sites, respectively

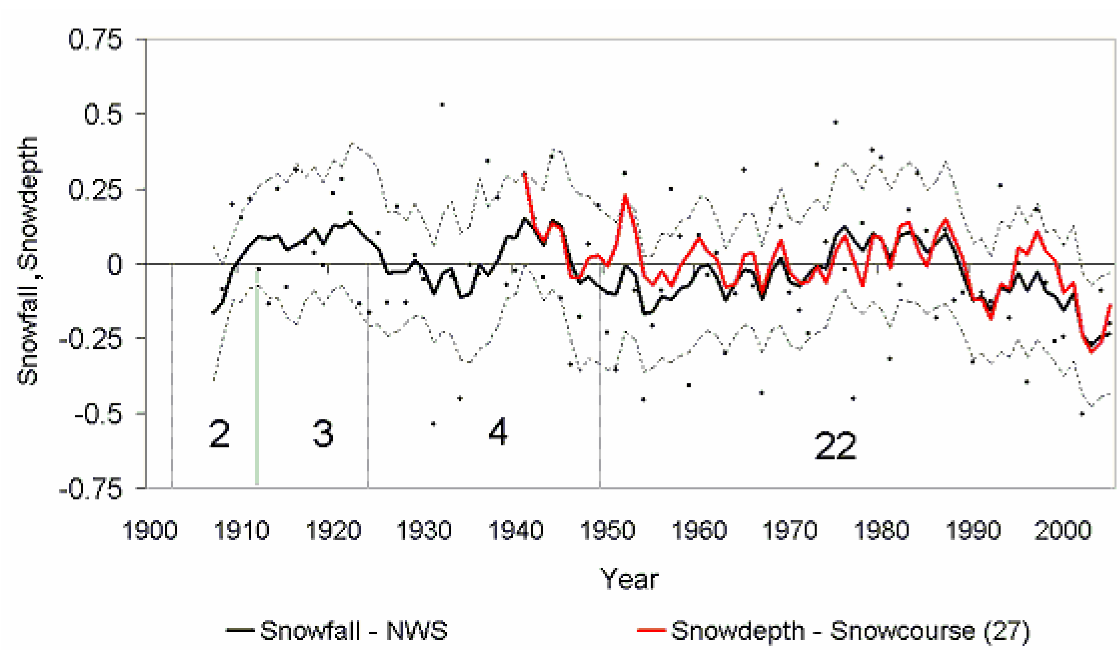

Figure 5.21 Same as 5.19 but the red curve describe normalized snow-depth trends for Snow Course sites.

Figure 5.22 shows decadally averaged anomalies in snowfall and snowdepth between 1936 and 2005. The snowdepth follows the snowfall trend. There are decreasing trends in both snowdepth and snowfall since the mid-1980s and it is most significant during the

1996-2005 period – 20% reduction in snowfall and 10% reduction in snowdepth from the base values. However, the trend in snowdepth is highly variable on a monthly basis. Figure 5.23 shows the decadally averaged snowdepth trend between 1936 and 2005 for February through May. For the 1996-2005 period, the snowdepth decreases during all months. However, the largest decrease occurs in April, although the snowfall during April has not changed significantly during that period, and in fact it seems to have increased slightly as shown in Figure 5.24.

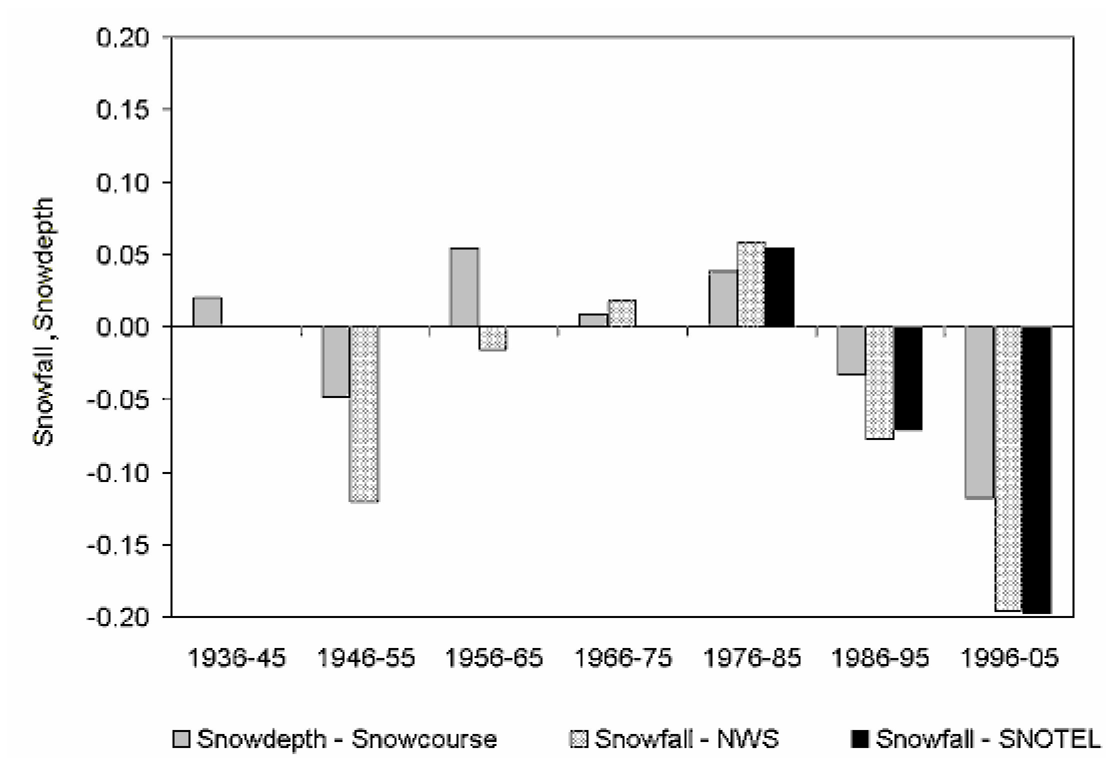

Figure 5.22 Normalized decadal anomalies in snowfall (NWS and SNOTEL) and snowdepth (Snow Course) in the San Juan Mountain Region from 1936-2005.

Figure 5.25 shows that snowfall and winter temperature in the SJM region appear to be negatively correlated over most of the 1906-2005 period. Even though the relationship does not appear to be strong, the warm phase of Pacific Decadal Oscillation (PDO) is associated with higher snowfall, and the cool phase of PDO with lower snowfall between

1906 and 1985 (r = 0.19). However, this relationship does not hold true, and is in fact opposite, between 1985-2005. Similarly, it appears that between 1950 and 1970, La Nina is associated with lower snowfall (r = 0.27). However, the generally accepted relationship between El Nino and higher snowfall, and La Nina and lower snowfall for the Southwest Colorado as described by *Edwards and Redmond* [2005] seems to completely break down since the mid-1970s.

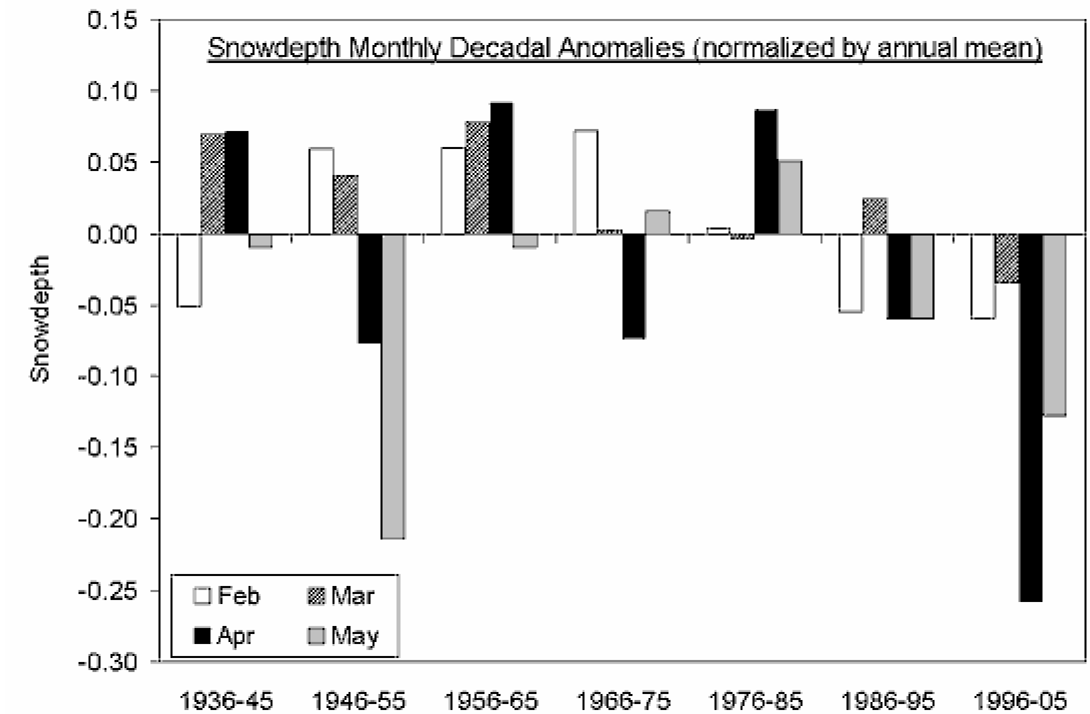

Figure 5.23 Normalized monthly decadal anomalies in snowdepth (Snow Course) in the San Juan Mountain Region from 1936-2005.

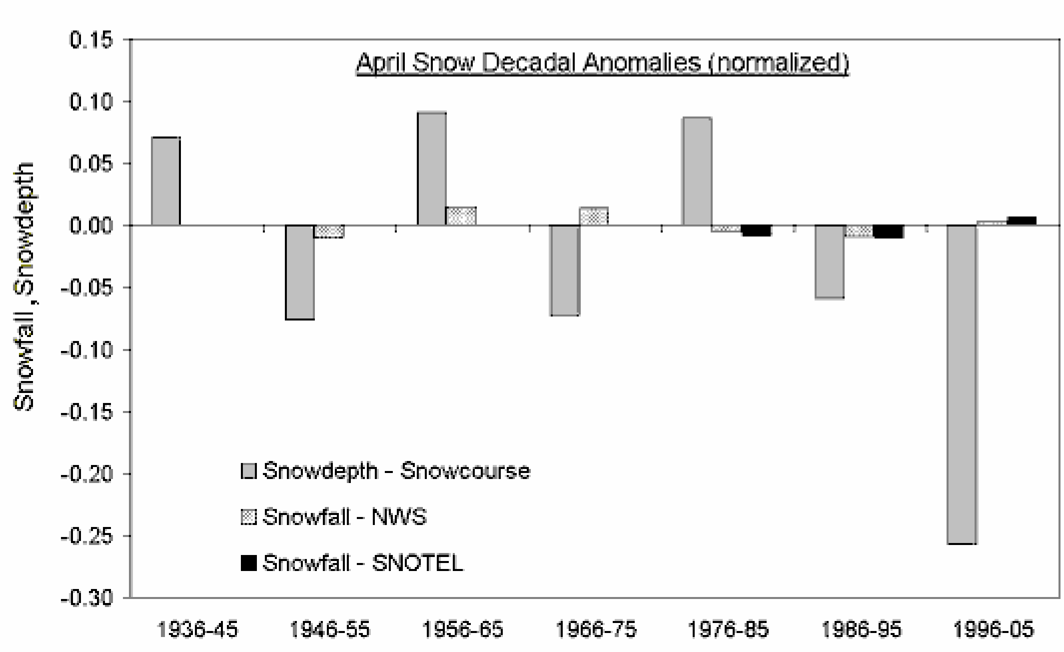

Figure 5.24 Normalized decadal anomalies in snowfall (NWS and SNOTEL) and snowdepth (Snow Course) during April in the San Juan Mountain Region from 1936-2005.

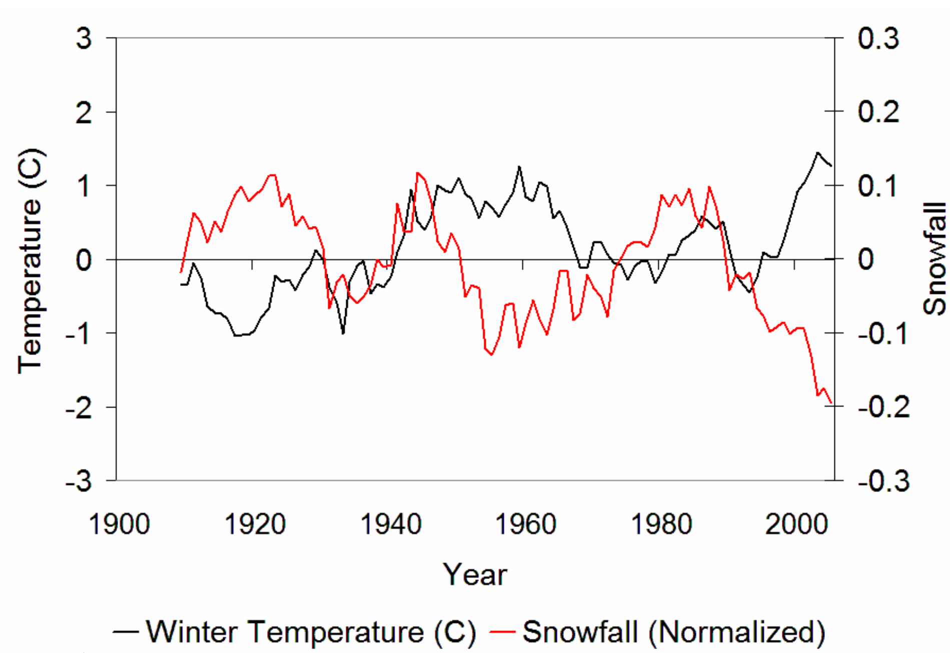

Figure 5.25 20th century trends in winter temperature (^{o}C) and snowfall (normalized) in the San Juan Mountain Region. Curves are 10 year running mean.

The behavior of monsoon (Jul-Aug) precipitation over the SJM region does not show any long term trend during the 1906-2005 period and varies between ± 30% of the mean for the 1960-1990 period (Figure 5.26). In the more recent decades, the monsoon seems to have been overall strong between 1980 and 2000, and sharply reduced (-30%) between 2000-2005. There is a strong correlation (r = 0.91) between the trends from NWS and SNOTEL sites for the 1979-2005 period. Moreover to validate the long-term trend, a comparison of trends between 4 long-term stations for which data are available before 1949 and all 22 stations shows a strong correlation (r = 0.94) for the 1949-2005 period.

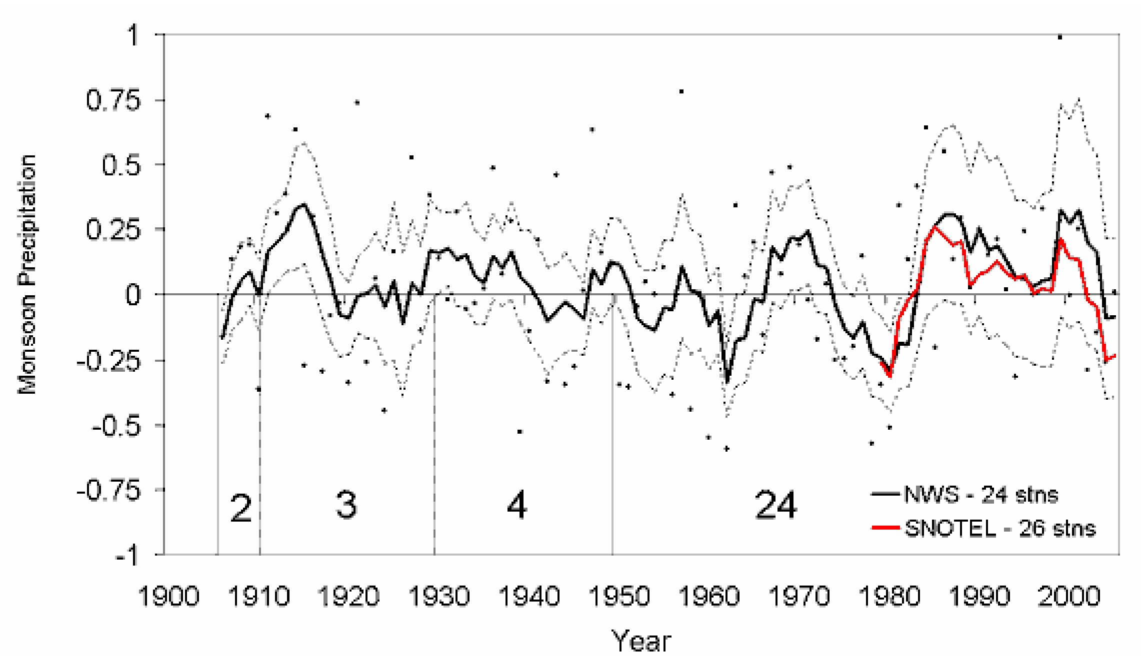

Figure 5.26 Same as Figure 5.19 but for normalized monsoon (Jul-Aug) precipitation trends.

Both El Nino (r = 0.23) and the warm phases of PDO (r = 0.22) are associated with higher monsoon precipitation between 1906 and 1985. However, similar to the behavior of snowfall, these relationships do not hold true between 1985 and 2005, and in fact appear to have an opposite behavior (ENSO: r = -0.18; PDO: r = -0.13).

Significant decreases in snowfall in the recent decades (1990-2005) in SJM region could not be explained by the climatic oscillations in the Pacific Ocean (PDO and ENSO). It is possible that changes in the pattern of atmospheric circulation, unrelated to PDO and ENSO, is in part modulating these trends in the snowfall over the SJM region.

Moreover, it appears that both SWE and snowdepth have decreased significantly during this period. A greater decrease in snowdepth during the spring months (April and May), without any significant changes in snowfall during these months, suggests that the snow melting processes have intensified during the spring months in the recent decades, at elevations corresponding to the Snow Course sites in the SJM region. An absence of snowdepth observations at NWS sites does preclude any understanding of annual and monthly trends in snowdepth at lower elevations (< 8500 ft) in the SJM region. The next section provides an analysis on the streamflow trends in the region.

5.4 Effect of climate change on streamflow in the SJM region

A total of 56 observation stations in the SJM region that comprised 34 stations maintained by the United States Geological Survey (USGS) and 22 stations by Colorado's Decision Support Systems (CDSS), were used to estimate the 20th century trends in streamflow. Figure 5.27 shows the normalized anomalies in the annual streamflow from all 57 stations. The streamflow in the region has been generally higher in the early half of the 20th century and lower the latter half. The annual flow between 1900-1950 is more than five times higher than the flow between 1951-2007. The lowest flow in the record occurred between 2000-2004; 2002 recording the lowest ever in the instrumental record.

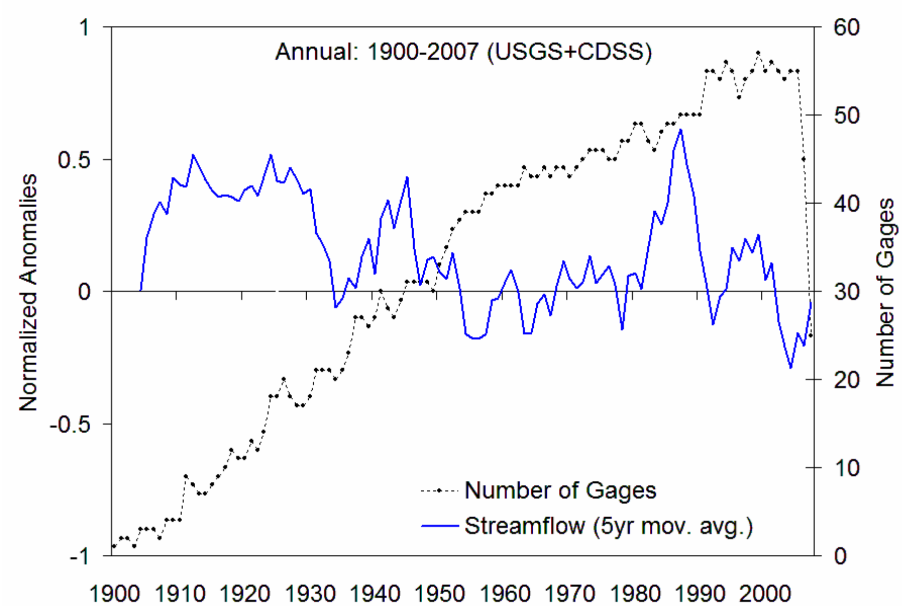

Figure 5.27 Annual streamflow anomalies (blue curve is a five-year running mean of the anomalies normalized by the mean of the 1990-2005 period in the SJM region between 1900 and 2007, relative to the mean of the 1990-2005 period, measured at both the USGS and CDSS gages. The black dots represent the total number of gages for which the streamflow anomalies were measured for a particular year.

A comparison between the annual streamflow trends at USGS and CDSS, as shown in Figure 5.28, demonstrates a high correlation (r = 0.92). Seasonally, more than 80% of the flow occurs in spring and summer, which is approximately equally distributed during the two seasons, and about 10% during fall. Moreover evaluating the long term trends during each season, as shown in Figure 5.29, I find that summer shows the largest decrease in flow in recent decades (see also Figure 5.30).

Table 5.3 Relationship of annual (USGS + CDSS) streamflow trends with snowdepth, SWE and precipitation in the SJM region between 1941-2005.

	R^2
Snowdepth	0.61
SWE - Snow Course	0.57
SWE - SNOTEL	0.61
Precipitation (Nov-May)	0.58

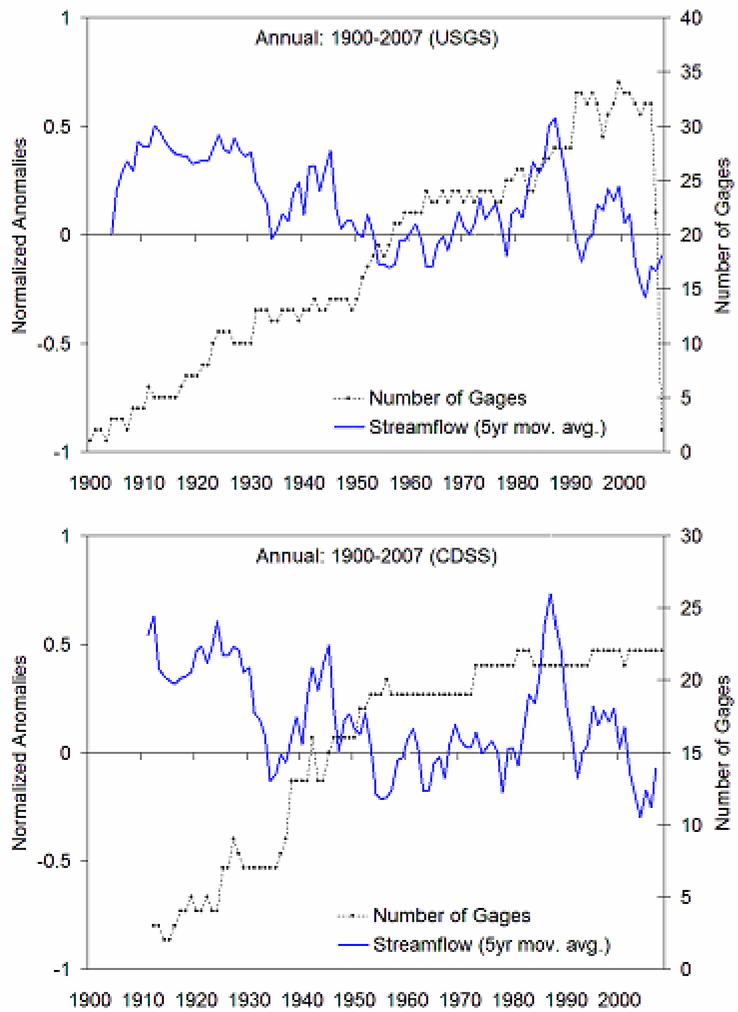

Figure 5.28 Same as Figure 5.27 but the annual streamflow anomalies are separated between USGS (above) and CDSS (below).

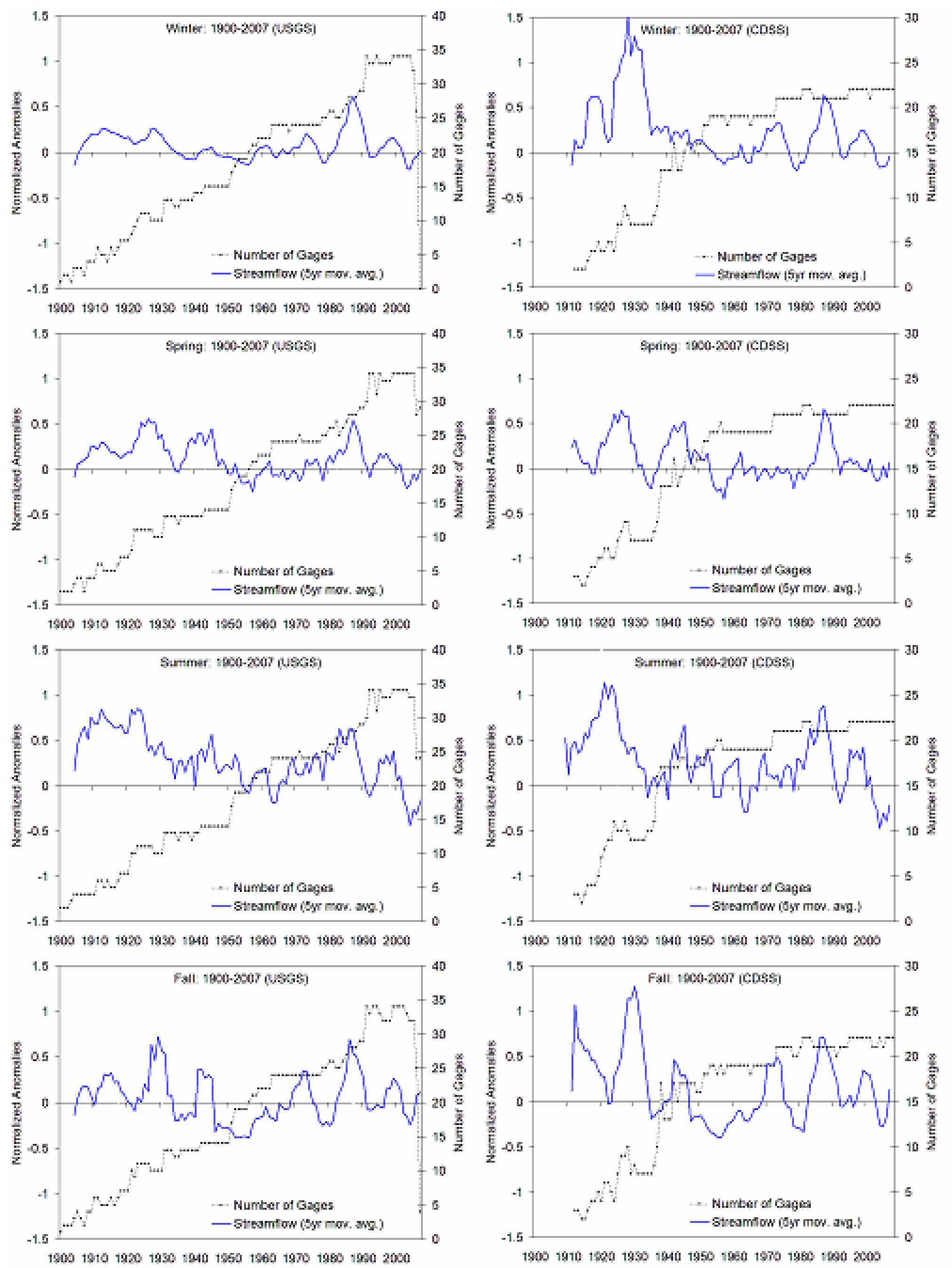

Figure 5.29 Same as Figure 5.27 but for seasonal streamflow anomalies, which are compared between the USGS (left column) and CDSS (right column) gages.

Figure 5.30 compares the linear trends of annual and seasonal flows between USGS and CDSS stations for the 1975-2005 and 1990-2005 periods. For both periods, there are large decreases in the flow annually and during summer and fall. The largest decreases occur during summer. However, the summer decreases are much larger for the 1990-2005 period. A similar scenario is true during fall. On the contrary, the decreases in flow during spring are becoming smaller between 1990-2005 as compared to 1975-2005. In fact, the CDSS trends show a slight increase in the streamflow during the 1990-2005 period. The large decreases in the annual, summer and fall flows in recent decades and relatively little change during spring months suggest that large increases in the snowmelt during spring is having a strong impact on the seasonal flows – particularly during the summer. Large increases in snowmelt in the recent decades are also suggested by large decreasing trends in the snowdepth during April and May (see Figure 5.23). Moreover, annual trends in snowfall, snowdepth and SWE explain 60% of the variability in the annual streamflow trends between 1941-2005 (Table 5.3).

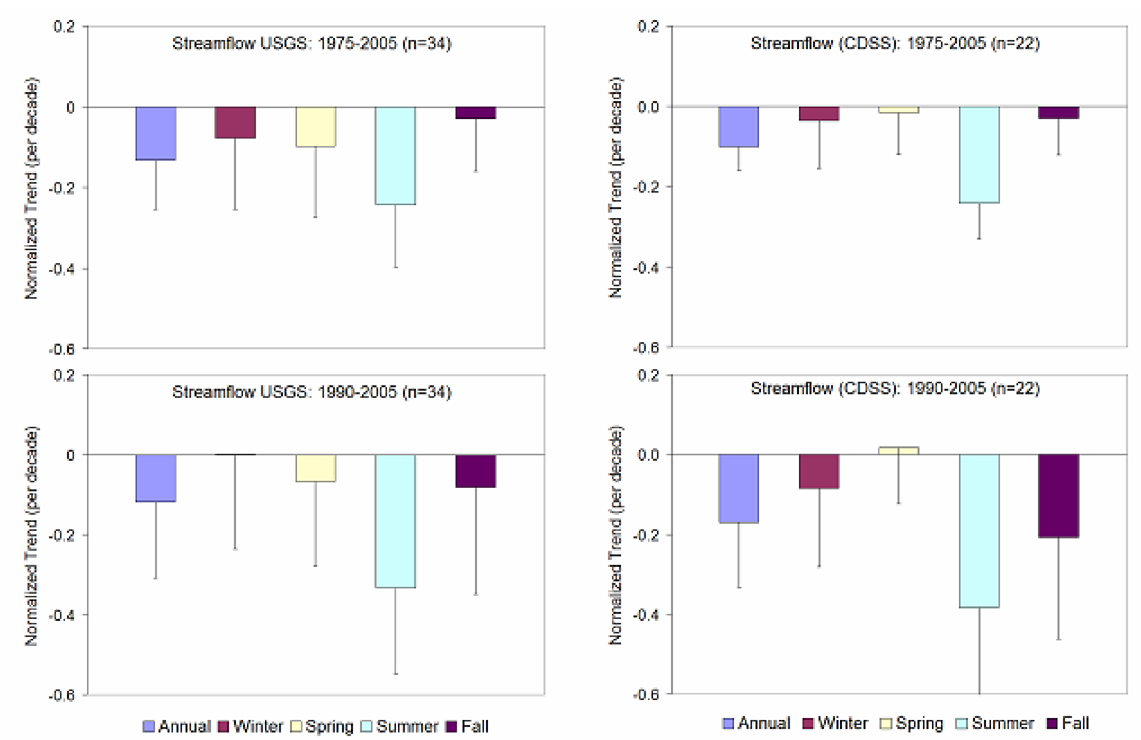

Figure 5.30 Linear trends in streamflow (normalized by the mean of the 1990-2007 period) for the 1975-2005 (above) and 1990-2005 (below) periods compiled separately for USGS (left) and CDSS (right) gages.

5.5 Discussion

The 20th century trend in surface temperature in the SJM region is similar to the trend observed globally – gradual warming in the early half of the century, slight cooling in the mid-century and a rapid cooling during the late century. The mid century cooling started later in the SJM region and so did the late century warming, however the latter has been much more rapid. Overall, the SJM region has warmed by 2^{o}C between 1906-2005. Half of this warming occurred between 1906-1950, however there are fewer than six observation stations to confidently validate this trend. More recently, between 1996-2005, the SJM region has experienced the most rapid warming trend in the instrumental record of 1^{o}C/decade, which has been observed at more than 20 stations each at the NWS and SNOTEL sites. The SNOTEL sites, which are about 2,500 ft higher than the NWS sites, show a 20% higher increase in the surface temperature in recent decades. The largest warming at the SNOTEL sites occurs during spring and summer while it is larger during winter at the NWS sites.

Analysis of trends in specific humidity (q) from a single station in the vicinity of the SJM region from 1990-2007 suggests that increases in q explain more than 50% of the variability in temperature increases during colder months such as January and November. Using the relationship between observed downward longwave radiation (DLR) and q from two high elevation stations in the region, I estimate large increases in DLR during November, December and January between 1990-2005 that coincide with large warming trends during these months. Future work needs to address the cooling trend in February.

A large warming trend in the SJM region during spring, particularly at the SNOTEL sites appears be related in part to the changes in snow cover. Snow Water Equivalent

(SWE) and snowdepth trends at both the SNOTEL and Snow Course sites show the largest decreases between 1996 and 2005. Moreover, the largest decreases in snowdepth occur during April and May. The decrease in snowdepth during spring in the recent decades appears to be related to decreases in precipitation and an increase in surface warming; the latter would lead to more snow melting during spring. Trends in streamflow in recent decades are consistent with the process of a large spring melt as well as a reduction in the precipitation in the region. There are large decreases in flow annually as well as during summer and fall; whereas there is little change in the flow during spring. The largest decrease in flow occurs in summer – more than 30% reduction per decade between 1990 and 2005. Therefore, the recent decreases in precipitation and increases in early spring melt have had a large impact on the seasonal pattern of streamflow in the region. Moreover, recent decreases in precipitation cannot be explained by trends in ENSO and PDO. Weak relationships that existed between precipitation and these climate indices do not appear to hold since the late 1970s.

Chapter 6: Conclusions and Future Directions

This dissertation evaluated the importance of low-level atmospheric water vapor in mediating the rate of climate changes processes, particularly at the high elevation regions in the world. I analyzed observed and modeled climate change in the late 20th and 21st century for China and its major mountain region, the Tibetan Plateau. To compare the results for the Tibetan Plateau with other high altitude sites, I compiled a long-term climate and hydrological trend for the San Juan Mountain (SJM) region in Southwest Colorado using the existing digitized record of the instrumental measurements.

The analysis of the GISS-AOM model simulations for China between 1950-2000 suggests that the simulated trends in climate variables, such as temperature, insolation, cloud cover and vapor pressure, have the same sign as the observed trends [*Che et al.*, 2005; *Kaiser*, 2000; *Kaiser and Qian*, 2002; *Liu et al.*, 2004; *Liu et al.*, 2005; *Liu et al.*, 2004a; *Qian et al.*, 2006; *Thomas*, 2000], although the magnitude of the modeled changes is smaller. During this time period, there is an observed warming of 1°C despite a 3.27 W/m^2 per decade decrease in surface insolation. The modeled results suggest that this warming is, in part, a result of an increase in downward longwave radiation (DLR), which is a consequence of an increase in anthropogenic greenhouse gases and the associated atmospheric water vapor feedbacks. Both observed and modeled cloud cover decrease during this period, thus trends in cloud cover are not expected to significantly increase DLR.

A similar scenario of warming is reported by *Philipona et al.* [2005] for Central Europe (another mid-latitude region) between 1995-2002 – a mean temperature increase of 0.8°C despite a 1.1 W/m^2 decrease in insolation between 1995-2002. During the same time period they find a 5.3 W/m^2 increase in DLR. Moreover, when they separate the different forcings contributing to the increases in DLR, using a stand-alone radiative transfer model, they find that the influence of water vapor increases on DLR are 2.3 times greater than the influences of all other greenhouse gases combined. The mid-latitude atmospheric boundary layer over China, in similarity to Central Europe, may not be optically saturated to the longwave radiation from the surface. Therefore, an increase in the lower atmospheric water vapor content can directly increase the infrared heating of the surface.

An additional cause of surface warming in China between 1950-2000 could be a reduction in latent heat fluxes from the surface caused by significant decreases in insolation. *Thomas* [2000] estimates large decreases in potential evapotranspiration during the same time period and, further, finds that these decreases are most strongly associated with sunshine duration south of 35^{o}N. Approximately for the same time period, *Robock and Li* [2006] find increases in soil moisture over Ukraine and Russia, and their analysis suggests decreases in insolation to be a major factor. Reduction in insolation leads to a decrease in evapotranspiration and thus an increase in soil moisture. A comprehensive soil moisture data set has not been accessible for China to verify the overall trends. However, I expect that large decreases in insolation over China in the latter half of the 20th century [*Che et al.*, 2005; *Kaiser and Qian*, 2002; *Liu et al.*, 2004] will tend to decrease evapotranspiration and exert a negative feedback on soil moisture. The model, however, shows a much smaller decreasing trend in evaporation (-1.3 mm/decade) over China as compared to the potential evapotranspiration trends (-23 mm/decade) estimated by *Thomas* [2000]. Therefore, most of the simulated warming between 1950-2000 appears to be a result of increases in DLR.

Furthermore, the decreases in the model's insolation between 1950-2000 are 4-5 times smaller than the observed decreases in insolation. This suggests that either black and organic carbon aerosols and dust have a greater role to play in the observed solar dimming over China than sulfate aerosols alone [Chameides *et al*., 1999; Qian *et al*., 2003], or the model insolation has lower sensitivity to changes in sulfate aerosols, or the estimates of aerosols used in the model calculation were incorrect. Menon *et al.* [2002] were able to simulate the observed summer cooling trend in southeast China only with the inclusion of black carbon aerosols in their model in addition to the non-absorbing aerosols. Therefore, inclusion of a more heterogeneous atmospheric aerosol composition in the model might produce trends in temperature and vapor pressure more consistent with observations.

For the 21st century, the model predicts a downward trend in surface insolation until the middle of the 21st century forced by the atmospheric sulfate burden, after which there is an upward trend as the atmospheric sulfate burden decreases. The model also predicts a continuous rise in surface temperature (2^{o}C) and surface vapor pressure (1 mb) during the 21st century for the SRES A1B scenario. These changes are much greater than for the period from 1850-2000. Overall, the model's prediction of the changes in climate variables between 1950-2000 is conservative. Therefore, the large changes in annual mean insolation, temperature and vapor pressure at the surface predicted by the model for China in the 21st century, may also be conservative estimates.

For the Tibetan Plateau, analysis of available climate datasets from *Xu et al.* [2006] for the 1961-2000 period confirms the general pattern of warming, described in earlier studies [*Du et al.*, 2004; *Liu and Chen*, 2000; *Shenbin et al.*, 2006; *You et al.*, 2007] for the region, that includes a strong warming trend in winter and fall. For the same time period, the model simulates a similar pattern of warming annually with the largest warming trend during winter. Overall, the model shows a 4^{o}C warming between 1951-2100 relative to the pre-industrial climate under the SRES A1B scenario. The model experiment also generates an elevation dependent warming (EDW) trend over the plateau between 1951-2100. This trend becomes larger in the latter half of the 21st century. An EDW over the plateau is simulated for all seasons in the model between 1950-2100, however the effect is more significant during winter and spring. For the 1961-1990 period, the model's EDW trend is comparable to the observed trend obtained by *Liu and Chen* [2000]. Similar to the temperature trend, there are elevation based increases in surface vapor pressure, absorbed solar radiation (ASR), downward longwave radiation (DLR) and latent heat fluxes, and decreases in snow cover between 1951-2100. The atmospheric sulfate burden, which peaks around 2030 and decreases in the latter half of the 21st century, shows the largest increases at lower elevations and much smaller increases at the highest elevations.

The model simulation suggests that an accelerated wintertime warming results from larger increases in DLR during the winter months relative to other months. These increases in DLR are in part responding to an increase in specific humidity, particularly when the specific humidity is low, which occurs most prominently during the winter months and at high elevations. From observations in the Swiss Alps, *Ruckstuhl et al.*

[2007] found that an increase in DLR is proportional to the logarithm of near-surface humidity because of the distribution of lines of absorption and emission of thermal radiation by water vapor. This mechanism, therefore, tends to cause the largest net increases in DLR at higher elevations during the winter months in the model and consequently appears to cause an EDW in the plateau during winter. This mechanism is also important during spring and fall, although not as strong.

Another factor in the large warming over the plateau is the snow albedo effect. However, it is more important during spring and summer in the model simulation. There are large increases in absorbed solar radiation (ASR) at higher elevation, particularly during these seasons, which can increase the surface temperature. These increases in ASR are largely associated with decreases in snow cover. Previous modeling studies have suggested that snow-albedo feedback is one of the primary factors in causing an EDW in the high mountain regions [*Chen et al.*, 2003; *Giorgi et al.*, 1997]. Moreover, there is a decreasing trend in the ASR in the low elevation region in the early half of the 21st century owing to large increases in the atmospheric sulfate burden relative to the high elevation sites. The net effect of changes in snow cover and atmospheric sulfate burden is to produce an elevation dependent increase in ASR during the 21st century. Trends in snowdepth and precipitation over the plateau suggests that snow cover has not been significantly affected during spring in the latter half of the 20th century. However, as the greenhouse warming continues into the 21st century, a continuous reduction in snow cover could contribute to an accelerated surface warming during spring and summer, particularly at higher elevations.

Overall, the model experiments suggest that the Tibetan Plateau will warm rapidly during the 21st century under the SRES A1B scenario. This warming is likely to be more pronounced at higher elevations in the plateau due to (a) increases in DLR caused by surface humidity increases during cold seasons, (b) increases in ASR caused by decreases in the snow cover extent during spring and summer and (c) larger aerosol concentrations at lower elevations. The elevation-based changes in surface energy balance affected by changes in surface humidity, snow cover and atmospheric aerosol will tend to produce an EDW trend over the plateau during the 21st century.

For the San Juan Mountain (SJM) region in southwest Colorado, long term trends in climate (temperature and precipitation) and hydrological (SWE, snowdepth and streamflow) variables are constructed from the digitized instrumental records. Trends in temperature, precipitation and streamflow extend to the first decade of the 20th century, however data from many fewer stations are either digitized or available in the early half of the 20th century to provide us with greater confidence in the trends of these variables – particularly temperature and precipitation – prior to 1950. Nonetheless, I find that those few stations for which the data are available from the early period do represent the mean trend from all stations combined for the latter period.

My analysis shows that the SJM region experienced a gradual warming of greater than $1^{o}C$ during the early half of the 20th century (1906-1955), a cooling of $0.5^{o}C$ (1960-1975) and very rapid warming of $1^{o}C$ between 1995-2005. The general trend in the warming is similar to the trend observed globally as well as for the contiguous US, however the mid century (post-1950) cooling and the accelerated late century warming occurred later and in a shorter duration in the SJM region. One of the causes for mid-century cooling in the

SJM region might be the solar dimming effect caused by an increase in the atmospheric aerosol loading, which is similar to that phenomenon proposed, in large part, for a general cooling trend globally, specifically the northern hemisphere. Based on the estimates from *Boucher and Pham* [2002], the 20th century trends in the atmospheric sulfate aerosol over the SJM is similar to the trends for the contiguous US which show sharp increases in the atmospheric sulfate concentrations between 1960-1980. Interestingly, the SJM region has not experienced a secular warming trend since the mid-1970s as observed globally. Instead, a much more rapid and secular warming trend in the region started later, since the mid-1990s. The rapid warming between 1995-2005 is also correlated with large decreases in annual precipitation, SWE, snowdepth and streamflow. Therefore, it appears that the recent warming is, in part, associated with decreases in annual snowfall. Furthermore, it appears that this warming has accelerated the spring snowmelt process, as noted by the largest decreases in SWE and snowdepth and smallest decreases in streamflow in spring.

On a monthly basis, some of the largest warming trends in the recent decades occur during January, July and December in addition to the spring months – particularly April and May. Warming during January, July and December is less likely to be caused by the snow-albedo feedback mechanism proposed for the large spring warming. There is almost no snow cover in July. During January and December, even though the annual precipitation and snowdepth have decreased significantly, there are relatively much smaller changes in precipitation and snowdepth which leads us to expect that snow cover may not have changed significantly during these months.

To explain the large winter warming trend in the SJM region during recent decades, I investigated the influence of increases in specific humidity (q). Owing to unavailability of humidity data for the region that extends for at least a decade, most of this analysis is based on the humidity trends from Gothic, CO which lies in close proximity of the region. Moreover, I find that the warming at Gothic is representative of the warming in the SJM region in general, and particularly at the high elevation sites. The normalized increases in q are only significant (> 10% per decade) from October through January. Moreover, only during these months do diurnal changes in q explain large variability (> 50%) in the corresponding changes in temperature. The largest changes in the estimated downward longwave radiaton (DLR) also occur during these months. Large increases in DLR during January and December coincide with large increases in temperatures and, in part, indicate the causes for a large warming trend during these months.

For July, a preliminary analysis suggests an association between an increase in warming and a decrease in precipitation in the SJM region. Although, I haven't been able to access the record of cloud cover changes for the region, large decreases in precipitation during July might also signify decreases in cloud cover during that month. Moreover, large decreases in cloud cover will lead to greater increases in the maximum temperature than the minimum temperature, particularly during summer months such as July which I find to be true. There is a 60% greater increase in the maximum temperature as compared to the minimum temperature during July between 1990-2005.

In this dissertation, I have demonstrated the importance of a positive low-level water vapor feedback on warming trends observed in China, the Tibetan Plateau and the SJM region. Positive water vapor feedbacks induced by atmospheric warming is a much more important mechanism in amplifying DLR than the anthropogenic greenhouse gases [*Hall and Manabe,* 1999, *Rákóczi and Iványi,* 1999-2000]. The water vapor increases in the atmosphere, in response to the warming triggered by anthropogenic greenhouse gas forcing, has occurred such that the relative humidity has remained approximately constant at all vertical levels [*Rind,* 1991]. Moreover, such increases in water vapor amounts have been simulated to produce large perturbations in warming in the lower atmosphere owing to increases in water vapor absorption in both longwave and shortwave radiation [*Shine and Sinha,* 1991]. On a seasonal basis, winter has been one of the warmest in each of my study regions. In fact, the winter warming in China and the Tibetan Plateau has been at least two times greater than warming during the other seasons [*Liu et al.*, 2004a; *Liu and Chen*, 2000]. The analysis conducted for each of these regions demonstrates that the influence of increases in specific humidity on surface energy fluxes is in part responsible for large rates of winter warming. This analysis further suggests that the mid-latitude boundary layer, particularly at high altitudes, is under-saturated in longwave absorption in the water vapor absorption lines. Therefore, an increase in water vapor content during winter when the specific humidity is lowest will cause a large increase in the DLR at the surface, as suggested by the model. However, owing to limited observations on humidity and DLR it is difficult to ascertain the accuracy of this relationship on the study regions and calculate its effect on the surface energy balance. Hence, the specific role of surface humidity increases on accelerated wintertime warming needs to more fully addressed in the future research with more comprehensive measurements of both humidity and surface energy fluxes.

Overall, the model has shown a lower warming rate as compared to the observed trend for both China and the Tibetan Plateau in the latter half of the 20th century. One factor for this discrepancy could be an underestimation of the radiative warming potential of water vapor. The observed effect of the water vapor feedback in mid-latitudes is found to be 2-3 times stronger than what the model predicts [*Fomin and Udalova,* 2003; *Philipona et al.*, 2005]. *Fomin et al.* [2004] report that the inadequacies in water vapor continuum absorption in the radiative transfer simulations is the main source of uncertainty in the calculations of both longwave and shortwave absorption by water vapor. Moreover, the role of water vapor on shortwave absorption might be underestimated in the present models [*Hargrove,* 2007]. Radiative transfer calculations in global climate models need to realistically account for the effect of the water vapor absorption in both shortwave and longwave in order to obtain accurate simulations of global and regional climate change.

Appendices

Table A1. NWS stations used for temperature observations. All stations were considered in calculating the trends. The six highlighted stations are the only stations for which pre-1949 data are digitized to extend the observation to the year 1906

#	Name	Elevation (ft)	Duration
1	MESA VERDE NATL PARK (055531)	7070	1922-2005
2	CORTEZ (051886)	6180	1929-2005
3	YELLOW JACKET 2 W (059275)	6860	1962-2002
4	RICO (057017)	8850	1959-2001
5	AMES (050228)	8700	1970-72,75,77-85
6	TELLURIDE (058204)	8770	1911-2005
7	NORWOOD (056012)	7020	1949-2005
8	RIDGWAY (057020)	7000	1982-2005
9	OURAY (056203)	7840	1949-2005
10	SILVERTON (057656)	9330	1949-2005
11	LEMON DAM (054934)	8090	1982-2005
12	VALLECITO DAM (058582)	7650	1949-2005
13	FORT LEWIS (053016)	7600	1949-2005
14	DURANGO (052432)	6600	1900-1990
15	IGNACIO 1N (054250)	6460	1950-1993
16	PAGOSA SPRING (056258)	7100	1949-2005
17	LAKE CITY (054734)	8880	1959-2005
18	HERMIT 7 ESE (053951)	9000	1949-2005
19	WOLF CREEK PASS 1 E (059181)	10640	1958-2001
20	DEL NORTE (052184-5)	7880	1949-2005
21	MANASSA (055322)	7710	1949-2005
22	ALAMOSA WSO AP (050130)	7540	1949-2005
23	MONTE VISTA (055706)	7660	1949-2005
24	CENTER 4 SSW (051458)	7670	1949-2005
25	SAGUACHE (057337)	7690	1949-2005
26	MONTROSE (055722)	5785	1949-2005

Table A2. SNOTEL stations used for temperature observations.

#	Name	Elevation (ft)	Duration
1	BEARTOWN	11600	1984-2005
2	CASCADE	8880	1987-2005
3	CASCADE #2	8920	1991-2005
4	COLUMBINE PASS	9400	1987-2005
5	COLUMBUS BASIN	10785	1995-2005
6	EL DIENTE PEAK	10000	1987-2005
7	IDARADO	9800	1987-2005
8	LILY POND	11000	1984-2005
9	LIZARD HEAD PASS	10200	1986-2005
10	LONE CONE	9600	1987-2005
11	MANCOS	10000	1997-2005
12	MIDDLE CREEK	11250	1984-2005
13	MINERAL CREEK	10040	1987-2005
14	MOLAS LAKE	10500	1987-2005
15	RED MOUNTAIN PASS	11200	1986-2005
16	SCOTCH CREEK	9100	1987-2005
17	SLUMGULLION	11440	1984-2005
18	SPUD MOUNTAIN	10660	1987-2005
19	STUMP LAKES	11200	1987-2005
20	UPPER RIO GRANDE	9420	1987-2005
21	UPPER SAN JUAN	10200	1984-2005
22	VALLECITO	10880	1987-2005
23	WOLF CREEK SUMMIT	11000	1987-2005

Table A3. NWS stations used for precipitation observations. All stations are considered in calculating the trends. The six highlighted stations are the only stations for which pre-1949 data are digitized to extend the observation to the year 1906

#	Name	Elevation (ft)	Time Period
1	MESA VERDE NATL PARK (055531)	7070	1949-2005
2	CORTEZ (051886)	6180	1929-2005
3	YELLOW JACKET 2 W (059275	6860	1962-2002
4	RICO (057017)	8850	1959-2001
5	AMES (050228)	8700	1970-72,75,77-85
6	TELLURIDE (058204)	8770	1911-2005
7	NORWOOD (056012)	7020	1949-2005
8	RIDGWAY (057020)	7000	1982-2005
9	OURAY (056203)	7840	1949-2005
10	SILVERTON (057656)	9330	1906-2005
11	LEMON DAM (054934)	8090	1982-2005
12	VALLECITO DAM (058582)	7650	1949-2005
13	FORT LEWIS (053016)	7600	1949-2005
14	DURANGO (052432)	6600	1900-90
15	IGNACIO 1N (054250)	6460	1950-93
16	PAGOSA SPRING (056258)	7100	1949-2005
17	LAKE CITY (054734)	8880	1959-2005
18	HERMIT 7 ESE (053951)	9000	1949-2005
19	WOLF CREEK PASS 1 E (059181)	10640	1958-2001
20	DEL NORTE (052184-5)	7880	1949-2005
21	MANCOS (055327)	10820	1949-2005
22	DOLORES (052326)	10830	1949-2005
23	PLACERVILLE (056524)	10800	1949-2005
24	TACOMA (058154)	10750	1949-2005

Table A4. SNOTEL stations used for precipitation and SWE observations. All stations are considered in calculating the trends (Mancos was not considered for snowfall analysis). The ten highlighted stations are the only stations for which pre-1980 SWE data are available to extend the data to the year 1941.

#	Name	Elevation (ft)	Time Period
1	BEARTOWN	11600	1983-2005
2	BUTTE	10160	1961-2005
3	CASCADE	8880	1939-2005
4	CASCADE #2	8920	1991-2005
5	COLUMBINE PASS	9400	1987-2005
6	COLUMBUS BASIN	10785	1995-2005
7	CUMBRES TRESTLE	10040	1961-2005
8	EL DIENTE PEAK	10000	1987-2005
9	IDARADO	9800	1987-2005
10	LILY POND	11000	1981-2005
11	LIZARD HEAD PASS	10200	1981-2005
12	LONE CONE	9600	1961-2005
13	MANCOS	10000	1995-2005
14	MIDDLE CREEK	11250	1981-2005
15	MINERAL CREEK	10040	1961-2005
16	MOLAS LAKE	10500	1987-2005
17	PORPHYRY CREEK	10760	1940-2005
18	RED MOUNTAIN PASS	11200	1961-2005
19	SCOTCH CREEK	9100	1987-2005
20	SLUMGULLION	11440	1981-2005
21	SPUD MOUNTAIN	10660	1951-2005
22	STUMP LAKES	11200	1987-2005
23	UPPER RIO GRANDE	9420	1987-2005
24	UPPER SAN JUAN	10200	1940-2005
25	VALLECITO	10880	1987-2005
26	WOLF CREEK SUMMIT	11000	1961-2005

Table A5. Snow Course stations used for snowdepth and SWE observations. All stations were considered in calculating the trends.

#	Name	Elevation (ft)	Time Period
1	BIG MEADOWS	9260	1969-2005
2	COCHETOPA PASS	10000	1949-2005
3	CRESTED BUTTE	8920	1936-2005
4	GRAYBACK	11600	1973-2005
5	GROUND HOG	8940	1976-2005
6	IRONTON PARK	9600	1937-2005
7	KEYSTONE	9960	1961-2005
8	LA PLATA	9340	1976-2005
9	LAKE CITY	10160	1969-2005
10	LAKE HUMPHREY	9000	1963-2005
11	LEMON RESERVOIR	8700	1969-2005
12	LOVE LAKE	10000	1965-2005
13	MANCOS T-DOWN	10000	1969-2005
14	MOLAS LAKE	10500	1951-2000
15	PARK CONE	9600	1936-2005
16	PINOS MILL	10000	1962-2005
17	PLATORO	9800	1962-2005
18	POOL TABLE MOUNTAIN	9840	1962-2005
19	PORCUPINE	10280	1951-2005
20	RICO	8700	1937-1990
21	RIVER SPRINGS	9300	1937-1990
22	SANTA MARIA	9600	1939-2005
23	SILVER LAKES	9500	1937-2005
24	TELLURIDE	8800	1939-2005
25	TROUT LAKE	9780	1949-2005
26	TROUT LAKE #2	9780	1939-2005

Bibliography

Arnell, N., Effects of IPCC SRES emissions scenarios on river runoff: a global perspective, *Hydrology and Earth System Sciences*, *7* (5), 619-641, 2003.

Beniston, M., Climatic change in mountain regions: a review of possible impacts, *Climatic Change*, *59*, 5-31, 2003.

Beniston, M., H. Diaz, and R. Bradley, Climatic change at high elevation sites: an overview, *Climatic Change*, *36* (3-4), 233-251, 1997.

Boucher, O., and M. Pham, History of sulfate aerosol radiative forcings, *Geophysical Research Letters*, *29* (9), 22-1, 2002.

Chameides, W., H. Yu, S. Liu, M. Bergin, X. Zhou, L. Mearns, G. Wang, C. Kiang, R. Saylor, and C. Luo, Case study of the effects of atmospheric aerosols and regional haze on agriculture: An opportunity to enhance crop yields in China through emission controls, *Proceedings of the National Academy of Sciences of the United States of America*, *96* (24), 13626-13633, 1999.

Che, H., G. Shi, X. Zhang, R. Arimoto, J. Zhao, L. Xu, B. Wang, and Z. Chen, Analysis of 40 years of solar radiation data from China, 1961–2000, *Geophys. Res. Lett*, *32* (3), L06803, 2005.

Chen, B., W.C. Chao, and X. Liu, Enhanced climatic warming in the Tibetan Plateau due to doubling CO2: a model study, *Climate Dynamics*, *20* (4), 401-413, 2003.

Dettinger, M., and D. Cayan, Large-Scale Atmospheric Forcing of Recent Trends toward Early Snowmelt Runoff in California, *Journal of Climate*, *8* (3), 606-623, 1995.

Diaz, H., and R. Bradley, Temperature variations during the last century at high elevation sites, *Climatic Change*, *36* (3-4), 253-279, 1997.

Du, M., S. Kawashima, S. Yonemura, X. Zhang, and S. Chen, Mutual influence between human activities and climate change in the Tibetan Plateau during recent years, *Global and Planetary Change*, *41* (3-4), 241-249, 2004.

Duan, A., and G. Wu, Change of cloud amount and the climate warming on the Tibetan Plateau, *Geophys. Res. Lett*, *33*, L22704, 2006.

Edwards, L., and K. Redmond, Climate Factors on Colorado River Basin Water Supply, in *Colorado River Basin Climate*, pp. 14-22, 2005.

Fomin, B., and T. Udalova, Spectroscopic Databases and Models of Continuum Absorption for Computation of Atmospheric Radiation: A Ten-Year Retrospective and the Current State, *Izvestiya Atmospheric and Oceanic Physics*, *39* (4), 466–475, 2003.

Fomin, B., T. Udalova, and E. Zhitnitskii, Evolution of spectroscopic information over the last decade and its effect on line-by-line calculations for validation of radiation codes for climate models, *Journal of Quantitative Spectroscopy and Radiative Transfer*, *86* (1), 73-85, 2004.

Fu, C., Potential impacts of human-induced land cover change on East Asia monsoon, *Global and Planetary Change*, *37* (3-4), 219-229, 2003.

Giorgi, F., X. Bi, and Y. Qian, Indirect vs. Direct Effects of Anthropogenic Sulfate on the Climate of East Asia as Simulated with a Regional Coupled Climate-Chemistry/Aerosol Model, *Climatic Change*, *58* (3), 345-376, 2003.

Giorgi, F., J. Hurrell, M. Marinucci, and M. Beniston, Elevation Dependency of the Surface Climate Change Signal: A Model Study, *Journal of Climate*, *10* (2), 288-296, 1997.

Hall, A., and S. Manabe, The Role of Water Vapor Feedback in Unperturbed Climate Variability and Global Warming, *Journal of Climate*, *12* (8), 2327-2346, 1999.

Hansen, J., L. Nazarenko, R. Ruedy, M. Sato, J. Willis, A. Del Genio, D. Koch, A. Lacis, K. Lo, and S. Menon, Earth's Energy Imbalance: Confirmation and Implications, *Science*, *308* (5727), 1431-1435, 2005.

Hargrove, J., Water dimer absorption of visible light, *Atmos. Chem. Phys. Discuss*, *7*, 11123-11140, 2007.

Held, I., and B. Soden, Water vapor feedback and global warming, *Annual Reviews in Energy and the Environment*, *25* (1), 441-475, 2000.

Hoerling, M., J. Eischeid, X. Quan, and T. Xu, Explaining the record US warmth of 2006, *Geophys. Res. Lett*, *34*, 2007.

Houghton, J., Y. Ding, D. Griggs, M. Noguer, P. van der Linden, X. Dai, K. Maskell, and C. Johnson, Climate change 2001: the scientific basis, 2001.

Julander, R., Difficulties in the measurement and interpretation of high elevation climate data in Utah, in *MTNCLIM 2008*, Silverton, 2008.

Kaiser, D., Decreasing Cloudiness Over China: An Updated Analysis Examining Additional Variables, *11th Symposium on Global Change Studies, Long Beach, CA (US), 01/10/2000--01/14/2000*, 2000.

Kaiser, D., and Y. Qian, Decreasing trends in sunshine duration over China for 1954-1998- Indication of increased haze pollution?, *Geophysical Research Letters*, *29* (21), 38-1, 2002.

Leathers, D., A. Ellis, and D. Robinson, Characteristics of Temperature Depressions Associated with Snow Cover across the Northeast United States, *Journal of Applied Meteorology*, *34* (2), 381-390, 1995.

Levitus, S., J. Antonov, T. Boyer, and C. Stephens, Warming of the World Ocean, *Science*, *287* (5461), 2225, 2000.

Liepert, B., J. Feichter, U. Lohmann, and E. Roeckner, Can aerosols spin down the water cycle in a warmer and moister world?, *Geophys. Res. Lett.*, *31* (L06207), 2004.

Liu, B., M. Xu, M. Henderson, and W. Gong, A spatial analysis of pan evaporation trends in China, 1955–2000, *J. Geophys. Res*, *109*, 1–9, 2004.

Liu, B., M. Xu, M. Henderson, and Y. Qi, Observed trends of precipitation amount, frequency, and intensity in China, 1960–2000, *J. Geophys. Res*, *110*, 2005.

Liu, B., M. Xu, M. Henderson, Y. Qi, and Y. Li, Taking China's Temperature: Daily Range, Warming Trends, and Regional Variations, 1955–2000, *Journal of Climate*, *17* (22), 4453-4462, 2004a.

Liu, X., and B. Chen, Climatic warming in the Tibetan Plateau during recent decades, *International Journal of Climatology*, *20* (14), 1729-1742, 2000.

Manabe, S., and R. Wetherald, Thermal Equilibrium of the Atmosphere with a Given Distribution of Relative Humidity, *Journal of the Atmospheric Sciences*, *24* (3), 241-259, 1967.

Menon, S., J. Hansen, L. Nazarenko, and Y. Luo, Climate Effects of Black Carbon Aerosols in China and India, *Science*, *297* (5590), 2250, 2002.

Nijssen, B., G. O'Donnell, A. Hamlet, and D. Lettenmaier, Hydrologic Sensitivity of Global Rivers to Climate Change, *Climatic Change*, *50* (1), 143-175, 2001.

Niu, T., L. Chen, and Z. Zhou, The characteristics of climate change over the Tibetan Plateau in the last 40 years and the detection of climatic jumps., *Advances in Atmospheric Sciences*, *21* (2), 193-203, 2004.

Pepin, N., and M. Losleben, Climate change in the Colorado Rocky Mountains: free air versus surface temperature trends, *International Journal of Climatology*, *22* (3), 311-329, 2002.

Pham, M., O. Boucher, and D. Hauglustaine, Changes in atmospheric sulfur burdens and concentrations and resulting radiative forcings under IPCC SRES emission scenarios for 1990-2100, *Journal of Geophysical Research*, *110* (D06112), 2005.

Philipona, R., B. Dürr, A. Ohmura, and C. Ruckstuhl, Anthropogenic greenhouse forcing and strong water vapor feedback increase temperature in Europe, *Geophys. Res. Lett*, *32* (5), 2533–2536, 2005.

Qian, Y., D. Kaiser, L. Leung, and M. Xu, More frequent cloud-free sky and less surface solar radiation in China from 1955 to 2000, *Geophys. Res. Lett*, *33*, 2006.

Qian, Y., L. Leung, S. Ghan, and F. Giorgi, Regional climate effects of aerosols over China: modeling and observation, *Tellus B*, *55* (4), 914, 2003.

Rákóczi, F., and Z. Iványi, Water vapour and greenhouse effect, *Geofizika*, *16-17*, 65-72, 1999-2000.

Ramanathan, V., P. Crutzen, J. Kiehl, and D. Rosenfeld, Aerosols, Climate, and the Hydrological Cycle, *Science*, *294* (5549), 2119-2124, 2001.

Rangwala, I., J. Miller, G. Russell, and M. Xu, Analysis of global climate model experiments to elucidate past and future changes in surface insolation and warming in China, *Geophysical Research Letters*, *33* (20), 2006.

Redmond, K., Recent Accelerated Warming in Western United States Mountains, in *presentation to American Geophysical Union, San Francisco, December*, pp. 18-30, 2007.
www.fs.fed.us/psw/cirmount/meetings/agu/pdf2007/redmond_talk_agu2007.pdf

Rind, D., E.-W. Chiou, W. Chu, J. Larsen, S. Oltmans, J. Lerner, M.P. McCormick, and L. McMaster, Positive water vapour feedback in climate models confirmed by satellite data, *349* (6309), 500-503, 1991.

Robock, A., and H. Li, Solar dimming and CO 2 effects on soil moisture trends, *Geophys. Res. Lett*, *33*, 2006.

Roderick, M., and G. Farquhar, The Cause of Decreased Pan Evaporation over the Past 50 Years, in *Science*, pp. 1410-1411, 2002.

Ruckstuhl, C., R. Philipona, J. Morland, and A. Ohmura, Observed relationship between surface specific humidity, integrated water vapor, and longwave downward radiation at different altitudes, *Journal of Geophysical Research*, *112* (D03302), 2007.

Russell, G., J. Miller, and D. Rind, A coupled atmosphere-ocean model for transient climate change studies, *Atmosphere-Ocean*, *33* (4), 683-730, 1995.

Saunders, S., C. Montgomery, T. Easley, and T. Spencer, Hotter and Drier: The West's Changed Climate, pp. 54, The Rocky Mountain Climate Organization (RMCO) and Natural Resources Defense Council (NRDC), March 2008.
http://www2.nrdc.org/globalWarming/west/west.pdf

Shenbin, C., L. Yunfeng, and A. Thomas, Climatic change on the Tibetan Plateau: Potential Evapotranspiration Trends from 1961-2000, *Climatic Change*, *76* (3), 291-319, 2006.

Shine, K.P., and A. Sinha, Sensitivity of the Earth's climate to height-dependent changes in the water vapour mixing ratio, *354* (6352), 382-384, 1991.

Soden, B., D. Jackson, V. Ramaswamy, M. Schwarzkopf, and X. Huang, The Radiative Signature of Upper Tropospheric Moistening, in *Science*, pp. 841-844, American Association for the Advancement of Science, 2005.

Stanhill, G., and S. Cohen, Global dimming: a review of the evidence for a widespread and significant reduction in global radiation with discussion of its probable causes and possible agricultural consequences, *Agricultural and Forest Meteorology*, *107* (4), 255-278, 2001.

Thomas, A., Spatial and temporal characteristics of potential evapotranspiration trends over China, *International Journal of Climatology*, *20* (4), 381-396, 2000.

Trenberth, K., P. Jones, P. Ambenje, R. Bojariu, D. Easterling, A. Klein Tank, D. Parker, F. Rahimzadeh, J. Renwick, and M. Rusticucci, Climate Change 2007: The Physical Science Basis, Contribution of Working Group I to the Fourth Assessment Report of the Intergovernmental Panel on Climate Change, Cambridge: Cambridge Univ Press, 2007.

Wild, M., H. Gilgen, A. Roesch, A. Ohmura, C. Long, E. Dutton, B. Forgan, A. Kallis, V. Russak, and A. Tsvetkov, From Dimming to Brightening: Decadal Changes in Solar Radiation at Earth's Surface, in *Science*, pp. 847-850, American Association for the Advancement of Science, 2005.

Xu, M., C. Chang, C. Fu, Y. Qi, A. Robock, D. Robinson, and H. Zhang, Steady decline of east Asian monsoon winds, 1969-2000: Evidence from direct ground measurements of wind speed, *J. Geophys. Res*, *111*, 2006.

Xu, Z., T. Gong, and J. Li, Decadal trend of climate in the Tibetan Plateau - regional temperature and precipitation, *Hydrological Processes*, 2007.

You, Q., S. Kang, N. Pepin, and Y. Yan, Relationship between trends in temperature extremes and elevation in the eastern and central Tibetan Plateau, 1961–2005, *Geophys. Res. Lett*, *35* (L04704), 2008.

Curriculum Vita

Education

Rutgers University, New Brunswick, New Jersey GPA 3.9/4.0
Ph.D., Department of Environmental Sciences (October, 2008)

Rutgers University, New Brunswick, New Jersey GPA 3.8/4.0
M.S. (2003), Department of Environmental Sciences

University of Mumbai, Mumbai, India
B. Engg. (1999), Department of Chemical Engineering

Research Experience

Dept. of Environmental Sciences, Rutgers University (Sept. 1999- Present)

- Analysis of observed and modeled climate data to elucidate the mechanisms of past and projected future climate change in high altitude regions
- Aquatic chemistry, culturing of marine and freshwater algae and crustaceans
- Sampling and analysis of organic pollutants

Bhabha Atomic Research Center, Mumbai, India (Aug 1998 – Jul 1999)

- Chemical engineering design of a denitrification process to treat the heavy metal effluent.

Teaching experience

As Teaching Assistant	Concepts in Biology (01:119:100)	Spring 2002 - Present
(Rutgers University)	Principles in Biology (01:119:103)	Fall 2001
	Introduction to Env. Sc. (11:375:101)	Spring 2000
	General Biology (01:119:101)	Fall 2000

Publications

1. **Rangwala I.**, J. Miller, G. L. Russell, and M. Xu, (2006). Analysis of global climate model experiments to elucidate past and future changes in surface insolation and warming in China. *Geophysical Research Letters*, 33 (20), CiteID L20709. DOI 10.1029/2006GL027778.

2. **Rangwala I.** and K.I. Keating, (2007). Silver deprivation limits fecundity and survivability in the freshwater crustacean Daphnia magna. *Biological Trace Element Research*. DOI: 10.1007/s12011-007-0016-x